

Microrheology for studying collagen solutions and collagen based ECM substitutes during cell proliferation and differentiation

Zur Erlangung des akademischen Grades eines

DOKTORS DER INGENIEURWISSENSCHAFTEN
(Dr.-Ing)

von der KIT-Fakultät für Chemieingenieurwesen und Verfahrenstechnik des
Karlsruher Instituts für Technologie (KIT)
genehmigte

DISSERTATION

von

Johanna Hafner
aus Markdorf-Leimbach

Tag der mündlichen Prüfung: 15.09.2020

Erstgutachter: Prof. Dr. Norbert Willenbacher

Zweitgutachter: Prof. Dr. Cornelia Lee-Thedieck

Danksagung

Nach so langer, intensiver Arbeit an einem einzigen Projekt fällt es schwer allen Wegbereitern in angemessenem Maße zu danken. Hier ein Versuch:

Ich bedanke mich bei meinem Doktorvater und Prüfer, Professor Willenbacher. Danke Norbert, dass Du mir dieses so faszinierende und gleichzeitig so nervenaufreibende Thema überlassen hast, meine Eskapaden im Biolabor zugelassen, sie produktiv mit mir diskutiert und größtenteils finanziert hast.

Danke Connie Lee-Thedieck, dass Du mein Zweit-gutachten übernommen hast und dass Du mir schon vorher mit Rat und Tat zur Seite gestanden hast. Danke auch dir, Claude Oelschlaeger. Du hast Du mir vieles abgenommen und mir in vielen wissenschaftlichen Fragen gezeigt, wie einfach die Dinge sein können.

Danke auch euch, liebe (Ex-)Kollegen, dass ihr euch mein Gejammer über mein einsames Leben am Rande der Rheo-Welt so geduldig angehört habt. Besonders danken möchte ich dir, Steffen Recktenwald für 1000 gute Ratschläge und Mut machende Gespräche vor und nach Feierabend. Annika Völp, dir möchte ich danken für die vielen Diskussionen über zweckentfremdete Apparate und vor allem dafür, dass Du mir mein allerletztes Laborexperiment bei der MAB organisiert hast. Danke, Ceren Yüce, dass Du deine Rheo- und Latex-Skills mit mir geteilt hast. Danke Bernhard Hochstein, dass Du mich durch den Verwaltungs-Dschungel begleitet hast. Danke euch allen, verrückte AMEler, für die doch ziemlich gute Zeit.

Und dann gibt es da ja noch mein zweites Arbeits-Zuhause, das Labor von Prof. Bastmeyer. Erstmal Ihnen, lieber Herr Professor Bastmeyer, herzlichen Dank, dass Sie meine Experimente so bedingungslos unterstützt haben. Vor allem dir, liebe Sarah Bertels gebührt ein riesiges Dankeschön. Danke, dass Du mir die Grundlagen der Zellkultur beigebracht, mir zu allen möglichen Zeiten Zellen expandiert hast und aus meinen wirren Entwürfen lesbare Manuskripte gemacht hast.

Die nächste Eskalationsstufe meiner Zellexperimente hat mich dann an den Campus Nord in die AG Lee-Thedieck geführt. Auch dort wurde ich wahnsinnig herzlich und völlig vorbehaltlos aufgenommen. Danke, Connie, dass Du mir so unkompliziert weitergeholfen hast, dass Du mir Annamarija Raic zur Seite gestellt und dann meine Betreuung, die sich plötzlich doch ewig hingezogen hat, in Anita Ludwig-Husemanns liebevolle Hände gegeben hast. Danke, Anna, Danke Anita, Danke, dass ich stundenlang euer Labor blockieren und von euren super strukturierten Assays profitieren durfte. Danke, Kathrin Brändle, dass Du mir sogar das Pipettieren abgenommen hast, damit wir rechtzeitig fertig werden.

Wenn ich nicht mir nichts dir nichts nach Okinawa geflogen wäre, wäre das Projekt am Campus Nord vielleicht schneller fertig gewesen, aber wer konnte schon ahnen,

dass ich in der Micro/Bio/Nanofluidics Unit DNA-Polymeraseaktivität messen, statt wie geplant, ECM-Synthese von HUVECs dort zu studieren. Well, without knowing how all this happened, I am very, very grateful for this experience. It was a great time, thanks to Amy Shen and Nikhil Bhalla for fantastic supervision, Simon Harward and Kazi Toda-Peters for lots of input, Bruno Miranda and Ianto Cannon for being amazing companions. ありがとうございます!

Dank gebührt zudem dir, Frau Professor Karen Bieback und dir, Julian Gebauer für die fantastische Unterstützung bei den HUVEC-Experimenten.

Alle diese kleinen und großen, immer zeitlich knappen Projekte hätte ich nicht hinbekommen ohne meine Studenten, die mir hier im Labor den Rücken freigehalten haben und meine Arbeit mit ihren kreativen Ideen und ihrem Wissensdurst sehr bereichert haben. Danke, Lea Bensinger, David Grijalva Garces, Hannah Storm, Anna Ryl, Valentin Wieland, Tiago Ribeiro da Costa, Aicha Laghmani, Yezi Zhou, Natalia Danielewicz, Shirane Zedef, Marissa Utomo, Jenny Maahs.

Ich glaube ich war die letzten Jahre mehrheitlich ätzend oder gar nicht erreichbar, vor lauter Arbeit. Deswegen möchte ich meinem sozialen Umfeld für Liebe, aufmunternde Worte und Nachsicht danken. Danke, liebe Eltern, dass ihr irgendwann aufgegeben habt zu verstehen, warum ich das hier unbedingt will und Danke, dass ihr mich trotzdem meinen ganzen bisherigen Werdegang mit Wort und Tat unterstützt habt.

Das letzte meiner Dankes geht an meinen mittlerweile Mann. Ohne dich wäre ich entweder verhungert, verdurstet oder in meinem Sumpf versumpft. Ich bin sehr froh, dass Du jede dieser Eventualitäten wieder und wieder verhindert hast.

Preface

This publication based dissertation consists of four peer-reviewed scientific journal articles and one conference proceeding. These include the main results of my experimental work, done at the Karlsruhe Institute of Technology (KIT), Institute for Mechanical Process Engineering and Mechanics, Applied Mechanics Group, from November 2015 until December 2019.

The main part of this thesis follows a general introduction and it includes the following adapted publications:

1. J. Hafner, C. Oelschlaeger, N. Willenbacher: Microrheology imaging of fiber suspensions - case study for lyophilized collagen in HCl (2020), *Soft Matter*
2. J. Roether, A. Ryl, C. Oelschlaeger, N. Willenbacher: Mechanical Properties and Suitability for Cell Culture of Hyaluronic Acid, Chitosan, and Collagen Based Scaffolds Obtained from Cryogelation (2017), Conference proceedings of BioMAAP 2017 Conference, London, held by ASRANet Ltd.
3. J. Roether, C. Oelschlaeger, N. Willenbacher: Hyaluronic acid cryogels with non-cytotoxic crosslinker genipin (2019), *Materials Letters X*
4. J. Roether, S. Bertels, C. Oelschlaeger, M. Bastmeyer, N. Willenbacher: Microstructure, local viscoelasticity and cell culture suitability of 3D hybrid HA/collagen scaffolds (2018), *PLoS ONE*
5. J. Hafner, D. Grijalva, A. Ludwig-Husemann, S. Bertels, L. Bensinger, A. Raic, J. Gebauer, C. Oelschlaeger, M. Bastmeyer, K. Bieback, C. Lee-Thedieck, N. Willenbacher: Monitoring matrix remodelling in the cellular microenvironment using microrheology for complex cellular systems (2020), *Acta Biomaterialia*

The thesis concludes with a summary and an outlook, as well as a joint bibliography. The bibliography includes all references of all publications. Hereby the publications are slightly changed. Furthermore, some diagrams and images are modified in size and color, taking into account the format of this dissertation. For the reason of better readability, the term we is used throughout the thesis.

Abstract

All types of cells are able to recognize the mechanical properties of their environment and the most important cellular processes are influenced by mechanical stimuli. However, the range taken into account for mechanosensing is limited to several hundreds of micrometers around the cell. Thus, it is of great interest to study mechanical and structural properties of the direct cell surrounding on a length scale that can be sensed by cells, i.e. micrometers.

The so called multiple particle tracking (MPT) technique is a passive, non-invasive microrheology method and consequently a promising candidate to study the local structural and mechanical properties of natural and artificial cell environments. MPT is based on video tracking of the Brownian motion of tracer particles embedded in the sample and allows for a characterization of these local viscoelastic properties and hence spatial heterogeneities on a length scale that is relevant for cells' mechanosensing.

For studying cell-matrix-interactions *in vitro*, appropriate scaffolds are needed and one approach to fabricate such, is the cryogelation technique which delivers porous soft hydrogels with tuneable mechanical properties and represents a facile processing route to integrate tracer particles directly.

The successful formulation of biocompatible hydrogels requires a detailed characterization of the precursor solutions. As the local structure of the resulting cryogels is partly determined by the structural features that are already present in the precursor solution, we investigated the structural and local viscoelastic properties of acidic solutions of lyophilized collagen I (Coll).

Native collagen I is a key component of natural ECM and sourced from tendons or hides. After lyophilization, a valuable biopolymer with modified chemical properties results. This is employed in cosmetics and many scaffold formulations, but highly complex in terms of molecular structure. Suspensions of Coll in HCl appear transparent to the naked eye. However, we were able to visualize micrometer-sized network-like structures by using our novel microrheology imaging approach, i.e. overlaying subsequent images of MPT videos. MPT measurements yielded a broad distribution of mean square displacements (MSDs). Three fractions of tracer particles were found: At first, tracer particles freely diffusing in the aqueous phase, that yielded viscosities indicating that irrespective of solution concentration, a constant amount of collagen is dissolved in the aqueous phase.

Secondly, particles exhibiting time-independent MSDs were found. This elastically trapped fraction was subdivided into two populations with distinctly different absolute MSD values. Higher absolute MSD values correspond to particles located within soft regions of fibrous Coll structures and thirdly, low absolute MSD values were found for

tracers that were almost immobilized in their highly elastic surrounding.

Based on these findings we propose for such acidic Coll dispersions a structure comprising multiple non-banding fiber bundles with dense regions inaccessible for tracers and elastic regions of different stiffness in between. Such structures were found even below the sol-gel transition but densify with increasing concentration. The existence of such heterogeneities in the precursor solutions is exclusively uncovered by using MPT and helps to better understand the crosslinking process and to identify causes for the heterogeneities in resulting biohydrogel scaffolds.

Beyond that, these MPT experiments serve as a proof-of-concept for characterization of network structures in fiber suspensions with poor optical contrast, for which typical imaging techniques fail.

For application in TE and cell culture, scaffolds need to be cost-effective and should have chemical and structural properties close to natural cell environment. This includes macroporous structure and mechanical properties in the same range as those of natural extracellular matrix. Chemically crosslinked cryogels based on biopolymers are perfectly suitable to fulfil those requirements.

We adapted the fabrication procedures for production of cryogels based on hyaluronic acid (HA), the mayor carbohydrate component of natural ECM and chitosan, a cost-effective, easily available alternative with similar chemical composition, both crosslinked with ethylene glycol di-glycidyl ether (EGDE). For enhanced biofunctionality, Coll as model for the mayor protein component of natural ECM was used for fabrication of cryogels and introduced in mixtures with chitosan and HA.

All resulting cryogel scaffolds were macroporous ($\sim 100 \mu\text{m}$ pore size) and their bulk mechanical properties can be tailored in the range of natural cell environments in different tissues. The combination of macroscopic (Young's modulus in uniaxial compression) and local (MPT) characterization with investigation of structural properties (pore architecture) allowed for the estimation of the influences of geometry and material properties of polymer networks on overall mechanical properties of scaffolds. Coll and HA cryogels showed a regular sample spanning network with spherical interconnected pores, while chitosan gels were heterogeneous, consisting of densely crosslinked areas and elongated macro pores. Those led to lower bulk moduli, but the local elasticity of the network was even higher than in samples containing Coll. Despite the high degree of heterogeneity in Coll precursor solutions, the local heterogeneity in the crosslinked state was reduced.

Additionally, for Coll gels the influence of initial freezing rate and crosslinker concentration on structural and mechanical properties was investigated in detail. Initial freezing in liquid nitrogen led to needle shaped pores, whereas after initial freezing in -20°C regular spherical pores occurred. However, local mechanical properties of the gels were not affected. In contrast, increased crosslinker concentration led to higher crosslink density in the pore walls which resulted in an increase in local elasticity.

Based on these results, cryogels' bulk mechanical and biofunctional properties can be tailored independently to generate a broad range of scaffolds, fitting application specific needs in cell culture. Despite the chemical similarity between HA and chitosan, latter forms cryogels with more heterogeneous microstructure and different elastic properties, so that chitosan cannot be considered a cheap alternative for HA, but chitosan can still serve as versatile component for the formation of heterogeneous cryogels.

Besides appropriate physical properties, suitable cell culture scaffolds need a high degree of biocompatibility. This was proven during 18 days of fibroblast cell culture in the scaffolds. All investigated scaffold compositions yielded a high number of living cells ($\sim 80\%$ of total cell count after 18 days). In contrast to pure HA, Coll containing gels furthermore enabled cell migration, adhesion and proliferation inside the gels.

For further reducing the cytotoxicity, not only of cell culture scaffolds, but also for a broad range of materials for drug delivery and aesthetic surgery applications, we aimed at using a less toxic crosslinker.

For the first time, pure HA cryogels were prepared with genipin as plant-based, non-cytotoxic crosslinking agent. These cryogels were characterized by a lamellar porous structure with a homogeneous pore size of $\sim 100 \mu\text{m}$ and bulk shear elasticity of $\sim 2 \text{ kPa}$. MPT revealed the formation of a heterogeneous network, as already seen for EGDE cryogels. This novel biomaterial owns great potential as non-cytotoxic alternative for application in drug delivery, as tissue engineering scaffold or wound healing substrate and can help reducing toxicity of artificial skin grafts or tissue equivalents.

Finally, we seeded different types of cells in cryogel scaffolds and employed MPT to monitor the development of extra cellular matrix (ECM) mechanical properties in the direct surrounding of these. Studying differentiating mesenchymal stem cells, we were able to prove that the osteogenic differentiation, induced by specific composition of the cell medium, led to a significant increase in local elastic modulus $G_{0,\text{MPT}}$ of the Coll/HA based scaffolds. In contrast, during adipogenic differentiation, the scaffold was predominantly degraded and $G_{0,\text{MPT}}$ was significantly decreased.

A separate modification of our MPT setup, namely the combination with a cell culture chamber, enabled us to study the ECM elasticity in the direct surrounding of single 3T3 fibroblasts continuously during the first 8 h of culture in the aforementioned gels.

In context of endothelial cells, that naturally form 2D layers, properties of newly secreted ECM are more interesting. For human umbilical vein endothelial cells (HU-VECs), serving as model for endothelial cells, the effect of varied concentrations of protease inhibitor on local ECM was investigated, showing the expected increase of ECM elasticity with increasing inhibitor concentration.

These novel techniques based on MPT and their combination provide great potential not only for live-cell studies on cell-material interactions in hydrogels, but also for the characterization of newly secreted ECM and its homeostasis, as well as all other soft, delicate (bio)materials. MPT possesses the unique potential to elucidate local structural and mechanical properties in-situ in a non-invasive manner, that was proven to be compatible with living cell cultures and suitable for delicate networks.

The non-invasive measurement allows for continuous monitoring of mechanical and structural properties, including kinetic investigations. Thus, it serves as powerful tool for the investigation of the development of mechanical stimuli on the cellular level and their effects on living systems. Such information needs to be systematically collected to finally understand the mechanically driven processes in cell-growth and metabolism, including wound healing, angiogenesis, tumor formation, cancer metastasis, but also cell-adhesion, migration and differentiation.

Zusammenfassung

Alle Arten von Zellen können die mechanischen Eigenschaften ihrer Umgebung wahrnehmen. So werden die wichtigsten zellulären Prozesse von mechanischen Stimuli beeinflusst. Der Bereich, der von einer Zelle im Rahmen des sog. *Mechanosensing* wahrgenommen wird, ist beschränkt auf einige hundert Mikrometer um die Zelle. Daraus erwächst ein besonderes Interesse die mechanischen und strukturellen Eigenschaften der direkten Zellumgebung auf der Mikrometer-Längenskala zu untersuchen.

Bei der sogenannten *Multiple particle tracking* (MPT)-Methode handelt es sich um eine passive, nicht-invasive Mikrorheologie-Methode, welche sich deshalb besonders zur Untersuchung von lokalen mechanischen und strukturellen Eigenschaften von natürlichen und synthetischen Zellumgebungen eignet. MPT basiert auf dem Video-Tracking der Brown'schen Molekularbewegung von Tracerpartikeln, welche in der Probe eingebettet sind. Weil die Bewegung der Partikel von den viskoelastischen Eigenschaften des umgebenden Materials abhängt, können diese viskoelastischen Eigenschaften der Umgebung und Heterogenitäten auf einer Längenskala bestimmt werden, die für das *Mechanosensing* der Zellen relevant ist.

Um Zell-Matrix-Interaktionen *in vitro* zu betrachten bedarf es geeigneter Gerüststrukturen (engl. *scaffolds*). Eine Möglichkeit diese herzustellen ist die Kryogelierung, mit welcher poröse, weiche Hydrogele mit einstellbaren mechanischen Eigenschaften hergestellt werden können. Die Kryogelierung bietet zudem die Möglichkeit, Tracerpartikel effizient in die Matrix einzuarbeiten.

Für die erfolgreiche Formulierung von Hydrogelscaffolds ist eine detaillierte Charakterisierung der verwendeten Rohstoffe entscheidend, da die lokale Struktur der resultierenden Kryogele zumindest teilweise von den strukturellen Eigenschaften der Ausgangslösungen abhängen. Deshalb haben wir die strukturellen und lokalen viskoelastischen Eigenschaften von gefriergetrocknetem Kollagen I in saurer Lösung untersucht.

Natives Kollagen I ist einer der Hauptbestandteile der natürlichen Extrazellulären Matrix (ECM) und wird aus Sehnen und Haut gewonnen. Durch die Gefriertrocknung entsteht ein wertvolles Biopolymer mit modifizierten chemischen Eigenschaften und hoch komplexer molekularer Struktur, welches in der kosmetischen Formulierung und bei der Herstellung von Scaffolds Verwendung findet.

Obwohl Suspensionen dieses gefriergetrockneten Kollagen I in Salzsäure dem bloßen Auge transparent erscheinen, konnten wir mittels eines bildgebenden Verfahrens basierend auf der Mikrorheologie-Methode *Microrheo Imaging* das mikrometergroße Netzwerk sichtbar machen. Hierfür wurden die Bilder einer MPT-Videsequenz übereinander gelegt und so verschiedene Bereiche der Mikrostruktur sichtbar gemacht. Die MPT-Messungen zeigten eine breite Verteilung der mittleren Verschiebungsquadrate

(MSD) der Tracerpartikel. Diese konnten drei Fraktionen zugeordnet werden: Die erste Gruppe bilden Tracerpartikel, die frei in ihrer Umgebung, hier der wässrigen Phase der Suspension, diffundieren und konstante Viskositätswerte liefern. Dies deutet darauf hin, dass unabhängig von der Kollagenkonzentration eine konstante Menge Kollagen in der wässrigen Phase gelöst ist.

Hiervon zu unterscheiden sind Partikel, welche zeitunabhängige MSDs zeigten. Diese Fraktion elastisch fixierter Partikel wurde in zwei Gruppen unterteilt, welche sich hinsichtlich der Absolutwerte der MSDs signifikant unterscheiden. Höhere Absolutwerte stehen für Partikel, welche sich in den weicheren Bereichen der faserigen Kollagensuspensionen befinden, während niedrige Absolutwerte für beinahe immobilisierte Tracerpartikel in hochelastischer Umgebung gefunden wurden.

Auf der Grundlage dieser Beobachtungen schlagen wir für die untersuchten sauren Dispersionen gefriergetrockneten Kollagens eine Mikrostruktur aus vielen Faserbündeln mit dichten, für Tracerpartikel zugänglichen Regionen unterschiedlicher Steifigkeit und gänzlich unzugänglichen Regionen vor. Solche Strukturen wurden sogar unterhalb der Sol-gel-Übergangskonzentration gefunden, aber sie verdichten sich mit steigender Konzentration.

Die Existenz dieser Heterogenitäten in den Kollagenlösungen ist einzig durch MPT erkennbar und trägt zum besseren Verständnis des späteren Vernetzungsprozesses bei der Gelierung bei. Ferner kann hierdurch die Heterogenität der resultierenden Biohydrogele teilweise erklärt werden.

Allgemein zeigen diese MPT-Experimente, dass es generell möglich ist, Netzwerkstrukturen in Fasersuspensionen mit schlechtem Kontrast und schwierigen optischen Eigenschaften, bei denen konventionelle bildgebende Verfahren scheitern, sichtbar zu machen.

Für die Anwendung im *Tissue Engineering* und in der Zellkultur müssen Scaffolds kosteneffizient sein und chemische, strukturelle und biofunktionale Eigenschaften haben, welche der natürlichen Zellumgebung so ähnlich wie möglich sind. Dies beinhaltet eine makroporöse Struktur und ähnliche mechanische Eigenschaften wie die der natürlichen ECM. Chemisch vernetzte Kryogele auf Biopolymerbasis erfüllen diese Anforderungen in höchstem Maße. Deshalb haben wir die Kryogelierungsmethode zur Verwendung von Hyaluronsäure, dem Hauptkohlenhydrat in der natürlichen ECM, und Chitosan, einem kostengünstigen leicht verfügbaren Alternativmaterial mit ähnlicher Zusammensetzung, angepasst. Beide werden mit Ethylenglykol-Diglycidylether (EGDE) vernetzt. Um die Biofunktionalität zu verbessern wird zudem Kollagen I, Hauptproteinbestandteil der natürlichen ECM, für die Scaffoldherstellung verwendet und in Mischungen mit den Kohlenhydraten eingesetzt.

Alle resultierenden Kryogel-Scaffolds waren makroporös (Porengröße $\sim 100 \mu\text{m}$) und ihre makromechanischen Eigenschaften können angepasst werden im Wertebereich, in dem auch die natürlicher Zellumgebungen in verschiedenen Geweben liegen.

Die Kombination des makroskopischen Elastizitätsmoduls (E-Modul in uniaxialer Kompression ermittelt) mit der lokalen Charakterisierung mittels MPT und der strukturellen Untersuchung der Porenstruktur ermöglichte es, den Einfluss der Geometrie und der Materialeigenschaften auf die mechanischen Eigenschaften der Scaffolds abzuschätzen. Kollagen- und Hyaluronsäuregele zeigten ein regelmäßiges, die gesamte Probe durchziehendes Porennetzwerk mit runden, miteinander verbundenen Poren,

wohingegen Chitosangele eine heterogene Porenstruktur, bestehend aus dicht vernetzten Bereichen und länglichen Makroporen aufwiesen. Diese führten zu reduzierten Bulk-Moduln, aber die lokale Elastizität des Netzwerkes war sogar höher, als in den reinen Kollagengelen. Trotz der großen Heterogenität in den Kollagenlösungen war hier die lokale Heterogenität in den vernetzten Gelen reduziert.

Zudem wurde für Kollagengele der Einfluss der initialen Gefriereschwindigkeit und der Vernetzerkonzentration auf die strukturellen und mechanischen Eigenschaften detailliert untersucht. Anfängliches Gefrieren in flüssigem Stickstoff führte zu Gelen mit nadelförmigen Poren, wohingegen Gele, die zu Beginn bei -20°C gefroren wurden, regelmäßige, runde Poren aufwiesen. Die lokalen mechanischen Eigenschaften der Gele waren hiervon nicht beeinflusst, aber erhöhte Vernetzerkonzentrationen führten zu einer erhöhten Vernetzungsdichte in den Porenwänden. Hieraus resultierte eine erhöhte lokale Elastizität. Auf der Grundlage dieser Ergebnisse können die makromechanischen und biofunktionalen Eigenschaften unabhängig voneinander variiert werden, um so eine Palette von Scaffolds mit verschiedenen Eigenschaften herzustellen, welche verschiedensten anwendungsspezifischen Anforderungen in der Zellkultur genügen können.

Trotz der Ähnlichkeit der chemischen Eigenschaften von Chitosan und Hyaluronsäure, bildet Chitosan Kryogele mit wesentlich heterogenerer Mikrostruktur und deutlich anderen elastischen Eigenschaften, sodass Chitosan nicht einfach als günstige Alternative zu Hyaluronsäure betrachtet werden kann. Dennoch kann Chitosan als vielseitige Komponente für die Formulierung von heterogenen Kryogelen eingesetzt werden.

Neben passenden physikalischen Eigenschaften müssen geeignete Scaffolds eine hohe Biokompatibilität aufweisen. Dies wurde nachgewiesen, indem Fibroblasten für 18 Tage in den Scaffolds kultiviert wurden. In allen untersuchten Gelen zeigte sich auch nach 18 Tagen ein hoher Anteil lebender Zellen ($\sim 80\%$ der Gesamtzellzahl). Im Gegensatz zu reinen Hyaluronsäuregelen ermöglichten Gele mit Kollagenanteil zusätzlich die Zellmigration, Adhäsion und Proliferation in den Gelen.

Um die Zytotoxizität von Zellkulturscaffolds, aber auch von vielen Materialien, die in der ästhetischen Chirurgie und für die verbesserte Wirkstofffreigabe eingesetzt werden, weiter zu verbessern, ist die Verwendung ungiftiger Vernetzer erstrebenswert. Zum ersten Mal konnten reine Hyaluronsäuregele mit Genipin vernetzt werden. Diese Kryogele zeichnen sich durch eine lamellare Porenstruktur mit homogener Porengröße von ca. $\sim 100\ \mu\text{m}$ aus und einer Bulk-Elastizität von $\sim 2\ \text{kPa}$ aus. MPT zeigte hier die Bildung eines heterogenen Netzwerkes, wie sie auch schon für mit EGDE vernetzte Kryogele beobachtet wurde.

Dieses neuartige Biomaterial besitzt großes Potential als nicht zytotoxische alternative für die Anwendung bei der verzögerten Wirkstofffreisetzung, als Tissue Engineering Scaffold oder innovatives Wundabdeckungssubstrat und kann dazu beitragen, die Toxizität künstlicher Hautsubstitute oder Gewebeersatzmaterialien zu reduzieren.

Schließlich haben wir verschiedene Zelltypen in Kryogelen kultiviert und MPT verwendet, um die Entwicklung der mechanischen Eigenschaften der ECM in deren direkter Zellumgebung zu untersuchen. Indem mesenchymale Stammzellen während der Differenzierung untersucht wurden, konnten wir zeigen, dass die osteogene Differenzierung, welche durch die Zusammensetzung des Zellmediums induziert wurde, zu einem signifikanten Anstieg des lokalen elastischen Moduls $G_{0,\text{app}}$ der Kollagen/Hyaluronsäure-Scaffolds führte. Im Gegensatz dazu wurde während der adipogenen Differenzierung

das Scaffold vorrangig degradiert und folglich $G_{0,app}$ signifikant reduziert.

Eine separate Modifikation unseres MPT-Aufbaus durch Hinzufügen einer Zellkulturkammer ermöglichte es uns die Elastizität der ECM in der direkten Umgebung einzelner 3T3 Fibroblastenzellen in den ersten 8 h nach dem Aussäen in den o.g. Gelen kontinuierlich zu beobachten.

Im Zusammenhang mit Endothelzellen, welche natürlicherweise zweidimensionale Schichten ausbilden, sind die Eigenschaften neu sekretierter ECM von größerem Interesse. Nabelschnurepithelzellen, (Human umbilical vein endothelial cells; HUVECs) wurden hier als Modell für Endothelzellen verwendet. Der Effekt der Proteaseinhibitorkonzentration auf die lokale ECM wurde hier untersucht. Es resultierte der erwartete Anstieg der Elastizität der ECM mit steigender Inhibitorkonzentration.

Diese neuartigen MPT-Methoden und ihre Kombination besitzen großes Potential um Zell-Matrix-Interaktionen an lebenden Zellen zu studieren und um neu sekretierte ECM und ihre Homöostase zu charakterisieren, aber auch zur Untersuchung anderer weicher, empfindlicher (Bio-)Materialien. MPT ermöglicht es lokale strukturelle und mechanische Eigenschaften nicht-invasiv und in-situ zu bestimmen. Hier wurde gezeigt, dass die Methode zytokompatibel und für sensible Materialien geeignet ist. Die nicht-invasive Methode ermöglicht die kontinuierliche Beobachtung mechanischer und struktureller Eigenschaften, sowie kinetischer Untersuchungen in der Zellkultur und dient so als hilfreiches Tool zur Untersuchung der Entwicklung mechanischer Stimuli auf zellulärer Ebene und deren Auswirkungen auf lebende Systeme. Solche Informationen müssen systematisch gesammelt werden um schlussendlich mechanisch getriebene Prozesse hinsichtlich Zellwachstum und Metabolismus im Zusammenhang mit Wundheilung, Angiogenese, Tumorbildung, Metastasierung, aber auch grundlegend Zelladhäsion, Migration und Differenzierung besser zu verstehen.

Notations

Abbreviations

AGE	Advanced glycation endproducts
adip	condition with induced adipogenic differentiation
AFM	Atomic Force Microscopy
BDDE	1,4-butanediol diglycidyl ether
BSA	Bovine serum albumin
CAM	high speed camera
CLSM	confocal laser scanning microscope
Coll	lyophilized Collagen I
DAPI	4',6-diamidino-2-phenylindole
DMEM	Dulbeco's modified Eagles medium
DMSO	Dimethyl sulfoxide
ECs	Endothelial cells
ECM	Extracellular Matrix
EDC	Carbodiimide
EDTA	Ethylenediaminetetraacetic acid
EdU	5-ethynyl-2'-deoxyuridine
EGDE	Ethyleneglycol diglycidylether
Coll	Collagen I
FCS	fetal calf serum
GSE Relation	generalized Stokes Einstein Relation
HA	Hyaluronic Acid
hMSCs	Human mesenchymal stem cells \equiv human mesenchymal stromal cells
HUVECs	Human umbilical vein endothelial cells
iPS	Induced pluripotent stemcells
LED	Light emitting diode
LSM	Laser scanning microscope
MMP	Matrix metalloproteinase
MPT	Multiple Particle Tracking
MSC	Mesenchymal stem cell or mesenchymal stromal cell
MSD	Mean square displacement
mMSD	Mean Mean square displacement of a particle collective
NHS	n-hydroxysuccinimide
ost	condition with induced osteogenic differentiation
PA	Polyacrylamide

PBS	Phosphate buffered saline
PEG	Polyethylene glycol
PS	Polystyrene
PTFE	Polytetrafluoroethylene
SR	Swelling ratio
TE	Tissue Engineering
TIMP	Tissue inhibitors of metalloproteinase
2D	Two dimensional
3D	Three dimensional

Symbols

Latin Symbols

a	Particle radius	μm
E	Young's modulus	Pa
G^*	complex Modulus	Pa
G'	Storage modulus	Pa
G''	Loss modulus	Pa
G_0	Plateau modulus	Pa
$G_{0,\text{app}}$	apparent modulus determined from MPT	Pa
$G_{0,\text{bulk}}$	Plateau modulus, measured in oscillatory shear	Pa
$G_{0,\text{MPT}}$	Plateau modulus from multiple particle tracking experiments	Pa
k_B	Boltzman Constant = $1.38064852 \times 10^{-23}$	$\text{m}^2\text{kg}/\text{s}^2\text{K}$
l_0	Initial sample height	mm
m_{dry}	Sample weight prior to swelling	g
n	number of particles	
M_W	Molecular weight	kDa
m_{wet}	Sample weight after swelling	g
r	Displacement	μm
T	Temperature	$^\circ\text{C}$

Greek symbols

α	Non-Gaussian parameter	[-]
Δl	Change in length during compression test	mm
Δr^2	Mean square displacement	μm^2
$\langle \Delta r^2 \rangle$	statistical error	μm^2
ν	Poisson's ratio	[-]
ξ_{bulk}	Mesh size according to rubber elasticity theory, calculated from G'_{bulk}	nm
ξ_{MPT}	Mesh size according to rubber elasticity theory, calculated from G'_{MPT}	nm
π	Pi-Number	[-]
τ	Lag time in MPT experiments	s
τ	Stress amplitude in oscillatory shear experiments (only in Chapter 2)	Pa
ω	Angular frequency	rad/s

Contents

Danksagung	i
Preface	iii
Abstract	v
Zusammenfassung	ix
Notations	xiii
Contents	xv
1 Introduction	1
1.1 Tissue Engineering (TE) and 3D cell culture	1
1.1.1 Cells for TE	2
1.1.2 Requirements for cell culture scaffolds	3
1.1.3 Mechanical and structural requirements	3
1.2 Hydrogels as 3D scaffolds	4
1.2.1 Biopolymers as building blocks for TE materials	4
1.2.2 Biobased cryogels	5
1.2.3 Cell-Matrix Interactions	6
1.3 Mechanical properties of ECM and substitutes	7
1.3.1 Bulk mechanical properties of ECM substitutes	7
1.3.2 Local mechanical properties of ECM substitutes	7
1.4 Multiple particle tracking microrheology	8
1.4.1 MPT Principle	8
1.4.2 MPT for characterizing ECM substitutes	9
1.4.3 Characterization of newly secreted ECM	10
1.5 Motivation and organization of manuscripts	10
2 Characterization of Coll precursor solutions	13
2.1 Introduction	14
2.2 Experimental	16
2.2.1 Preparation of lyophilized Coll in HCl	16
2.2.2 Multiple particle tracking microrheology	17

2.2.3	Bulk rheological characterization in oscillatory shear	19
2.3	Results and Discussion	19
2.3.1	Sol- gel transition of lyophilized Coll suspensions from bulk rheometry	19
2.3.2	Visualization of fibers using MPT tracer particles	20
2.3.3	Local elasticity and microstructure of lyophilized Coll suspensions obtained using MPT	21
2.3.4	Concentration dependence of local elasticity and network structure	23
2.3.5	Structural properties of native collagen I solutions	29
2.4	Conclusions	30
3	Cryogel scaffolds from HA, Coll, Chitosan and mixtures	33
3.1	Introduction	34
3.2	Materials and Methods	35
3.2.1	Preparation of HA/Coll/Chit solutions	35
3.2.2	Scaffold pore size and shape, network thickness and topology characterizations	38
3.2.3	Multiple particle tracking based optical microrheology	38
3.2.4	Mechanical Compression tests and Texture Profile Analysis	38
3.3	Results	39
3.3.1	Formation and structure of single component cryogels	39
3.3.2	Fabrication and structure of stable hybrid gels	40
3.3.3	Comparison of polymer types	40
3.3.4	Influence of fabrication process on mechanical and structural properties of cryogels	43
3.4	Conclusion	43
4	Fabrication of non-cytotoxic HA scaffolds	45
4.1	Introduction	45
4.2	Materials and methods	46
4.2.1	Preparation of cryogels and determination of swelling capacity	46
4.2.2	Rotational rheometry	46
4.2.3	Multiple particle tracking	46
4.3	Results and discussion	47
4.3.1	Cryogels structural properties and swelling capacity	47
4.3.2	Mechanical properties	48
4.4	Conclusion	49
5	Structure and cell-culture suitability of HA/Coll scaffolds	51
5.1	Introduction	51
5.2	Materials and Methods	53
5.2.1	Preparation of HA/Coll cryogels	53
5.2.2	Scaffold pore size and shape, network thickness and topology characterizations	54
5.2.3	Multiple particle tracking based optical microrheology	54
5.2.4	Bulk mechanical properties	56

5.2.5	Degradation Kinetics	56
5.2.6	In vitro assessment of biocompatibility	56
5.3	Results and Discussion	57
5.3.1	Structural properties of HA, Coll and hybrid cryogels	57
5.3.2	Swelling and bulk mechanical properties	58
5.3.3	Local viscoelastic properties from multiple particle tracking microrheology	61
5.3.4	Degradability	64
5.3.5	Biocompatibility of HA/Coll cryogels	65
5.4	Conclusions	67
6	Local elasticity of natural and synthetic ECM	71
6.1	Introduction	72
6.2	Materials and Methods	75
6.2.1	2D and 3D cell culture and differentiation	75
6.2.2	Characterization of local viscoelastic matrix properties using MPT	77
6.2.3	Proof of hMSC differentiation by staining	80
6.3	Results and Discussion	81
6.3.1	Continuous monitoring of matrix degradation by fibroblasts . .	81
6.3.2	ECM mechanics after adipogenic and osteogenic differentiation in 3D	85
6.3.3	ECM mechanics in 2D	87
6.4	Conclusion	90
6.5	Acknowledgements	91
7	Summary and outlook	93
	Bibliography	97

Chapter 1

Introduction

Multiple particle tracking microrheology is based on video tracking of the Brownian motion of micrometer-sized tracer particles embedded in the sample [204, 257, 262]. The assessment of many individual particle trajectories and corresponding mean square displacement as a function of lag time allows for a characterization of local viscoelastic properties and hence microstructural heterogeneities of the surrounding fluid [152]. MPT was presented by Mason and Weitz in the mid 1990s as alternative for characterization of mostly synthetic polymer solutions, allowing to reduce the required sample volumes down to few microliters [152]. However, access to the spatial resolution of viscoelastic properties and the characterization of microheterogeneities is of great interest for the characterization of complex, heterogeneous materials, such as biopolymer dispersions and tissue engineering scaffolds made thereof. The spatial resolution of viscoelastic properties on the micrometer length scale allows for the characterization of material properties on a length scale that can be probed by cells, i.e. is relevant for cells' mechanosensing [11, 15, 52, 57, 60, 71, 72].

For studying cell-matrix-interactions *in vitro*, appropriate scaffolds are needed and one procedure to produce these is the cryogelation technique, which delivers porous, soft hydrogels with tuneable mechanical properties [143, 144]. Additionally, cryogelation represents a facile processing route to integrate tracer particles directly in the matrix [174]. Not only for research applications, but especially in therapeutic approaches, such scaffolds need to be biocompatible and non-cytotoxic [83, 187, 222].

1.1 Tissue Engineering (TE) and 3D cell culture

Tissue engineering is a promising technique for replacement and regeneration of diseased tissues by fabricating biological tissues artificially. Healthy cells are gathered from the patient, targetedly multiplied *in vitro* and the resulting tissues are finally re-implanted into the patients' body [129] and references within. Providing such autologous cells is beneficial in terms of immune response i.e. the cells or rather the surface protein structures are recognized as patient-specific so that the implant will not be repelled. However, one current mayor limitation is organizing the interplay of multiple cell types in co-cultures *in vitro* [101]. This includes further the vascularization of tissues, which requires the formation of blood vessel endothelial layers and is existential

for the nutrient and oxygen supply in multilayered TE constructs [36, 37, 216]. Consequently, to date only smaller TE constructs, based on one single cell type, such as cartilage based on chondrocytes and single skin layers based on fibroblasts are commercially available [129, 165, 246]. These can be produced either as 2D cell layers, obtained from cells that are cultured on cell culture plastic, or as three-dimensional cell-laden structures. Therefore, cells are seeded into 3D scaffolds or embedded in gelling products during fabrication [31, 44]. Besides the scaffold or surface employed as mechanical support, nutrient media and growth factors determine the successful cell growth *in vitro* [94].

In addition to the application for transplantation, TE approaches are widely used to study cellular function and interplay under near-natural conditions in fundamental research. Such artificially derived tissue constructs can be employed e.g. for studying toxicity and drug efficacy [83, 195].

1.1.1 Cells for TE

For growing a specific tissue, healthy differentiated cells of the targeted tissue can be harvested from the patient and expanded *in vitro*. Alternatively, stem cells, that are able to differentiate to various cell types, can be harvested and differentiated *in vitro*. Totipotent cells, that are able to form a full organism, including all extra-embryonal tissues, exist only during the initial cell divisions at the beginning of the embryonic development. Afterwards, only pluripotent stem cells remain. These are able to differentiate into each cell type of all germ layers of the organism. In adult organisms, during specification, differentiation potency is further reduced so that the differentiation potential of tissue specific cells is mostly limited to other cell types of the same tissue.

Mesenchymal stem cells (or mesenchymal stromal cells, MSCs) for example, can be derived from various tissues, including adipose tissue and bone marrow. They are able to differentiate towards all cell types of the connective tissue, including osteoblasts (bone cells), adipocytes (fat cells), chondrocytes (cartilage cells) or myocytes (muscle cells). More recently, pluripotency was re-induced to such somatic cells, resulting in so called iPS cells (induced pluripotent stem cells). iPS cells offer a great potential for TE, because adult cells, obtained e.g. from the bone marrow, can be re-programmed to all desired cell types *in vitro* [50, 106]. In contrast, chondrocytes and fibroblasts, both suitable for TE, are specified tissue cells with limited differentiation potential. Fibroblasts belong to the connective tissue and one of their key responsibility is the formation and remodelling of extracellular matrix by secreting glycosaminoglycans, collagen and other proteins, but also enzymes for the degradation of these ECM components.

To finally overcome the limitation of angiogenesis in TE, blood vessel cells, such as vein and arterial endothelial cells (ECs) gained attention in research [185]. E.g. Human umbilical vein endothelial cells (HUVECs) are widely used as a model system for investigating function and pathology of angiogenesis. In contrast to mesenchymal cells, ECs naturally form 2D layers lining the inner surfaces of an organism.

1.1.2 Requirements for cell culture scaffolds

Independent of the desired cell type, a scaffold for successful TE must be biofunctional, biodegradable and biocompatible [129, 171] and references within. Biofunctional means that all ligands that are necessary for near-natural cell behaviour and cell-matrix interactions need to be available in appropriate number. This includes e.g. the availability of protein structures on the scaffold surface that are required for cell adhesion and thus allow cell spreading [118]. A scaffold is furthermore designed to provide mechanical stabilization, especially in the early stage of the cultivation. However, as soon as the newly arising tissue is able to take over this function, the scaffold should preferentially be degraded [97, 136]. Biodegradability is consequently a key requirement and needs to be balanced with the stability in cell-culture conditions.

Biocompatibility includes all aspects of avoiding negative effects on the growing cells, including low acute and long-term toxicity, reducing interactions with degradation products and in the best case providing bioactive features, that are even beneficial for the cell culture [95].

For closely mimicking the structural properties of natural ECM and to ensure sufficient nutrient and oxygen supply, a material with porous architecture and high degree of pore interconnectivity is useful [171]. Furthermore, the chemical properties of the extracellular matrix matter. It is consequently desirable to use natural ECM components, such as collagen and hyaluronic acid or similar polymers and to combine these with non cytotoxic crosslinkers to form stable and at the same time biocompatible hydrogels. Finally, appropriate mechanical properties in a similar range as those of the natural ECM are required [95].

1.1.3 Mechanical and structural requirements

The mechanical properties of a TE scaffold play a fundamental role in the functionality of later implants. Especially during the initial period of tissue formation, the artificial matrices need to take over full mechanical stability of the replaced tissue. Thus, besides high shape fidelity, mechanical properties should meet those of the original healthy tissue. For replacing different tissues, consequently, a broad range of requirements results, which makes configurable stiffness and elasticity desirable [210].

However, not only the initial mechanical properties determine the suitability of a material. The degradation kinetics during tissue growth play another fundamental role, i.e. as the growing cell population/ tissue is increasingly able to take over mechanical stability, the scaffold needs to be degraded. After accomplishing this process, preferentially a healthy tissue with normal mechanical properties results.

In terms of structure, porous materials turned out to be advantageous for enhanced nutrient and oxygen supply of cells in the depth of the scaffold constructs [116, 194, 210]. Furthermore, a high number of interconnected pores in the size range of cells facilitate seeding and later vascularization and migration of cells into the scaffold [88, 175]. Besides these general recommendations, mechanical properties, i.e. local elasticity of the substrate or scaffold also alter cell migration, adhesion, proliferation and metabolism [3, 86, 96, 115, 206, 214, 234, 250] see further details in section 1.2.3.

1.2 Hydrogels as 3D scaffolds

To fulfill the requirements mentioned in section 1.1.2, in early studies, either scaffolds derived from animals and or cadavers were used or later on, scaffolds were based on fully synthetic artificial polymer gels, including poly-amide, poly-vinyl alcohol, polyethylene glycol, silicone and polylactic acid. Many of them were functionalized with additional protein groups to ensure biofunctional properties (reviewed in [216]). Instead of combining a purely mechanical scaffold with biologically active additives, it is meanwhile common to bring both tasks together and employ a biobased scaffold, that fulfills both, biofunctionality and the mechanical requirements [194, 243] and references within.

1.2.1 Biopolymers as building blocks for TE materials

Potential candidates for formation of biocompatible materials are all components of the natural ECM, which include mainly proteins, such as all types of collagen and its processed form gelatin, elastin, fibronectin and laminin, as well as glycosaminoglycans, e.g. hyaluronic acid (HA) or chondroitin sulfate. Furthermore, a broad range of proteins from non-mammalian origin, e.g. silk, fish gelatin and multiple carbohydrates, such as chitosan, alginate and a broad range of cellulose derivatives are used individually and in combinations [243].

The mayor advantage of non-mammalian proteins is the reduced immune-response and in many cases the improved availability, but this is ever accompanied by a less accurate mimicry of natural conditions and the drawback of reduced biofunctionality [171]. In terms of polysaccharides, mainly the low-cost production of microbial hyaluronic acid and the less laborious purification process matter. For many applications, chitosan, derived from shrimp shells and chemically similar to HA, serves as promising cost efficient alternative. HA is a key polysaccharide component of vertebrates ECM and is composed of repeating disaccharide units of n-acetyl glucosamine and glucuronic acid linked by β -1,3 and β -1,4 glycosidic bonds. HA chains can reach a molecular mass of several millions of Daltons, corresponding to a molecule contour length of up to 10 μ m. HA is mainly produced by fibroblasts and serves for the maintenance of the viscoelasticity of liquid connective tissue, control of tissue hydration and water transport. Furthermore, HA plays a key role in receptor-mediated cell detachment, mitosis, migration, tumor metastasis and inflammation [8, 85, 232, 239].

The mayor protein components of the ECM belong to the collagen family. To date, more than 12 types of collagen were identified, covering a broad range of physico-chemical properties. The most prominent type is the fibrous collagen I. It is the most abundant protein in vertebrates and forms fibrils and fibers determining the mechanical properties of the natural ECM. Collagen I is extracted from human or mammal tissues, e.g. rat tails, bovine hides or tendons and is commercially available in aqueous solutions with concentrations up to 1 wt% or as lyophilized powder with altered chemical properties [64, 65, 169] (referred to as Coll). For more details please refer to chapter 2. Collagen I is a biopolymer widely used for all kinds of biological replacements, including tissue engineering, wound dressing and *in vitro* 3D cell models.

For obtaining stable, self-supporting scaffolds with high shape-fidelity from these biomaterials, a chemical crosslinking process is required and in order to allow penetra-

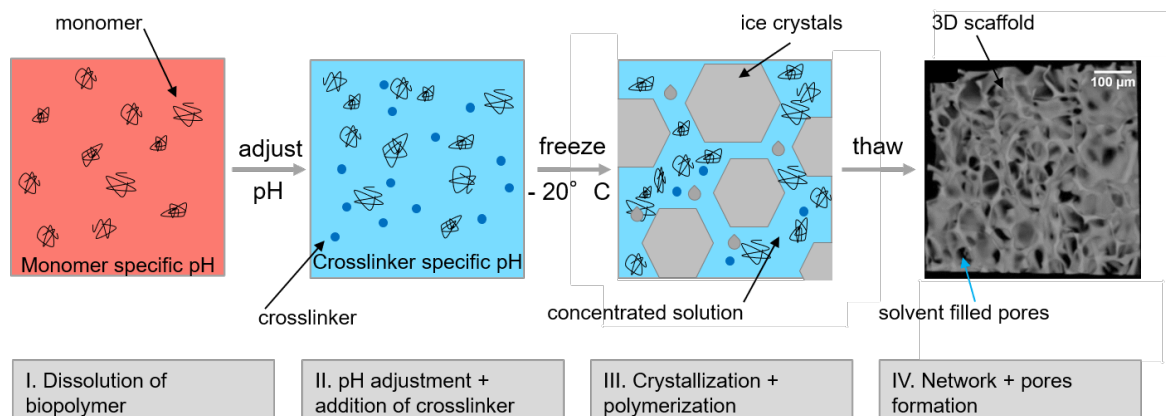


Figure 1.1: Preparation of cryogels (scheme), reproduced from chapter 3

tion of cells and their nutrient supply, preferentially interconnected pores need to be induced.

For fabrication of HA and HA-mixture based porous scaffolds, electrospinning [166], phase separation [35] freeze-drying [115], rapid prototyping [107], critical fluid technology [13] and porogen leaching [61] have been established. Therefore, BDDE (1,4-butanediol diglycidyl ether) [124] and glutaraldehyde [35] were used as crosslinkers. Crosslinkers that are reactive with HA at low temperatures are ethyleneglycol diglycidylether (EGDE) [174, 199, 224] and EDC/NHS (carbodiimide/N-hydroxysuccinimide) [89]. Mixed cryogels of HA with collagen, gelatine and chitosan were also crosslinked by EDC/NHS [33] and glutaraldehyde [123, 231]. Most of the crosslinkers and especially their non-reacting residues are cytotoxic [141, 170], so that currently, non-cytotoxic alternatives are sought-for.

1.2.2 Biobased cryogels

An alternative method to produce porous scaffolds that does not require any specific equipment nor dangerous treatments with organic solvents, is the cryogelation technique as proposed by Lozinski et al. [143]. Thus, many studies deal with cryogels as potential TE scaffolds [88, 144, 188], including a few studies showing scaffolds based on HA-mixtures [30, 116, 224].

Starting from an aqueous solution of the polymer (mixture), a chemical crosslinking agent is added prior to freezing. At temperatures well below the crystallization point of the solution, water forms crystals, that serve as a template for the pores. At the same time, the polymer concentration in the liquid phase is increased, which facilitates crosslinking of the polymer rich phase. After thawing, a sample spanning network is obtained, with pores remaining at all locations, where ice crystals had been present [174]. Besides the tuneable pore size and mechanical properties, it is considered beneficial that stable porous scaffolds can be obtained at relatively low polymer concentrations and that the molding process allows fabrication of scaffolds of nearly any desired shape. Due to the interconnected pore architecture, cryogels possess a characteristic high swelling capacity, i.e. when immersed in water, they swell instantly and take up large amounts of water. Cells can be seeded to such cryogels by taking advan-

tage of the swelling behavior, i.e. a dry scaffold is impinged with a cell suspension, so that the nutrient media together with the cells is sucked directly into the depth of the scaffold.

1.2.3 Cell-Matrix Interactions

After cells are seeded into scaffolds, they interact with their local surrounding, depending on the initial matrix properties. Mostly all cellular processes, namely motility, adhesion, spreading, proliferation, differentiation and metabolism of cells, depend on matrix mechanical properties [57, 58, 86, 96, 135, 149, 206, 234]. Besides that, cells themselves affect ECM mechanical properties during remodeling, which is in turn depending on initial structural and mechanical scaffold properties [60, 133, 209, 220]. In an iterative process, those altered properties of the remodeled matrix feedback to cell growth.

Maintaining the homeostasis of ECM properties is one key responsibility of fibroblast cells. Therefore, they actively synthesize and secrete ECM components, such as collagen, proteoglycans, fibronectin and others. Additionally, cells increase ECM network density by contraction during remodeling [76]. Furthermore, they produce matrix metalloproteinases (MMP) which degrade the peptide-bonds in the ECM, as well as the corresponding inhibitors, called tissue inhibitors of metalloproteinase (TIMP). The combination of both, together with the matrix secretion regulates ECM composition and its mechanical properties. The underlying metabolism is further regulated by the complex interplay of cell-cell and cell-matrix interactions [156].

At the molecular level, interactions of cells with the ECM are mediated by various adhesion receptors, among which integrins and transmembrane proteoglycans take a principal role. Cells probe the elasticity of their surrounding in the range of up to five times their length (reviewed in [60]) by actively pulling fibers they are adhered to. Whether the displacement of fibers or the corresponding force of the material is sensed, is subject of current discussion [206]. According to the fiber pulling theory, the local mechanical properties of pore walls in water filled macroporous scaffolds are more relevant than bulk elasticity. But pore wall/ material thickness should be taken into account, as the force a cell has to apply for buckling of a strut depends on the geometry and elasticity of this object [60].

The ideal healthy mechanical conditions are not only continuously adjusted, but also tissue specific. For instance, tissues such as brain or adipose tissue are softer, compared to bone or cartilage - consequently their ECM is softer, too. The elasticity of ECM substitutes was even shown to determine stem cell fate: For *in vitro* mesenchymal stem cell cultures, soft polyacrylamide (PA) matrices that mimic mechanical properties of the brain ($E \sim E_{\text{brain}} = 0.1\text{-}1 \text{ kPa}$) were shown to induce neurogenesis—i.e. active production of new neurons and other brain cells—while rigid matrices that mimic bone rigidity ($E \sim 25\text{-}40 \text{ kPa}$) induced osteogenesis. Intermediate elasticity ($E \sim E_{\text{muscle}} = 8\text{-}17 \text{ kPa}$) was proven to induce myogenic differentiation [58, 59].

Besides matrix stiffness, the surface topography of the microenvironment around the cells matters; it has been established that the nano-topography of the substrate has a remarkable influence on cell behavior. In the case of stem cells, nano-topography can contribute in undifferentiated cell proliferation or in directing differentiation into

a specific cell lineage (reviewed in[196]).

1.3 Mechanical properties of ECM and substitutes

Studies dedicated to characterize ECM mechanical properties or to investigate their impact on cell behavior, deal either with the properties of natural ECM itself or, in most cases with ECM substitutes, such as gels, coatings and scaffolds onto which cells are seeded. With regard to the available amount of sample and the delicacy of newly secreted ECM, only artificial scaffold substitutes can be characterized in bulk.

1.3.1 Bulk mechanical properties of ECM substitutes

Mechanical properties of hydrogels can be determined using bulk rheological shear measurements. In continuous shear, network structures can be ruptured. Thus, mainly oscillatory shear experiments were employed to reduce the impact on delicate network structures [3, 16, 18, 96, 214, 217, 234]. From such measurements in the linear viscoelastic deformation regime, storage modulus $G'_{\text{bulk}}(\omega)$ and loss modulus $G''_{\text{bulk}}(\omega)$ are obtained.

In order to determine the widely used Young's modulus E , uniaxial tension [53, 176, 198], and compression tests [19, 30, 35, 142, 178, 198] are performed. E is calculated from the slope in the initial linear regime of the stress strain diagram and characterizes bulk elasticity of an entire sample on a macroscopic scale. Different Young's moduli are connected to different tissue applications, from soft mucosa with $E \sim \text{kPa}$ to hard bone tissues with $E \sim \text{GPa}$.

Shear elasticity and Young's modulus can be linked by the Poisson's number ν . For incompressible, uniform, homogeneous, isotropic, crosslinked polymers, in theory $\nu \sim 0.5$ is obtained. However, it is obvious, that cell-laden, potentially porous scaffolds, in some cases even flooded with liquid media do not fulfill these assumptions.

Furthermore, these methods characterize such often macroporous materials with their given heterogeneity as a homogeneous material on a continuum mechanical level. This limits the explanatory power of such methods and cells' sensitivity for the local mechanical properties [60, 236] rises the need for mechanical characterization on shorter length-scales.

1.3.2 Local mechanical properties of ECM substitutes

One potential approach for the characterization of the local properties of ECM substitutes is using atomic force microscopy (AFM) and other indentation experiments [54, 110, 122, 157, 221, 236, 259, 268].

The underlying measurement principle is indenting a (nano-) tip with defined geometry and measuring the sample deformation resulting from the application of a defined force. Alternatively, the necessary force for reaching a defined deformation can be measured. However, AFM is limited to the surface of a sample. Here it is important to keep in mind, that cells do not necessarily sense the scaffold surface. An additional limitation is the softness of the bio-hydrogels. Nano-indentation techniques are usually

established for stiff materials with $E > 1$ GPa. The apparent elasticity measured for soft materials is often affected by measurement artefacts and thus depends on the used measurement method [157]. Furthermore, the surface tension of water/nutrient media is troublesome, due to the difficulty to identify the point of zero force in a water filled hydrogel.

To circumvent these major limitations, microrheology methods, in particular active microrheology methods, were employed for studying ECM substitutes. Single tracer particles of $\sim 1 \mu\text{m}$ diameter or particle collectives were placed in the cellular surrounding and their motion was actively triggered, while the resulting displacement was measured. For example optical tweezers were employed for studying the elasticity of ECM substitutes laden with breast cancer cells [223, 228] and laser tweezers were used for the characterization of ECM elasticity in sprouting angiogenesis [105].

A more gentle method to study local mechanical properties of delicate materials is passive microrheology based on monitoring the Brownian motion of the embedded tracer particles. One advanced microrheology technique is MPT, which allows for the characterization of the viscoelastic properties sensed by an entire particle collective ($n > 100$). Based on this, local distributions in viscoelasticity and local heterogeneity can be characterized [174, 199].

1.4 Multiple particle tracking microrheology

1.4.1 MPT Principle

The underlying principles and fluid mechanics of MPT microrheology have been described in detail [68, 252] and further background information is presented in chapters 2 and 5.

In brief, the Brownian motion of inert colloidal probe particles embedded in a material is monitored. Thereby, quantitative information about the rheological properties of the surrounding fluid is obtained [154] based on a fundamental relationship between tracer mean square displacement (MSD; $\langle r^2(\tau) \rangle$) as a function of lag time τ and the complex shear modulus $G^*(\omega)$ as a function of the frequency. The Laplace transform of the particle MSD is related to the complex modulus G^* of the sample via a generalized Stokes-Einstein equation (GSE, general form, see Eq 1) [153, 262]:

$$G^* = \frac{2k_B T}{3\pi a i \omega \langle \Delta r^2(i\omega) \rangle} \quad (1.1)$$

a stands for the radius of the embedded beads, k_B for the Boltzmann constant and T for the temperature. $\Delta r^2(i\omega)$ is the mean square displacement as function of frequency. This GSE relation is valid in 2D under the assumption that the material surrounding the tracer particles can be treated as an isotropic and homogeneous continuum, i.e. that the particle size is larger than the structural length scales of the probed material. Furthermore, tracer particle and fluid inertia need to be neglectable, which is appropriate here, since Reynolds number and Stokes number both are well below 1. For 2D

tracking of beads suspended in an ideal elastic material, Eq 1 reduces to Eq 2 [98, 262]

$$G_{0,MPT} = \frac{2k_B T}{3\pi a \langle \Delta r^2(\tau) \rangle} \quad (1.2)$$

where $G_{0,MPT}$ stands for the frequency independent shear modulus of the material and $\Delta r^2(\tau)$ for the mean square displacement as function of the lag time. As confirmed by the time independency of the MSDs, all materials investigated here, behave like elastic solids.

In the first step of MPT evaluation procedure, all particle trajectories are represented in a trajectory plot. Trajectories of freely diffusing particles cover a larger area compared to trajectories of elastically trapped particles, that are more restricted in their motion. Furthermore, areas in which no particles were present throughout the whole measurement can be identified. Then from these trajectories, the coordinates of the particle centroids were transformed into MSD traces.

Time independent MSDs correspond to elastically trapped particles, whereas for freely diffusing particles, a linear increase over lag time τ is expected. Complex polymer materials often yield ensembles of MSDs including tracers of both limiting cases, and often also curved MSDs representing diffusion in a viscoelastic environment. Thus, the variation of obtained MSDs in one measurement provides insight into the heterogeneity of the material within the field of view ($127 \times 127 \mu\text{m}$). In order to characterize the material heterogeneity often the Van Hove correlation function [241] is used and the non-Gaussian parameter α is calculated according to Eq. 3[256].

$$\alpha = \frac{\langle r^4(\tau) \rangle}{3\langle r^2(\tau) \rangle^2} - 1 \quad (1.3)$$

r stands for the displacement and the resulting parameter α describes the derivation of the MSD values from a Gaussian distribution expected for an ideal homogeneous uniform sample ($\alpha = 0$) at a fixed lag time τ . Real fluids with $\alpha \leq 1$ are considered homogeneous on the probed length scale typically ranging from 0.1 to 1 μm .

MPT was initially used for characterization of intracellular elasticity [238], but heterogeneity in the cellular lumen, filled with cytoskeleton, vesicles, organelles and more, and additionally cell-cell variation were large. Thus, low statistical reliability resulted and it was further decreased by the low number of particles that was successfully phagocytosed. Thus, no moduli could be derived from these measurements [238]. Furthermore, the pericellular matrix layer, covering some micrometers on the cellular surface was characterized [242]. To our knowledge, MPT was never used for studying natural ECM.

1.4.2 MPT for characterizing ECM substitutes

A broad range of ECM substitutes and biohydrogels was characterized with MPT, including the local elasticity of synthetic ECM in tumors [102]. In another study, cells were encapsulated in a biogel doped with particles for MPT measurements [103]. A series of MPT measurements allowed for the semi-continuous monitoring of the elasticity of PEG-based ECM substitutes during several days of cell culture and revealed a

decrease in matrix elasticity in the direct surrounding of encapsulated MSCs [45, 208]. The decreasing matrix elasticity was found to be caused mainly by the secretion of matrix metalloproteinases (MMPs) by the cells. Although these approaches delivered a spatially resolved elasticity profile for semi-continuous measurements, they possess severe limitations in terms of the cell surrounding: Cells need to be encapsulated in highly homogeneous PEG-based gels and the number of analyzed particles is still limited.

1.4.3 Characterization of newly secreted ECM

For characterizing the newly secreted ECM in scaffold free cell cultures, AFM was employed, despite the above mentioned limitations (see section 1.3.2). Gambini et al.[67] used a passive single particle tracking method for studying the mechanical properties of the ECM of jellyfish which were microscopied as a whole and Nijenhuis et al. [168] studied the elasticity of the pericellular matrix of chondrocytes by a combined approach of positioning the tracer particle with an optical trap and studying their Brownian motion for rheological measurements.

Li et al. [137] used magnetic twisting beads that were conjugated to the collagen fibers of the adventitial layer of porcine aortas for studying ECM local elasticity. To our knowledge, a sound mechanical characterization of the cellular surrounding in mammalian cell culture had never been achieved. But we consider this indispensable to ultimately understand and control cellular processes depending on mechanical cues. Further challenges arise from the fact that mechanical properties of synthetic and natural ECM, such as stiffness and elasticity, cannot be expressed as one single value but underlie the continual impact of the cells.

1.5 Motivation and organization of manuscripts

For understanding cell-matrix interactions, a local characterization on the length scale sensed by cells is crucial and as cells embedded in ECM or 3D scaffolds sense local mechanical properties in the depth of the material, a surface characterization is not sufficient.

We aimed at providing suitable, non-cytotoxic scaffolds to the cells and tailor their bulk and local mechanical properties to fulfill tissue specific requirements. Controlling the mechanical properties of cryogels requires a sound understanding of the polymer distribution and structure in the underlying precursor solutions. HA solutions were well characterized before (see [172] and references within), but little was known about microstructure and local properties of Coll. Hence, we performed a comprehensive microrheology study of acidic solutions of lyophilized collagen I.

Using these precursor solutions and combining them with chitosan or HA, we aimed at producing cost effective cryogels, that closely mimic the composition of natural ECM. By employing EGDE, a conventional crosslinker for this, we hoped to obtain stable scaffolds with desired mechanical properties and high shape fidelity.

However, especially in cell-free applications, including wound-covering and drug delivery, protein-free scaffolds with good biocompatibility are required. For such ap-

plications, we tried to reduce the cytotoxicity of HA based cryogels by using a novel crosslinker, namely genipin. Genipin is plant based and due to its usage in traditional Chinese medicine, known to be non-toxic. It had been utilized to crosslink biopolymers, such as chitosan [158] and gelatin [25] or hybrid systems like chitosan/HA [164] but it has never been used to form pure HA gels before.

We employed multiple particle tracking microrheology and conventional bulk mechanical tests to characterize structure and mechanical properties of the resulting one component cryogels, as well as a broad range of HA/Coll hybrid scaffolds crosslinked with conventional crosslinker EGDE. Furthermore, we wanted to ensure the cell-culture suitability and hence performed long-term cell viability tests and studied the degradation of the scaffolds *in vitro*.

Our scaffolds served as appropriate platform for studying cellular effects on mechanical properties of the ECM. As currently, little is known about the impact of matrix remodelling on the mechanical properties of ECM and its substitutes, we aimed at gaining deeper insight into temporal changes of the local elasticity in direct cell surrounding. Developing a method for continuous characterization of local elasticity in the direct surrounding of living cells in-situ was our main goal. With this, we intended to study matrix degradation by fibroblasts, which are known to remodel their ECM intensively.

Furthermore, hMSCs, most important progenitor cells, that help to regenerate in wound healing and ensure function and replacement of many different kinds of tissues in our body, are expected to cause massive changes in matrix elasticity. Thinking of their differentiation into adipocytes and osteocytes, i.e. fat tissue and bone with obviously totally different bulk mechanical properties, it is quite surprising that the matrix elasticity during this differentiation was never investigated before. We aimed at gaining deeper insight into the mechanical cues resulting from ECM remodelling during differentiation in 3D cultures and making this measurable.

This thesis covers the fabrication of collagen/ HA based cryogels, their structural and mechanical characterization and finally their application as cell culture scaffolds for studying the effects of cell proliferation and differentiation on the local mechanical properties of artificial scaffolds and natural ECM.

Following the processing route for fabricating biobased cryogels, we first characterized the microstructural and rheological properties of Coll precursor solutions (1) and further elucidated the fabrication of biocompatible cryogels based on HA, Chitosan, Coll and mixtures thereof (2). For reducing cytotoxicity, we used genipin as crosslinking agent with reduced toxicity to form pure HA gels (3). Cryogels based on collagen, HA and mixtures thereof were characterized in terms of structure, mechanics and cell culture suitability (4) and finally, we developed a set of advanced MPT methods for studying local ECM elasticity in complex systems. Using three model cell types, we tested our approaches to perform continuous MPT measurements during fibroblast proliferation, studied the effect of hMSC differentiation on local elasticity in 3D scaffolds, and characterized mechanical properties of newly secreted ECM in scaffold-free 2D cultures of endothelial cells (5).

This thesis consists of the following 5 chapters, based on five manuscripts. Each manuscript is presented in a separate chapter with detailed bibliographic information. A full list of publications is included in my academic CV in the appendix.

1. J. Hafner, C. Oelschlaeger, N. Willenbacher: Microrheology imaging of fiber suspensions - case study for lyophilized collagen in HCl, (2020), *soft Matter*
2. J. Roether, A. Ryl, C. Oelschlaeger, N. Willenbacher: Mechanical Properties and Suitability for Cell Culture of Hyaluronic Acid, Chitosan, and Collagen Based Scaffolds Obtained from Cryogelation (2017), Conference proceedings of BioMAAP 2017 Conference, London, held by ASRANet Ltd.
3. J. Roether, C. Oelschlaeger, N. Willenbacher: Hyaluronic acid cryogels with non-cytotoxic crosslinker genipin (2019), *Materials Letters X*
4. J. Roether, S. Bertels, C. Oelschlaeger, M. Bastmeyer, N. Willenbacher: Microstructure, local viscoelasticity and cell culture suitability of 3D hybrid HA/collagen scaffolds (2018), *PLoS ONE*
5. J. Hafner, D. Grijalva, A. Ludwig-Husemann, S. Bertels, L. Bensinger, A. Raic, J. Gebauer, C. Oelschlaeger, M. Bastmeyer, K. Bieback, C. Lee-The dieck, N. Willenbacher: Monitoring matrix remodelling in the cellular microenvironment using microrheology for complex cellular systems (2020), *Acta Biomaterialia*

Chapter 2

Characterization of Coll precursor solutions

- Full title: Microrheology imaging of fiber suspensions - a case study for lyophilized collagen in HCl solutions
- Authors: J. Hafner, C. Oelschlaeger, N. Willenbacher
- Bibliographic information: Soft Matter (2020)
- <https://doi.org/10.1039/D0SM01096K>

Abstract

In fiber suspensions with low optical contrast, the *in situ* characterization of structural properties with conventional microscopy methods fails. However, overlaying subsequent images of multiple particle tracking (MPT) videos including short trajectories usually discarded in MPT analysis allowed for direct visualization of individual fibers and the network structure of lyophilized collagen I (Coll) distributed in hydrochloric acid solutions. MPT yielded a broad distribution of mean square displacements (MSDs). Freely diffusing tracer particles yielded viscosities indicating that, irrespective of concentration, a constant amount of Coll is dissolved in the aqueous phase. Particles found elastically trapped within fibrous Coll structures exhibited a broad range of time-independent MSDs and we propose a structure comprising multiple fiber bundles with dense regions inaccessible to tracers and elastic regions of different stiffness in between. Bulky aggregates inaccessible to the 0.2 μm tracers exist even at low Coll concentrations, a network of slender fibers evolves above the sol–gel transition and these fibers densify with increasing Coll concentration. This novel MPT-based imaging technique possesses great potential to characterize the fiber distribution in and structural properties of a broad range of biological and technical suspensions showing low contrast when imaged with conventional techniques. Thus, MPT imaging and microrheology will help to better understand the effect of fiber distribution and network structure on the viscoelastic properties of complex suspensions.

2.1 Introduction

Fiber suspensions play an important role in processing of polymer composites, pulp and paper production and the food industry. The characteristic flow properties of fiber suspensions strongly depend on their microstructure, which is determined by the properties of dispersed fibers, i.e. their length distribution and aspect ratio, as well as hydrodynamic, thermodynamic or steric interactions among them. The bulk rheological behavior of model fiber suspensions with short, stiff fibers, such as glass, has been intensively studied theoretically [14, 51, 184] and experimentally [20, 183, 192, 213]. Experiments focusing on hydrodynamic interaction in dilute and semi-dilute regime yielded good agreement with available theories. For the rather short fibers, fiber orientation in shear was observed which determined the characteristic rheological behavior of the suspensions, i.e. shear thinning. In the concentrated regime, non-hydrodynamic particle interactions become increasingly relevant and cause a growing discrepancy between experimental results and purely hydrodynamic theories. Numerical simulations of concentrated fiber suspensions show the stress transfer through fiber contacts can increase the viscosity of the suspension [183, 226, 264]. This mechanical interplay depends on the fiber orientation and on fiber intrinsic properties, such as fiber elasticity, size and aspect ratio [112, 253]. However, numerical simulations for studying the influence of fiber elasticity on the rheological properties of the suspension deliver contradictory results, depending on the underlying geometrical model [104, 191, 227]. A sound characterization of fiber elasticity in-situ, would help to answer such questions. Especially for elastic fibers with mechanical properties that are altered during drying or precipitation, in-situ characterization of fiber elasticity is fundamental.

Most importantly, the flow behavior of fiber suspensions and the mechanical properties of products made thereof are determined by the size distribution and orientation of fibers in the continuous phase. Fiber localization, orientation and network structure can be studied using visualization and imaging techniques [47, 90, 112, 132, 148]. In case of glass fiber model systems, due to the difference in refractive index of the dispersed fibers and the continuous phase, visualization of suspension microstructure can be realized easily using light microscopy [148]. For combinations of dispersed and continuous phases with similar refractive index but different optical activity, e.g. cellulose and polymer fibers in organic solvents and polymer melts, the use of a polarization microscope is required [132]. Alternatively, optical contrast can be created by addition of specific dyes or in suspensions with colored fibers. However, such staining protocols might alter fiber interactions and can cause flocculation. Non-transparent suspensions cannot be investigated using light microscopy at all. NMR can help to visualize suspensions with chemically different components based on proton density, but the spatial resolution is limited [46]. Electron microscopy and X-ray tomography are other widely used imaging techniques, but they require a high electron density and sufficient contrast [128, 200, 205, 261]. Furthermore, radiation damage is especially likely for biological samples and electron microscopy is not suitable for liquid products [87, 200]. Thus, additional processing steps, such as drying or freezing, are needed prior to the investigation of aqueous suspensions. This can result in altered fiber network properties or, in the worst case, network collapse [2, 117].

Therefore, new gentle visualization methods with enhanced contrast are required to

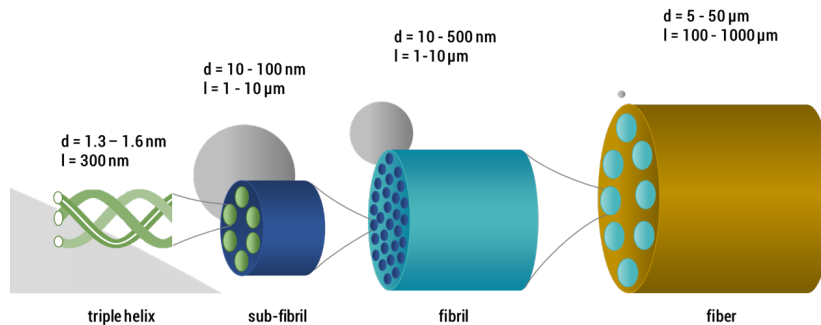


Figure 2.1: Hierarchical structure of collagen I as found in vivo (length not to scale): From left to right, single collagen I triple helices, sub-fibrils, fibrils and fibers are shown and the respective feature diameters are given. For size relation, a 100 nm particle is sketched in grey in respective scales.

study fiber microstructure in situ, especially for suspensions of sensitive fibers, such as DNA, proteins and other biomaterials. One prominent example of these delicate fibers is collagen I, which is a key structural protein in vertebrates. Due to its excellent biocompatibility and biodegradability [266] collagen I has diverse biomedical applications, recently as a promising bioink for 3D printing [150] and it is also a common constituent of many cosmetic and food products, partly in the processed form of gelatin. The complex hierarchical structure of collagen I includes several levels of structure (see Fig. 2.1). It is indisputable that the primary structure is the amino acid sequence, and the secondary and tertiary structure, referred to as α -chain, collagen I molecule or in some cases tropo-collagen, is a rod-like triple helix. An individual triple helix in type I collagen is $< 2 \text{ nm}$ in diameter and $\sim 300 \text{ nm}$ long [24, 63, 70, 84, 99, 108, 230]. The quaternary structures are supra-molecular forms called collagen fibrils and collagen fibers, which are formed by self-assembly in neutral pH and appropriate salt concentration [84] of several collagen I molecules. Native collagen fibers are up to several millimeters in length and $\sim 10 \mu\text{m}$ in diameter [24, 63, 70, 108]. A good overview about size estimate on the different levels is provided by Varma et al. [244].

An accurate characterization of microstructural properties of collagen fiber suspensions and/or collagen networks and a better understanding of the role of fiber architecture in cellular behavior and mechanical properties are of significant importance. Many studies have characterized the macromechanical properties of collagen I solutions through rotational rheometry [4, 73, 125, 167]. However, for such a complex protein, interpretation of bulk rheological features in terms of structural properties is essentially impossible. Consequently, atomic force microscopy (AFM) [34, 259] was employed. A drawback using AFM is that the sample needs to be dried prior to the measurements, which can lead to an increase of the stiffness of the collagen I structures [109]. Moreover, structures may be trapped in non-equilibrium conformations when deposited on substrate surfaces. To overcome this limitation, microrheological measurements were performed using optical-tweezers to determine viscoelastic and structural properties of collagen I solutions locally [131, 181, 215, 245]. A major drawback of this method for studying heterogeneities is the local measurement of the behavior of a small number of tracers that not always represents larger areas of the sample and limits statistical

reliability. On the other hand, the comparably large tracer particle size (about 2 μm used in these studies constraint the spatial resolution. However, results indicate a high degree of heterogeneity in the elasticity of the non-covalent network formed by entangled collagen I fibrils. Elasticity varies by more than one order of magnitude at different locations within the sample. Similar microheterogeneities were observed in other systems like actin filament solutions and networks [6, 237], human or animal mucus [12, 29, 77, 126, 163], cellular actin skeleton [41, 79, 238], but also for xanthan [180] or gellan gum solutions [26]. In these latter studies the presence of such heterogeneities served as an explanation for discrepancies observed between viscoelastic properties determined by bulk- and microrheology. To the best of our knowledge, for lyophilized collagen I (Coll), which has achieved great technical relevance in cosmetics and pharmaceutical formulations, in HCl, no detailed comparison between data from micro- and macro-rheology measurements has been performed so far. It is only for chemically crosslinked Coll networks, that such a comparison exists [199]. In that latter study, local elastic moduli of Coll cryogels determined from MPT measurements were much lower than the corresponding bulk shear moduli. Analogous to earlier investigations on intermediate filament networks [182], this was attributed to a pronounced contribution of stretched out of equilibrium chain segments between network junctions or to densely crosslinked areas not accessible for the tracer particles, thus not contributing to the MPT modulus, but showing up in the bulk modulus. Here, we use classical bulk mechanical rheometry and for the first time MPT microrheology to get new insight into structural and local viscoelastic properties of acidic lyophilized Coll suspensions in a large concentration range from 0.05 to 1 wt%. Previously, particle-tracking has been successfully used to study heterogeneous structures of fibrous porous media [27, 219] as well as complex heterogeneous biogels [45]. In our MPT experiments, we use tracer particles of particularly small diameter, down to 0.2 μm , allowing for characterization of rheological properties and for the first time for visualization of structural properties directly inside Coll structures. Furthermore, we use the image overlay technique to obtain a direct visualization of Coll fibers and the fiber network structure and its change with concentration of suspended Coll. Additionally, we monitor the self-assembly of Coll after filtration using MPT and bulk rheological measurements. Finally, we compare the microstructure of the Coll/HCl mixtures based on lyophilized powder with that of ready-to use native collagen I solutions at the same concentration.

2.2 Experimental

2.2.1 Preparation of lyophilized Coll in HCl

For preparation of Coll suspensions, 0.05 to 1wt% bovine collagen I (lyophilized fibrous powder from tendon, Advanced BioMatrix, USA) was dissolved in 5 mM hydrochloric acid (Carl Roth, Germany). During the freeze drying process, inter-molecular hydrogen bonds are formed [64, 65, 169], which stabilize Coll aggregates, so that intensive stirring is required for reconstitution. Thus, proper reconstitution required stirring with magnetic stirrer for 18h at 20°C, which finally led to highly viscous transparent liquids, that were characterized immediately. The preparation and characterization

of solutions was repeated 5 times per condition to ensure appropriate reproducibility. In order to elucidate the impact of altered chemical properties after the freeze-drying and re-wetting procedure during fabrication, samples based on lyophilized Coll were compared to a commercially available solution of native collagen I from similar origin. This was purchased from Advanced Biomatrix (FibriCol, Bovine collagen I solution, 10 mg/ml, Advanced BioMatrix, USA) and diluted to the respective concentrations with 5mM hydrochloric acid, pH \sim 2.3. This dilution experiment was done in triplicate for three separate investigations. Coomassie Brilliant Blue R250 (CBB, Merck, Germany), which exclusively stains proteins, was added for visualization of Coll using light microscopy. Additionally, in order to investigate the Coll self-assembly, all Coll fragments larger than 1.2 μm were removed by filtration. For this, we used cellulose acetate syringe filters (Puradisc FP 30, Whatman, GE Lifesciences, GB) with pore size 1.2 μm . Bulk shear and MPT measurements were performed prior to filtration, directly after filtration, after 7.5 h and after 24 h to monitor the Coll self-assembly via the change in viscoelastic properties of the sample. This set of experiments was done in triplicate. Protein concentration was determined from BCA assay (PierceTM BCA Protein Assay Kit, Thermo Fisher), by performing the assay in 96-well plates according to supplier's manual. Extinction measurements were performed with an Infinite 200 (Tecan, Switzerland) plate reader.

2.2.2 Multiple particle tracking microrheology

The underlying idea of MPT is to study mechanical properties of materials by monitoring the Brownian motion of inert colloidal probe particles embedded in the samples. Mason and Weitz proposed a quantitative relation between the tracer mean square displacement (MSD) $\langle \Delta r^2(\tau) \rangle$ as a function of lag time τ and the complex shear modulus of the surrounding material G^* as a function of the frequency ω [152]. The Laplace transform of the particle MSD $\langle \Delta \tilde{r}^2(i\omega) \rangle$ is related to the complex modulus G^* of the sample via a generalized Stokes–Einstein equation (GSE) [68, 252]:

$$G^*(\omega) = \frac{2k_B T}{3\pi R i \omega \langle \Delta \tilde{r}^2(i\omega) \rangle} = G'(\omega) + iG''(\omega) \quad (2.1)$$

R stands for the radius of the embedded beads, k_B for the Boltzmann constant and T is the temperature. This relation is valid in two dimensions under the following assumptions: tracer particles are suspended in an ideal elastic, isotropic and homogeneous continuum; probe particle and fluid inertia can be neglected; i.e. Reynolds number and Stokes number are both $\ll 1$. Thus, MPT allows for characterizing structural and mechanical properties of complex materials on a micrometer length scale [68, 240]. For beads suspended in an ideal elastic material with modulus G_0 , equation 2.1 reduces to [262]:

$$G_{0,MPT} = \frac{2k_B T}{3\pi R \langle \Delta r^2 \rangle_{\tau \rightarrow \infty}} \quad (2.2)$$

For ideal viscous fluids, the viscosity η is determined from the diffusivity coefficient D [152]:

$$\eta = \frac{k_B T}{6\pi R D} \text{ with } D = \frac{\langle \Delta \tilde{r}^2(\tau) \rangle}{4\tau} \quad (2.3)$$

A detailed scheme of the MPT setup used in this study is described in Kowalczyk et al. [120]. It is based on an inverted fluorescence microscope (Axio Observer D1, Carl Zeiss, Germany) equipped with a Fluar 100x objective (numerical aperture 1.3, 100x magnification, oil immersion lens, Carl Zeiss). We tracked the Brownian motion of green fluorescent, non-functionalized, surfactant stabilized polystyrene microspheres of 0.2 and 0.5 μm diameter (Bangs Laboratories, USA). To evaluate collagen adsorption on the surface of the tracer particle or other specific interactions among particles and dissolved polymer, we also performed MPT measurements using polystyrene particles functionalized with polyethylene glycol (donated by Xabier Murgia, Department of drug delivery, Helmholtz Institute for Pharmaceutical Research Saarland). No significant difference in particle diffusion in the two tests could be found suggesting that collagen adsorption on the particle surface is negligible here.

Two-dimensional images (field of view 127 x 127 μm , frame rate 50 frames/sec, total duration 10 s with at least 150 fluorescent beads per image) were recorded using a sCMOS camera Zyla X (Andor Technology, Ireland, with 21.8 mm diagonal sensor size, 2160 x 2160 square pixels). The obtained movies of the fluctuating microspheres were analyzed using the software Image Processing System (iPS, Visiometrics, Germany) and a self-written Matlab code, based on the widely used Crocker and Grier tracking algorithm [39]. We examined the distribution of displacements, known as the van Hove correlation function [241] and calculated the non-Gaussian parameter α [256]:

$$\alpha = \frac{\langle r^4(\tau) \rangle}{3\langle r^2(\tau) \rangle^2} - 1 \quad (2.4)$$

This parameter describes the deviation of the MSD values from a Gaussian distribution expected for a homogeneous, uniform sample and characterizes the heterogeneity of the sample on a 0.1-10 μm length scale. In our study, α was determined at lag time $\tau = 0.1$ s.

In order to perform MPT measurements, tracer particles were added to the samples prior to stirring with a magnetic stirrer for 10 min to ensure homogeneous distribution of the tracers. Liquid samples were injected into a self-built glass chamber, consisting of a cover slip and microscope glass slide with height ~ 150 μm . We have also determined the so-called static error χ as described by Savin et al. [204] for our experimental setup. This quantity corresponds to the apparent random motion of particles due to the noise of the camera and digitization effects. It has been evaluated by fixing tracer particles on a substrate, and by performing measurements under similar noise and signal conditions as for the rest of the experiments. The static error for the experimental setup and tracer particles used here was $\chi = 8 \times 10^{-5}$ μm^2 and defines the lower limit of accessible MSD.

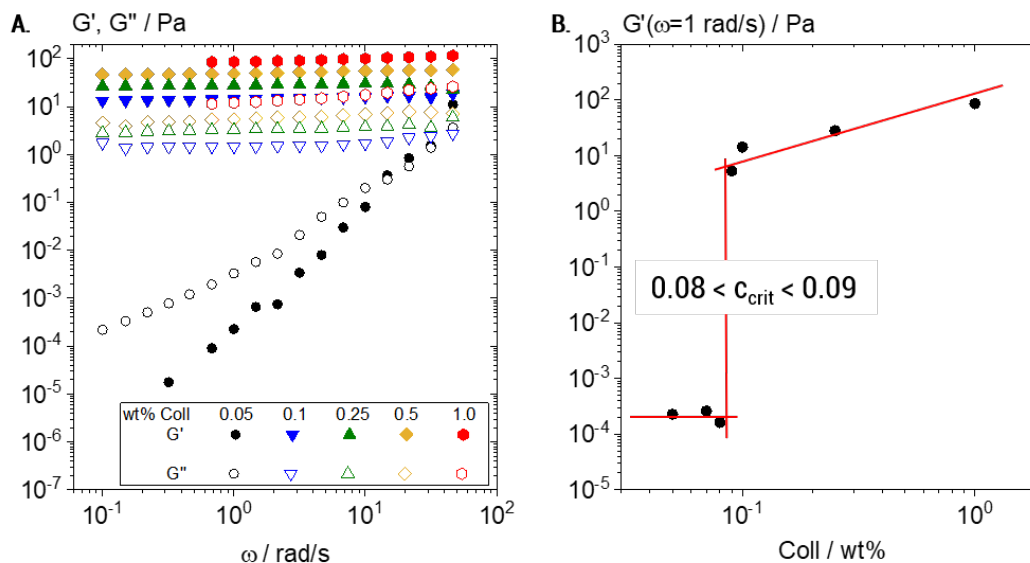


Figure 2.2: Bulk rheometry of Coll solutions: A) variation of dynamic shear moduli G' and G'' as a function of frequency obtained from oscillatory shear measurements for a series of Coll concentrations ranging from 0.05 to 1 wt% and B) determination of the sol/gel transition concentration c_{crit} from $G'(\omega=1 \text{ rad/s})$ as a function of Coll concentration.

2.2.3 Bulk rheological characterization in oscillatory shear

Oscillatory shear measurements were performed using a rotational rheometer (Physica MCR501, Anton Paar) with a plate-plate geometry (diameter 60 mm, gap 0.4 mm). Frequency sweeps, covering the frequency range from 0.01 to 10 rad/s, were performed at a stress amplitude of $\sigma_0 = 0.5$ Pa which corresponds to the linear viscoelastic response regime for the gel samples discussed in section 2.3.1. For the Coll solution in the sol-state as well as for the presumably heterogeneous filtrated samples discussed in section 2.3.4 a linear viscoelastic response regime was not clearly visible, so we decided to perform all frequency sweeps at the same stress amplitude of 0.5 Pa.

2.3 Results and Discussion

2.3.1 Sol- gel transition of lyophilized Coll suspensions from bulk rheometry

Under bulk oscillatory shear (Fig. 2.2A), 0.05wt% Coll suspensions appeared mainly viscous and only weak elasticity was observed. The obtained frequency sweep (black curve) shows $G' < G''$ with slopes of 2 and 1 for G' and G'' , respectively, in the log-log representation. This behavior is typical for predominantly viscous liquids and here the viscosity was found to be close to that of water ($\eta \sim 3$ mPa.s). In contrast, all Coll suspensions with concentrations of 0.1wt% and above, show a significant degree

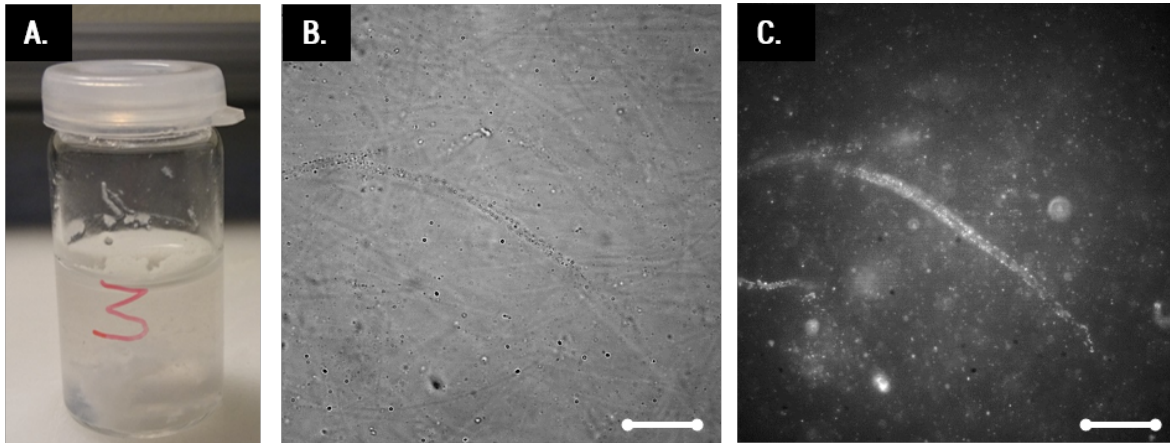


Figure 2.3: A) transparent 0.25 wt% Coll suspension, B) corresponding white light image of Coll stained with CBB, C) corresponding image of the same spot including fluorescent tracer particles of diameter $0.2 \mu\text{m}$. Scale bar represents $20 \mu\text{m}$.

of elasticity with $G' > G''$ and constant moduli in the measured frequency range. This is considered the typical behavior of elastic, gel-like samples. The plateau value of G' , termed G_0 , increases in this elastic regime from $G_0 = 13 \pm 1$ to $G_0 = 103 \pm 2$ Pa when the Coll concentration increases from 0.1 to 1 wt%, respectively. In order to determine the sol/gel transition concentration c_{crit} more accurately, a detailed concentration series has been characterized (Fig. 2.2B). The sudden increase of several decades in G' at a critical Coll concentration $0.08 < c_{\text{crit}} < 0.09$ wt% clearly indicates that in this concentration range, Coll structures start to entangle and interact with each other. The observed elasticity is not due to chemical crosslinking, but due to steric hindrance and colloidal interactions (van der Waals, electrostatic) among supramolecular Coll structures that lead to the formation of a sample spanning network.

2.3.2 Visualization of fibers using MPT tracer particles

Transparent Coll solutions (see Fig. 2.3A) offer low contrast and dispersed fibers were invisible in conventional light microscopy. Thus, CBB was employed as fluorescent staining agent for visualization of Coll structures. This dye is widely used to stain Coll and other protein suspensions, but corresponding images of Coll in HCl still possess only bare contrast. Fig. 2.3B shows the 0.25 wt.% Coll suspension, here fibers are visible and the formation of a network of fibers with a mesh size of about $50 \mu\text{m}$ covering the whole sample can be seen. The length of the fibers is several hundreds of μm and the diameter is about $5\text{-}10 \mu\text{m}$. For solutions with Collagen concentrations higher than 0.5 or lower than 0.1 wt% not even the above shown level of contrast can be achieved and information about changes in the fiber and/or network structure is not accessible. Visualization of these fiber networks is, however, enabled by adding fluorescent beads of $0.2 \mu\text{m}$ diameter (Fig. 2.3C) and tracking their Brownian motion. This will be discussed in the next section.

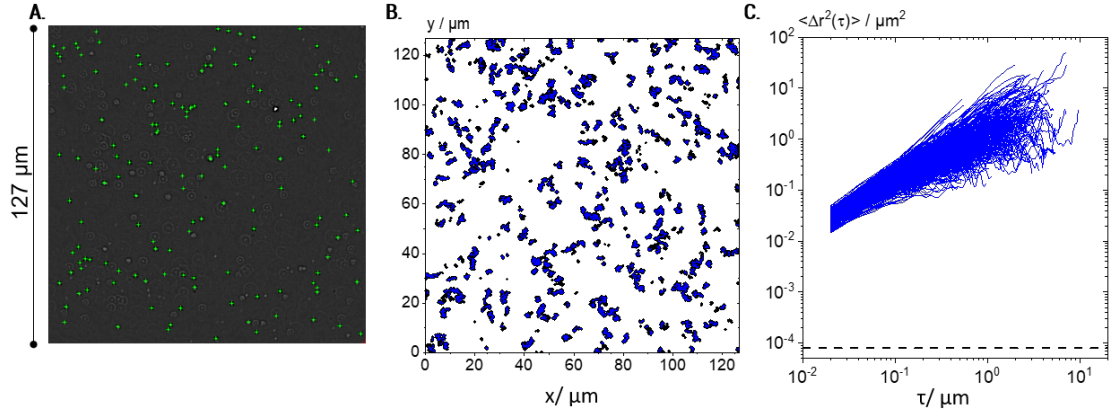


Figure 2.4: MPT results for a 0.25 wt% Coll suspension as probed with $0.5 \mu\text{m}$ particles: (A) exemplary localization of particle centres marked in green, measured at 488 nm fluorescence illumination, (B) all trajectories localized in the same field of view (trajectories shorter than 50 frames are shown in black, and those longer than 50 frames are shown in blue) and (C) the corresponding MSD plots for trajectories of minimum 50 frame-length. The minimum measurable MSD, that exceeds the static error [120, 204] $\chi=8 \times 10^{-5} \mu\text{m}^2$ is shown as dashed line. For each condition, 4 videos were recorded and analyzed per biological repetition and a representative set is shown here.

2.3.3 Local elasticity and microstructure of lyophilized Coll suspensions obtained using MPT

According to the results of bulk rheological measurements obtained in section 2.3.1, Coll suspensions at concentrations $> 0.1\text{wt}\%$ were in the gel state.

For a more detailed investigation of the underlying microstructure, MPT measurements were performed on 0.25 wt% Coll suspensions using tracer particles of diameter 0.5 and $0.2 \mu\text{m}$ (see Fig. 2.4 and Fig. 2.5, respectively). Fig. 2.4A indicates that $0.5 \mu\text{m}$ tracer particles are uniformly distributed all over the sample and Fig. 2.4B shows that trajectories are widely spread and the individual particles explore areas much larger than their diameter. In total, 1083 were detected, but only 343 trajectories longer than 50 frames, ensuring sufficient statistical significance, were used to calculate the MSD traces shown in Fig. 2.4C. These MSDs vary almost linearly with lag time τ , indicating that the motion of the tracer particles is purely diffusive, i.e., the microenvironment surrounding the particles responds like a viscous liquid. According to 2.3, the averaged MSD yields $\eta_{\text{MPT}} = 4.3 \pm 1.1 \text{ mPa}\cdot\text{s}$. Additionally, the value of the non-Gaussian parameter, calculated for the whole ensemble of MSDs is $\alpha = 0.11 \pm 0.04$, which indicates that all tracers explore a similar environment. These results clearly reveal that $0.5 \mu\text{m}$ tracer particles only probe the solvent and not the fiber network providing the elasticity seen in bulk measurements. Presumably, tracer particles are freely diffusing in the meshes of the sample spanning Coll network and accordingly the lower limit of network mesh size is well above $0.5 \mu\text{m}$. The viscosity of that liquid phase is about 4 times the viscosity of water indicating that Coll is partly dissolved in the aqueous

phase. Tracer particles with $0.2 \mu\text{m}$ diameter also exhibited a uniform distribution all over the sample (see Fig. 2.5A). A total number of ~ 450 trajectories, each composed of more than 50 frames corresponding to a lag time $\tau > 1\text{s}$, as typically used in conventional MPT analysis, are shown in Fig. 2.5B. Many particles probed areas that were much larger than their diameter, as similarly observed for the $0.5 \mu\text{m}$ particles (cf. Fig. 2.4B). However, including the shorter trajectories in the overlay of subsequent images of the video sequence showing all tracer particle trajectories (Fig. 2.5C) allows for a more detailed insight into the microstructure of the suspension. Here, the total number of trajectories is very large, around 50 000, since the small tracers in the low viscosity environment frequently enter and leave the focal plane. Surprisingly, the trajectories do not cover the whole sample, leading to the visualization of elongated white areas where no particles were present during the whole measurement. These white areas correspond to the Coll structures, which are densely packed and seem to be inaccessible to the diffusing tracer particles (see also Fig. 2.6).

MSDs obtained from the $0.2 \mu\text{m}$ particles based on the trajectories of >50 frames show results completely different from those obtained for the $0.5 \mu\text{m}$ particles (cf. Fig. 2.4C) and provide further insight into the Coll structure. A broad variation in absolute values and time-dependence of the individual MSDs was found for the $0.2 \mu\text{m}$ particles (Fig. 2.5D). The non-Gaussian parameter of all MSDs increased to $\alpha = 8.3 \pm 3.4$, indicating a high degree of heterogeneity in the environment probed by the tracers. The ensemble of MSDs splits up into three populations: population I includes all MSDs with slopes $m < 0.5$ and absolute values $< 10^{-3} \mu\text{m}^2$ (shown in green) close to the static error $\langle \Delta r^2 \rangle = 8 \times 10^{-5} \mu\text{m}^2$, determined for the setup and tracer particles used here. Population II consists of all MSDs with $m < 0.5$ and absolute values $> 10^{-3} \mu\text{m}^2$ (red curves) and all MSDs with $m > 0.5$ are summarized in population III (blue curves). The separation criteria were applied at $\tau = 0.1 \text{ s}$. Consequently, population I (green) corresponds to particles that are located within highly elastic regions where thermal motion is strongly restricted even at long lag times of about 10 s, and particles can be considered to be almost completely immobilized. This population comprises a broad variation of MSDs which extends over one decade from $\sim 10^{-4}$ to $\sim 10^{-3} \mu\text{m}^2$, corresponding to the static error limit, would be expected. Tracer particles corresponding to population II are located in regions of significantly lower elasticity whereas population III comprises freely diffusing tracers, located in predominantly viscous areas.

The black trajectories shown in Fig. 2.5C as well as in Fig. 2.6A correspond to short trajectories (<50 frames), which result from highly mobile particles in viscous environment, which enter and leave the focal plane of the microscope frequently. These short trajectories correspond to low viscosity regions of the sample, and although they are not used for further MSD data evaluation they are the key to visualization of the sample microstructure. Careful inspection of the localization of the trajectories corresponding to the different populations gives further insight into the heterogeneous organization of the Coll structure. For better visibility, colored trajectories were plotted with twice the size of the black ones.

Fig. 2.5A confirms that tracer particles of diameter $0.2 \mu\text{m}$ were uniformly distributed all over the sample. However, Fig. 2.5C and more clearly Fig 2.6A reveal that green trajectories corresponding to particles a highly elastic surrounding were located

Table 2.1: Non-Gaussian parameter α of all MSDs, derived from 4 independent measurements with $0.2 \mu\text{m}$ tracers, and fractions of Population I (green), II (red) and III (blue) at different Coll concentrations. Viscosity values η_{PopIII} of the continuous phase derived from the average MSD corresponding to population III.

Coll concentration	0.05 wt%	0.1wt%	0.25wt%	1wt%
α all MSDs	18 ± 2	31 ± 16	8 ± 3	2 ± 0
Population I (green)	75%	52%	38%	2%
Population II (red)	6%	26%	11%	3%
Population III (blue)	18%	22%	51 %	96%
η_{PopIII}	5.2 ± 2.8	3.6 ± 1.8	2.2 ± 0.9	4.8 ± 2.9

within the white areas representing the Coll structure, mainly in the center. Red trajectories corresponding to the particles exploring areas of lower elasticity, were located in the white regions, too. Blue trajectories, corresponding to freely viscous diffusing particles, were found on only in the easily accessible regions between the white areas.

For this population, a viscosity value of 2.2 ± 0.9 mPa.s was obtained, consistent with the results obtained for the $0.5 \mu\text{m}$ tracer particles. The relatively large experimental error obtained with $0.2 \mu\text{m}$ particles is due to a fast motion of the tracers leading to short length of the trajectories and to a broad variation of absolute MSD values (Fig. 2.5D, blue curves). Our data reveal that a substantial fraction of $0.2 \mu\text{m}$ tracer particles were able to penetrate into the Coll structures. In contrast, $0.5 \mu\text{m}$ particles cannot enter these fibrous structures. Thus, the mesh size of the Coll structures can be estimated to be less than $0.5 \mu\text{m}$. However, as there were regions inaccessible for $0.2 \mu\text{m}$ tracers, too, we propose a Coll structure comprising bundles of dense fibers embedded in elastic regions with a broad range of different stiffness as sketched in Fig. 2.6B). According to Eq. 2.2, time independent MSDs found for populations I and II correspond to elastic moduli $G_{0,\text{MPT}} = 58.3 \pm 7.2$ and 1.8 ± 0.2 Pa, respectively. These values are in the same range as the macroscopic elastic modulus obtained from bulk shear rheometry (Fig. 2.2). However, it has to be emphasized that this latter quantity is determined by the network of Coll structures, the steric hindrance and the colloidal interactions among fibers and thus the agreement between absolute $G_{0,\text{MPT}}$ and $G_{0,\text{bulk}}$ values is accidental. However, the MPT technique is a powerful and versatile tool to image the fiber network of gel-like Coll suspensions (Fig. 2.5C) and beyond that provides insight into the elastic properties of the Coll structures or fiber bundles with their heterogeneous organization.

2.3.4 Concentration dependence of local elasticity and network structure

In the following we will discuss the change in local viscoelasticity and network structure upon variation of Coll concentration based on MPT experiments performed using $0.2 \mu\text{m}$ tracer particles. Overlay images showing the complete trajectories of all tracers and the variation of corresponding MSDs as a function of lag time for Coll concentrations from 0.05 up to 1 wt% are shown in Figs. 2.7A and 2.7B, respectively.

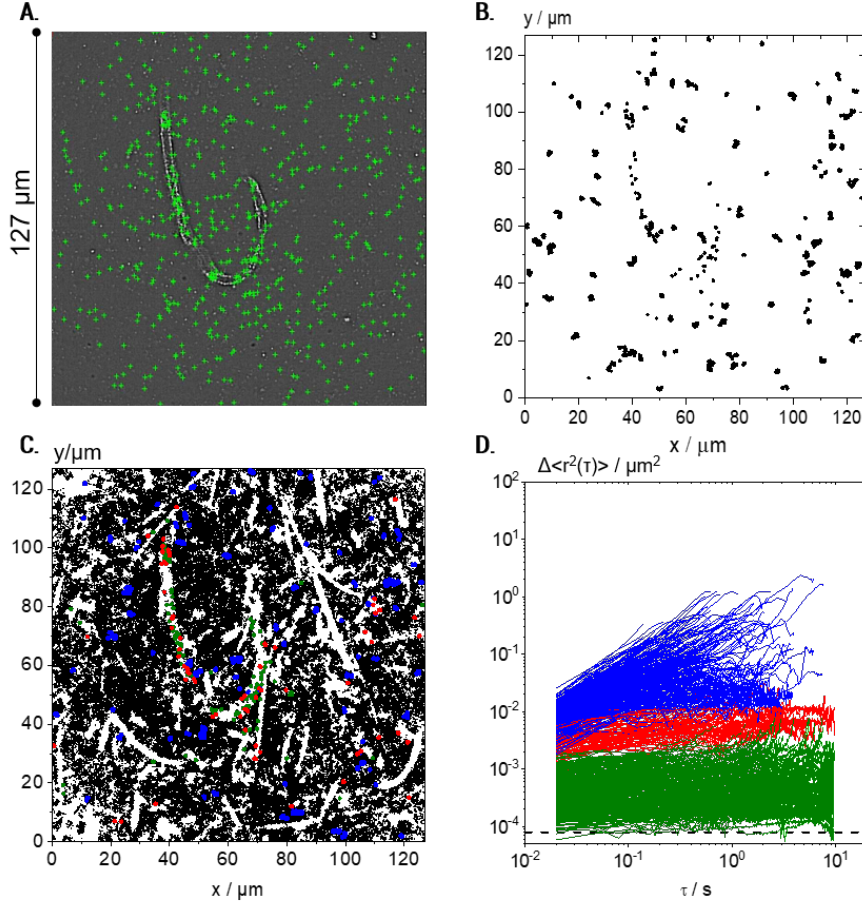


Figure 2.5: Visualization of microstructures in a 0.25 wt% Coll suspension using $0.2 \mu\text{m}$ particles: (A) exemplary localization of particle centers marked in green, and measured at 488 nm fluorescence illumination, and (B) all trajectories considered for MSD calculation (~ 450), i.e., short trajectories (< 50 frames) were eliminated. (C) All trajectories ($\sim 50\,000$) including short ones evaluated in the same field of view (the trajectories longer than 50 frames are marked in blue, red, and green according to the MSD classification described in D); for better visualization, red, blue and green trajectories are plotted at twice the size of the black ones. (D) Corresponding MSD plots for trajectories of minimum 50 frame-length. Green MSDs are MSDs with slopes < 0.5 and absolute values $< 10^{-3} \mu\text{m}^2$, red MSDs have slopes < 0.5 and absolute values $> 10^{-3} \mu\text{m}^2$, and blue curves correspond to MSDs with slope > 0.5 . The minimum measurable MSD, that exceeds the static error [120, 204] $\chi = 8 \times 10^{-5} \mu\text{m}^2$ is shown as dashed line. For each condition, 4 videos were recorded and analyzed per biological repetition and a representative set is shown here.

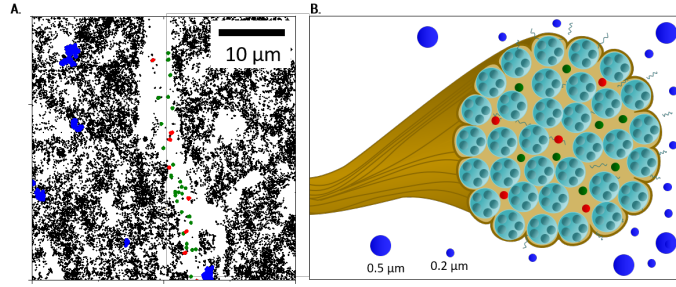


Figure 2.6: The fibrous Coll structure consisting of densely packed bundles: (A) close-up of Fig. 2.3B (lower area), to show localization of MPT particles in more detail, and (B) sketch of Coll dispersed in acidic solution, including the viscous surrounding, a bundle of fibrils (see Fig. 2.1) with areas accessible to $0.2 \mu\text{m}$ particles (shown in red and green, corresponding to particles trapped in elastic and highly elastic regions) and the dense, inaccessible core. In the viscous surrounding, 0.5 and $0.2 \mu\text{m}$ particles can be found.

At all investigated Coll concentrations, a broad variety in absolute values and time dependence of MSDs is found (Fig. 2.7B), and the calculated non-Gaussian parameter $\alpha \gg 1$, as summarized in Table 2.1. This latter value is maximal at the gelation concentration, as already reported for colloidal dispersions of spheres with weak attractive interactions [49] and clay suspensions [186] where a strong increase in heterogeneity was observed at the sol-gel transition. In all cases, three populations of tracer particles classified according to their slope in log-log representation of MSD vs τ as well as absolute MSD values are found. The separation criteria are the same as those defined in the previous section. The fraction of tracers in each population at different Coll concentrations is also summarized in Table 2.1. Besides that, many short trajectories (< 50 frames length) are observed (Fig. 2.7A) indicating a very low viscosity of the surrounding medium in accordance with the viscosity value of $5.2 \pm 2.8 \text{ mPa}\cdot\text{s}$ calculated from the MSDs of population III (see Table 2.1). At $0.05 \text{ wt}\%$ Coll concentration, large areas of the field of view are white, i.e. not accessible by the $0.2 \mu\text{m}$ tracer particles. Consistent with the measurements performed at higher concentrations, these large areas correspond to collagen fibers or aggregates loosely packed but obviously inaccessible for the tracers. The regions which are probed by the particles are heterogeneous even in this low viscosity sample well below the sol/gel transition. Three populations of tracer particles can be distinguished similar as for the gelled sample described above, i.e. some tracer particles explore a viscous matrix, others are trapped in a weakly elastic environment and a large fraction is found almost immobilized in highly elastic regions. Fiber like structures with a core-shell structure as outlined above exist even at Coll concentrations as low as $0.05 \text{ wt}\%$ well below the sol/gel transition. As mentioned before, these structures obviously cover large areas of the solution. Some individual fibers are visible due to the elastically trapped tracer particles lined-up along these structures. They do not, however, form a percolating network as indicated by the viscous response found in bulk rheometry. At $0.1 \text{ wt}\%$ Coll concentration, just

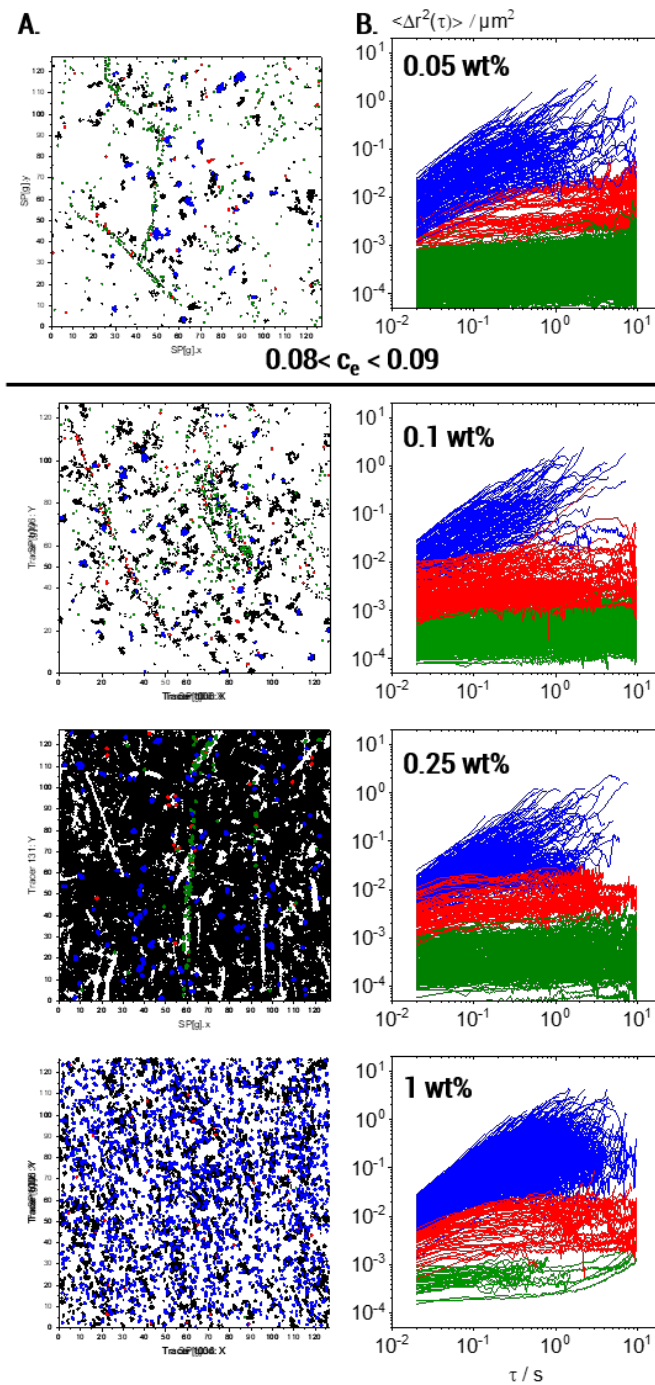


Figure 2.7: Effect of Coll concentration on MPT with $0.2 \mu m$ tracers: (A) all trajectories; (B) MSD plots corresponding to trajectories of min. 50 frames, showing three particle fractions: almost immobilized (green), elastically trapped (red) and freely diffusing (blue). For each concentration, 4 videos were recorded and analyzed per biological repetition and the results for one representative set are shown here.

above the sol/gel transition, the white areas shrink, i.e. the regions dilute enough to be accessible for the $0.2\ \mu\text{m}$ tracers increase in size. As the Coll concentration is doubled compared to the liquid sample discussed above, this indicates that the phase separation between dense Coll structures and the viscous matrix is more pronounced, the white areas must correspond to denser Coll structures than in the more dilute solution. In the overlay image of the 0.25 wt% Coll solution, the heterogeneity, i.e. the separation between dense Coll structures and the surrounding low viscosity solvent is even more pronounced. The inaccessible white areas show up as elongated, slender filaments or fibrils forming an extended percolating network providing the macroscopic gel-like texture. The Coll structures or fibers are denser than at lower concentrations. This shows up in the higher contrast between the dark areas of very low viscosity and the filamentous white areas as well as in the large fraction of tracers almost immobilized in the highly elastic areas of the fibers. Further increasing the Coll concentration up to 1 wt% results in a denser network of elongated fibers as expected in line with a higher bulk elastic modulus. The Coll structure seems to be further densified and the fraction of tracer particles able to diffuse into this structure and to be elastically trapped there, is clearly lower than at lower Coll concentrations. In particular, almost immobile tracers, that are embedded in highly elastic regions are hardly found, whereas a large fraction of tracers freely diffuses in the viscous matrix. In summary, MPT measurements inform us about the non-uniform structure of collagen aggregates and how collagen slender fibers or fiber bundles evolve at concentrations above the macroscopic sol-gel transition. As the collagen concentration increases, the inaccessible areas for the tracer particles shrink and re-arrange into slender bundles of collagen fibers, i.e. the collagen aggregates strongly densify with increasing collagen concentration. Another otherwise hardly accessible result, is that the diffusion coefficient corresponding to the linearly increasing MSDs of population III and hence the calculated viscosity of the continuous phase of the fiber suspensions is essentially independent of Coll concentration as shown in Table 2.1. This result indicates that the fraction of collagen molecularly dissolved in the aqueous phase is independent of the total collagen concentration in the solution. As the viscoelastic behavior of Coll solutions is determined by heterogeneous, supramolecular Coll structures present even at concentrations well below the sol-gel transition, we aimed at investigating this self-assembly phenomenon in more detail. Hence, large Coll structures were removed by filtration. Prior to filtration, 0.1 wt% Coll solutions showed, as already discussed above, a sample spanning network of elastic Coll structures. Consequently, in bulk measurements (see Fig. 2.8A), G' was frequency independent and dominating over G'' . Directly after filtration (Fig. 2.8A, row 2), results appear noisy and this is due to the fact that the sample is not in equilibrium anymore and its structure is heterogeneous on a macroscopic scale. In that sense rheological data obtained some seconds after filtration have to be treated as apparent values. However, a predominantly viscous behavior with a pronounced frequency dependence of G' and G'' was observed indicating that the gel structure was removed or destroyed. The viscosity deduced from the MSDs of the freely diffusing particles (blue) did not change upon filtration, but as expected, fewer elastically trapped tracer particles were seen when comparing row 2 to row 1 in Fig. 2.8B and C.

The measured protein concentration of $0.05 \pm 0.01\ \text{wt}\%$ after filtration corresponds to the sol state (see Fig. 2.2) and again, we find elastically trapped tracer particles

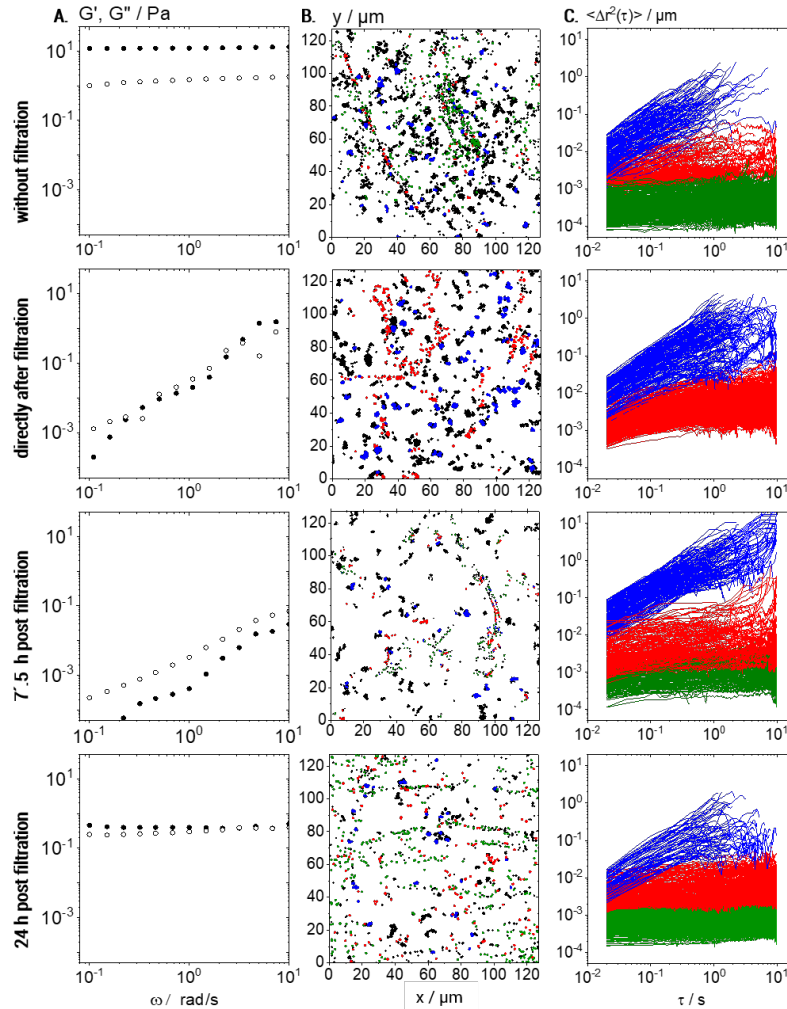


Figure 2.8: Coll self-assembly after removing large structures by filtration with $1.2 \mu\text{m}$ pore size: A) Storage and loss modulus, G' (full symbols) and G'' (hollow symbols), respectively, vs. frequency, obtained from rotational rheometry. B) Trajectories of all $0.2 \mu\text{m}$ tracer particles. Trajectories of tracers in viscous surrounding are shown in blue, those of elastically trapped tracers are shown in red and trajectories of almost immobilized particles are shown in green. Trajectories < 50 frames in length are shown in black but not considered for MSD calculations. C) MSD plots showing the different populations using the same color code as in B). Data is shown for $0.1 \text{ wt}\%$ Coll solutions prior to filtration (row 1), directly after filtration (row 2), 7.5 h (row 3) and 24 h (row 4) after filtration. For each time-point, 4 videos per biological repetition were recorded and analyzed and a representative set is shown here.

(compare Fig. 2.8B, row 2 to top row Fig. 2.7B). However, the size of continuous elastic areas was drastically reduced (compare Fig. 2.8B, row 2 to top row Fig. 2.7B) and the almost immobilized fraction (green trajectories) even disappeared completely. The fraction of elastically trapped (red) particles re-increases over time and even almost immobilized particles (green population) re-appear after 7.5 h waiting time but no percolating network can be seen (Fig. 2.8B, row 3). This is consistent with the still predominantly viscous behavior in bulk rheometry (row 3 in Fig. 2.8A). After 24 h post-filtration time, however, the gel-like behavior re-appears (G' , G'' independent of frequency) and MPT data show that a sample-spanning network structure of Coll fibers has recovered (row 4 in Fig. 2.8). However, the modulus $G_{0,\text{bulk}} = 1.6 \pm 0.5$ Pa was one order of magnitude lower than prior to filtration ($G_{0,\text{bulk}} = 13 \pm 1$ Pa) which is attributed to the lower Coll concentration and even 4 days after filtration, the initial plateau modulus is not recovered. Moreover, after 24h, G' and G'' are both independent of frequency and exhibit almost the same absolute values. Such a behavior is unphysical for homogeneous and isotropic materials and thus may be attributed to sample heterogeneities on a macroscopic level which can be seen in MPT data (Fig. 2.8B and C). It should be noted that the freshly prepared solution with 0.05 wt% Coll does not exhibit such a behavior and remains in the sol state even after 4 days of storage. This difference is attributed to the different size distribution of Coll aggregates or fibers in the filtrated compared to the untreated solution. From a comparison of samples measured in the same chamber after 24 h and newly filled channels, we were able to exclude any drying effects or mechanical influences on this network reformation. In summary, we conclude that MPT is a powerful tool to monitor the self-assembly of Coll in-situ.

2.3.5 Structural properties of native collagen I solutions

For comparison with lyophilized collagen solutions, ready-to use solutions of native collagen I were investigated, too. These solutions do not show the sol-gel transition observed in the solutions made from lyophilized Coll. Up to a concentration of 1 wt% these solutions behave like almost Newtonian low viscosity fluids as exemplarily shown in Fig. 2.9A for the 0.25 wt% solution with $\eta = 30.0 \pm 1.5$ mPa.s. Flow behavior changes from Newtonian to weakly viscoelastic in the concentration range up to 1 wt%, however, a sol-gel transition is not observed in this concentration range. The absolute viscosity of the 0.25 wt% solution is about 10 times higher than for the solutions made from lyophilized Coll below the sol-gel transition clearly indicating that a larger Coll fraction is molecularly dissolved. Trajectory plots and MSDs, derived from MPT measurements performed on a 0.25 wt% native collagen I solution with tracer particles of diameter $0.2 \mu\text{m}$ are shown in Fig. 2.9B and C, respectively. As for the solution made from lyophilized Coll, a broad variation in absolute values and time dependence of the calculated individual MSDs was found (see Fig. 2.3B). However, here we found only two populations of MSDs, one with slope $m > 0.5$ (blue) and the other with $m < 0.5$ and absolute value $< 10^{-3} \mu\text{m}^2$ (green). In native collagen I samples, the freely diffusing particles are the dominating fraction of tracers (96%) and the corresponding viscosity value $\eta_{\text{MPT}} = 78 \pm 8$ mPa.s agrees reasonably well with viscosity data from bulk mechanical rheometry. We hypothesize that the viscosity

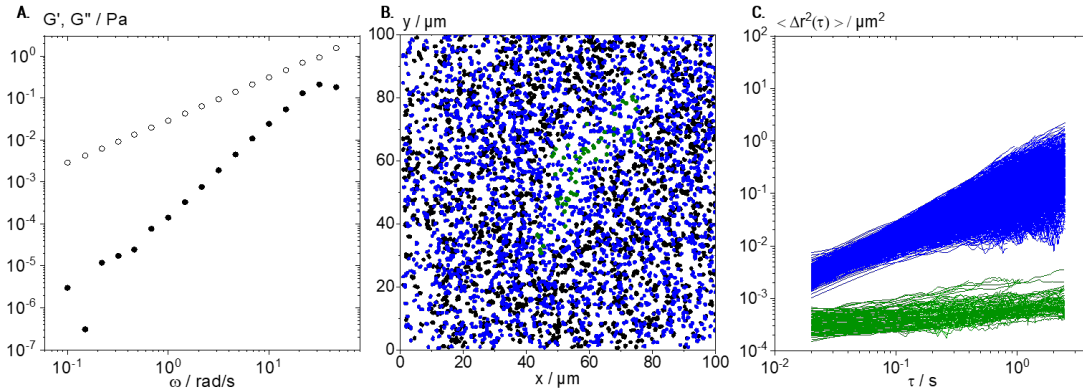


Figure 2.9: Characterization of 0.25wt% native collagen solution: A) G' (full symbols) and G'' (hollow symbols) obtained from small amplitude oscillatory shear rheometry versus frequency. B) Overlay of trajectories of elastically trapped $0.2 \mu\text{m}$ tracer particles (green) and freely diffusing tracers in viscous surrounding (blue). All trajectories shorter than 50 frames are shown in black. C) Respective MSD plots for all trajectories longer than 50 frames. For each biological repetition, 4 videos were recorded and analyzed and a representative set is shown here.

value deduced from MPT is systematically higher because of sample heterogeneity: besides the blue trajectories (Fig. 2.9C) used to calculate the viscosity, we observe a large fraction of very short trajectories presumably corresponding to areas of lower viscosity.

The small fraction of elastically trapped tracer particles exhibits a very low absolute MSD value close to the static error of our set-up, i.e. they are almost immobilized. These results indicate the formation of more homogeneous and stiffer structures in native collagen I solutions as compared to samples based on lyophilized Coll.

The plot of trajectories in Fig. 2.9B shows the formation of elastic areas (see green trajectories), as already observed for solutions of lyophilized Coll (see Fig. 2.5C) However, these areas are fewer in number, more roundish, shorter, and broader. These structures are not able to form a percolating network consistent with the predominantly viscous behavior found in bulk rheological measurements on native collagen I solutions (see Fig. 2.9A). However, the existence of such supramolecular aggregates even in low viscosity Coll solutions can be seen clearly in MPT experiments but not from conventional light microscopy. These results further confirm that MPT is a versatile tool to characterize different types of collagen solutions and the structure of included structures or fibers in-situ.

2.4 Conclusions

Classical bulk rheometry and multiple-particle tracking microrheology have been employed to gain insight into bulk viscoelasticity as well as structural and local viscoelastic properties of acidic Coll solutions. As already observed for a broad range of other materials, MPT and bulk data are not in agreement [12, 26, 29, 77, 163, 180] and the

explanation for this discrepancy is the presence of heterogeneities. Overlaying subsequent images of MPT video sequences allowed for a direct visualization of the fiber network in suspensions of lyophilized Coll. For all concentrations in the range from 0.05 to 1 wt%, MPT experiments performed with tracer particles of diameter $0.2\ \mu\text{m}$ yielded a very broad distribution of mean square displacements (MSDs) in terms of time dependence as well as absolute values. Some tracer particles diffused freely with a diffusion coefficient indicating that part of the Coll is dissolved in the aqueous phase, yielding similar viscosities as the bulk measurements for concentrations below the sharp sol-gel transition observed at $c_{\text{crit}} = 0.08\text{-}0.09\ \text{wt}\%$. According to these viscosity values, the amount of dissolved Coll is independent of the total Coll concentration. However, even at concentrations well below the macroscopic sol-gel transition, other MSD traces approached a constant value at long lag times, i.e. these particles were trapped in an elastic environment. We distinguished two populations of elastically trapped particles according to the order of magnitude difference in absolute MSD values. These particles were found within Coll structures. This suggests, that the Coll aggregates presumably comprise multiple dense bundles not permeable for the $0.2\ \mu\text{m}$ particles embedded in a swollen surrounding layer accessible by the $0.2\ \mu\text{m}$ tracer particles, but with largely varying stiffness according to the broad variation in absolute values of the corresponding time-independent MSDs. In contrast, $0.5\ \mu\text{m}$ particles were not able to penetrate these fiber bundle structures. These tracers diffused freely in the aqueous solution and the measured viscosity was found similar to the value obtained from the ensemble of freely diffusing smaller particles. The fraction of almost immobilized $0.2\ \mu\text{m}$ particles, found in the Coll structures, decreased with increasing Coll concentration, and we attribute this to an increasing packing density of the fibers progressively preventing to be accessed by the tracer particles. MPT and bulk rheological measurements were also used to monitor the Coll fiber self-assembly process. After removing larger Coll structures by filtration, the reformation of the sample-spanning network was observed within 24 h, resulting in a macroscopic sol-gel-transition. Surprisingly, this network structure recovers although the total Coll concentration after filtration is significantly lower than c_{crit} . The investigation of native collagen I solutions revealed a higher fraction of molecularly dissolved Coll, also fewer elastic regions that were less wide-spread than those in the samples based on lyophilized Coll at the same concentration, were observed. This is again in good accordance with the respective viscous behavior observed in bulk rheometry up to Coll concentrations of 1 wt%. According to our observations, particle tracking based microrheology imaging serves as a powerful tool for the in-situ analysis of the supramolecular structure and local viscoelasticity of dispersed Coll or other biopolymer fibers on a sub-micron length scale including the real-time monitoring of structure formation or structural transitions. Thus, this microrheology imaging method is perfectly suitable to study structural properties of fiber suspensions where conventional microscopy techniques fail.

Acknowledgements

We acknowledge the experimental assistance of Lea Bensinger, performing most of the MPT experiments in our lab and Dr. Carsten Radtke's help with BCA assays at the

KIT molecular separation group (MAB).

Chapter 3

Cryogel scaffolds from HA, Coll, Chitosan and mixtures

- Full title: Mechanical properties and suitability for cell culture of hyaluronic acid, chitosan, and collagen based scaffolds obtained from cryogelation
- Authors: J. Hafner, A. Ryl, C. Oelschlaeger, N. Willenbacher
- Bibliographic information: Conference Proceedings of BioMAAP 2017 Conference, publisher ASRANet Ltd.

Abstract

For 3D cell culture, scaffolds are required that obtain chemical, structural and bio-functional properties close to natural cell environment. This includes biocompatibility, macroporous structure and mechanical properties close to those of natural extracellular matrix. Chemically crosslinked cryogels based on biopolymers are perfectly suitable to fulfil those requirements. In this study we have adapted fabrication procedures for production of hyaluronic acid, chitosan and collagen cryogels, crosslinked with ethylene glycol diglycidyl ether, as well as hybrid gels thereof. Those cryogel scaffolds are macroporous ($\sim 100 \mu\text{m}$ pore size) and their mechanical properties can be tailored in the range of natural cell environments in different tissues. Besides bulk Young's modulus we have characterized the local viscoelastic properties by multiple particle tracking microrheology. The combination of macroscopic and local characterization with investigation of structural properties allowed the estimation of the influences of geometry and material properties of polymer networks on overall mechanical properties of scaffolds. Collagen and hyaluronic acid cryogels showed a regular sample spanning network with spherical, interconnected pores, while chitosan gels were heterogeneous, consisting of densely crosslinked areas and elongated macro pores. Those led to lower bulk moduli, but the local elasticity of the network was even higher than in collagen samples. Hybrid cryogels also showed a heterogeneous structure, but superior mechanical properties compared to single component gels. Additionally, for collagen gels the influence of initial freezing rate and crosslinker concentration on structural and mechanical properties were investigated in detail. Initial freezing in liquid nitrogen led to

needle shaped pores. After initial freezing in -20°C regular spherical pores occurred, and this structural difference influenced bulk modulus, while the local properties of the polymer network were not affected. Increased crosslinker concentration led to higher crosslink density in the pore walls which resulted in an increase in local elasticity but did not affect the pore geometry nor bulk properties. Based on these results, cryogels' mechanical and biofunctional properties can be tailored independently to generate a broad range of scaffolds, fitting application specific needs in cell culture.

3.1 Introduction

Tissue engineering scaffolds must be biocompatible, biofunctional and biodegradable. This leads to complex requirements regarding structure and composition. An open macroporous three-dimensional architecture is highly suitable to mimic natural cell environment and enables cells' migration into the scaffold but also their supply with nutrients and oxygen. Mechanical properties should be similar to those of the natural extra cellular matrix (ECM) to allow normal cell adhesion, growth and proliferation in culture [171]. In general, bulk rheological measurements [3, 16, 18, 96, 214, 234] and uniaxial compression tests [19, 30, 35, 142, 178] are considered for mechanical characterization of hydrogels. Young's modulus E or storage and loss modulus G' and G'' obtained from these. Both methods probe the bulk elasticity of the entire specimen under unidirectional stress. Elastic moduli of natural tissues vary in a broad range- from soft mucosa with $E \sim \text{kPa}$ to hard bone tissues with $E \sim \text{GPa}$ [58], so the properties of application specific suitable scaffolds are tailored in a broad range, too. However, in many studies the influence of gel macro elasticity on cell adhesion and proliferation has been investigated [3, 96, 214, 234]. But in fact, cell development and behavior are significantly influenced by the elasticity of the local environment and its deformability during adhesion. In particular changes in cell morphology, cell differentiation, cell spreading and proliferation [57–59, 149] have been observed to be a function of matrix stiffness, but the microenvironment that a cell can take into account therefor might be much smaller than the entire probe. ECM local viscoelastic properties have been investigated by atomic force microscopy (AFM) based nano-/micro-indentation [54, 110, 122], but only applied to the surface of non-porous hydrogels [52]. For soft ($E < 1 \text{ MPa}$), porous hydrogels, especially in the hydrated state, the indentation technique has several limitations [267]. Thus new techniques providing accurate information about local viscoelastic properties of hydrated soft cryogels are of great importance. Besides that, the development of bio-based scaffolds, offering the potential to fulfill cells needs regarding structure, mechanical and chemical properties, plays a crucial role in successful tissue engineering and cell research. Implanted scaffolds have to fulfill the mechanical function of a tissue initially, to allow the seeded cells to regenerate towards a functional tissue again. Mechanical functions are shifted towards newly grown tissue continuously, while the scaffold should be degraded, preferentially residue-free.

In this study we have used the cryogelation method to fabricate macroporous scaffolds from hyaluronic acid (HA), chitosan (Chit) and collagen (Coll) as single components and additionally mixtures of HA/Coll and Chit/Coll using ethylene glycol diglycidyl ether (EGDE) as chemical crosslinker to obtain a broad variety of scaffolds

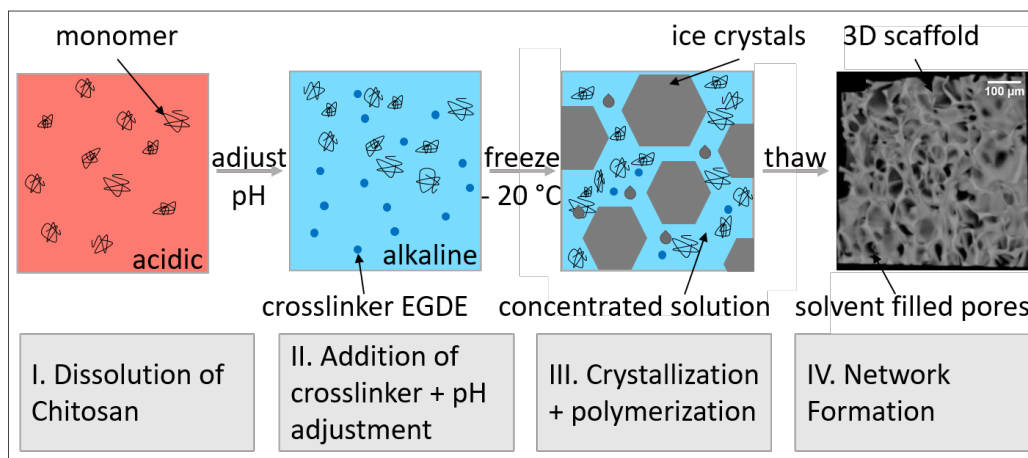


Figure 3.1: Fabrication of chitosan gels: Hybrid HA/Coll and Coll/Chit solutions were made of the two solutions by blending them under stirring.

with properties, that can be set to suit the requirements of specific applications. The goal is to produce non-toxic cryogels with controlled pore geometry and viscoelastic properties for application as cell culture scaffolds. For that, we develop a preparation method for production of HA, Coll and hybrid scaffolds and adapt this to fabricate stable Chit gels under alkaline conditions. We compare suitability of the different polymers and structure of obtained cryogels and investigate the influence of polymer and crosslinker concentration on bulk and local mechanical properties. The latter are characterized using multiple particle tracking (MPT) microrheology.

3.2 Materials and Methods

Macroporous gels were prepared starting from polymer solutions, using the cryogelation technique as described in [174].

3.2.1 Preparation of HA/Coll/Chit solutions

The initial step of the method was adapted, taking the individual dissolution needs of different polymer types into account. Briefly, to generate HA single component solutions, HA ($M_w=2.2$ Mio Da, Contipro, CZ) was dissolved in a 1 wt % sodium hydroxide aqueous solution under constant stirring, and this mixture was maintained for 16 h at 4°C until complete dissolution ($\text{pH} \geq 13$). Coll (Collagen I, fibrous powder from bovine tendon, AdvancedBiomatrix, USA) solutions were prepared in hydrochloric acid of pH 2.7, because Coll is not soluble in alkaline conditions. The solution had to be mixed for 18 h with magnetic stirrer at ambient temperature to ensure proper dissolution of collagen, leading to a highly viscous liquid. Chit (medium MW Chitosan, Sigma, USA) was dissolved in 2% acetic acid while stirred for 30 min. Chitosan solutions were left to rest for 4h (40°C) / 16h (4°C) / 4h (20°C) to study the dissolution behavior. Preparation procedure for Chit samples is described schematically in Fig. 3.1.

(a) Crosslinking

The crosslinker contains two highly reactive epoxy rings at both ends, and is suitable for nucleophilic crosslinking of e.g. hydroxyl or amine groups that all used biopolymers offer. However, under acidic conditions, protonation will lead towards ring opening in EGDE, which results in its deactivation. Accordingly, for all samples crosslinking took place under alkaline conditions. In case of HA there are two hydroxyl groups per disaccharide subunit, in Chit two amine groups and two hydroxyl groups. Coll offers the hydroxyl groups of hydroxyproline, lysine and hydroxyl-lysine residues of the protein chains. Crosslinking efficiency may be reduced here due to the complex rigid fibrous structure and low number of crosslinking site per polymer chain length unit, but stable crosslinks can be obtained.

As shown in Fig. 3.2 schematically, the crosslinker is generally able to crosslink all three types of polymers, but only under alkaline conditions. Those alkaline conditions are superior for processing of HA, because during dissolution in an acidic solvent, the HA backbone is degraded rapidly [69]. Collagen and chitosan are considered non-soluble under alkaline conditions, but after obtaining stable acidic solutions, pH was changed to alkaline, right when EGDE was added, and then crosslinking took place. Accordingly, after adjusting pH of polymer solutions to 13.3 ± 0.2 with concentrated NaOH, the crosslinker EDGE (Ethylene glycol diglycidyl ether, Sigma) was added. For hybrid samples, the method is similar: After blending both solutions, pH was adjusted to alkaline by using NaOH before addition of crosslinker. For Chit we compared mild and strong alkaline conditions (pH 9 and 13), in order to find a compromise between homogeneity of solution and activity of crosslinker.

(b) Freezing and Polymerization

All resulting solutions were poured into cylindrical PTFE molds (diameter 10 mm, height 3 mm) and tightly sealed. Thereafter molds were placed either into an ethylene glycol bath and stored at -20°C for 6 days polymerization (low freezing rate) or for accelerated initial freezing, samples in liquid nitrogen for 30 min and afterwards stored for the rest of the polymerization time at -20°C in an ethylene glycol bath.

(c) Thawing

After 6 days of freezing, gels were allowed to warm up to room temperature for at least 2 h before performing experiments. The cryogels obtained were spongy, elastic with large interconnected pores and swelled instantaneously when immersed in water. The swelling ratio was determined by measuring the ratio of the masses of the gels in the swollen (wet) and unswollen (dry) state. To ensure sufficient statistics, weight was averaged over 10 different gels of the same batch. In particular, dry gels were weighed directly after fabrication (m_{dry}) and again after being immersed in water for 4h (m_{wet} , measured in triplicate for each specimen, to take the influence of remaining surface water into account). Swelling ratio is mainly depending on the interconnectivity of the pores and the water up-taking capacity of the used polymers [100, 195].

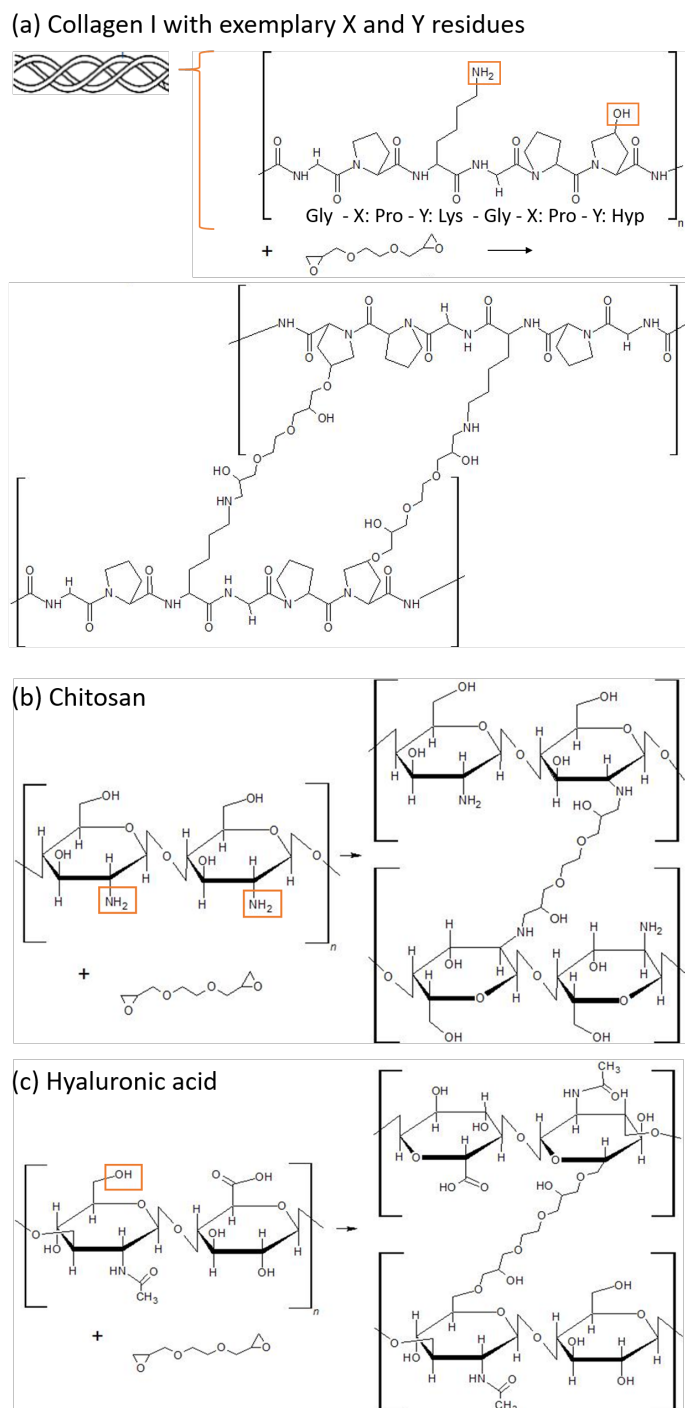


Figure 3.2: Crosslinking mechanism for (a) Coll, (b) Chit, (c) HA (following [62, 64, 134, 231])

3.2.2 Scaffold pore size and shape, network thickness and topology characterizations

The overall scaffold architecture has been investigated using laser scanning microscopy (Zeiss LSM 500). For the visualization of pore walls, green fluorescent polystyrene particles (diameter $0.19\ \mu\text{m}$, 10% in aqueous solution, Bangs Laboratories, USA) have been added to the solution before freezing. These tracer particles remain in the polymer phase during gelation and are finally entrapped in the pore walls, which reduces background noise compared to unspecific staining and requires no time consuming staining protocol. From parallel staining with Rhodamine B solution, we saw that observed structures are congruent to those obtained from staining (data not shown).

3.2.3 Multiple particle tracking based optical microrheology

Local viscoelastic properties of the matrix have been investigated using Multiple Particle Tracking (MPT) technique. With an inverted fluorescence microscope (Axio Observer D1, Zeiss), equipped with a Fluar $100\times$ objective (numerical aperture 1.3, $100\times$ magnification, oil immersion lens), we tracked the Brownian motion of green fluorescent polystyrene microspheres (see section 3.2.2). Images of these fluorescent beads were recorded with a sCMOS camera Zyla X (Andor Technology: $21.8\ \text{mm}$ diagonal sensor size, 2160×2160 square pixels). Displacements of particle centers were monitored in a $127 \times 127\ \mu\text{m}$ field of view, at a rate of 50 frames/sec. Movies of the fluctuating microspheres were analyzed by a custom MPT routine incorporated into the software Image Processing System (Visiometrics iPS) and a self-written Matlab program based on the widely used Crocker and Grier tracking algorithm [120]. Additionally, to perform the statistical analysis and characterize the microstructure heterogeneity, we examined the distribution of displacements, known as the Van Hove correlation function, and calculated the non-Gaussian parameter a as described in [174]. Based on the generalized Stokes Einstein relation, we also calculated local moduli ($G'(\text{MPT})$ and $G''(\text{MPT})$) using the average mean square displacements (MSDs) of a particle collective. For further details, please refer to [121].

3.2.4 Mechanical Compression tests and Texture Profile Analysis

Uniaxial unconfined compression tests were performed at room temperature using a commercial Texture Analyzer TA.XTplus (Stable Micro System, UK) machine with a 5 kg load cell. Tests were performed on cylindrically shaped gels (diameter \ll plate size) of different height and diameter depending on swelling. Samples were compressed up to 80% strain at a compression speed of $0.5\ \text{mm/s}$. The Young's modulus E was determined as the slope of the initially linear stress-strain curve in the 5 to 15% strain region.

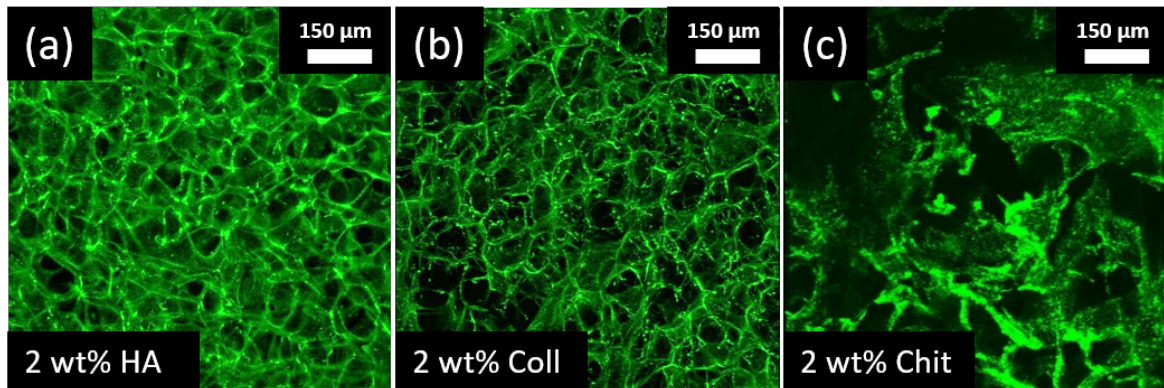


Figure 3.3: Structure of HA, Coll and Chit samples in LSM

3.3 Results

3.3.1 Formation and structure of single component cryogels

EGDE is not able to form stable crosslinks under acidic conditions, but based on alkaline solution, HA is perfectly able to form stable gels [22]. Initially dissolving Coll at acidic pH and subsequent adjustment of pH to 13 enabled us to produce stable collagen cryogels. However, it was not possible to obtain reproducible and stable crosslinking in Chit samples, because the increase in pH led to immediate phase separation. Chit was concentrated only in a part of the initial solution which formed stable gels, but there remained some specimen, that contained almost no Chit and were thus unstable and showed poor mechanical properties and stability during swelling. The solubility of chitosan was improved by increasing temperature to 40°C during pH exposure. This led to formation of heat gels, without addition of crosslinker, indicating that the crosslinking mechanism was different and nonporous thermal gels were obtained. Preferentially, porous Chit cryogels are produced in mild alkaline pH (pH 9), but the phase separation still cannot be avoided, so that only some of the samples formed stable gels containing the main fraction of initially added Chit. As the amount of both phases was not quantifiable, the dry mass content of obtained samples is to be regarded with suspicion. Homogeneity of polymer solutions is crucial for homogeneous structural properties of resulting cryogels. Homogeneous HA and Coll solutions formed uniform sample spanning networks around regular spherical pores (see Fig. 3.3a and b). Both showed a high degree of pores interconnectivity and similar pore size. Chit gels (Fig. 3.3c) also had porous structure, but besides areas with thick pore walls around angular pores, there occurred at the same time huge pores without defined shape, similar to cracks with low degree of connection. The Chit gels seem to consist of gel flocks with dense structures that are only loosely connected to each other. This is further corroborated by the fast degradation of some of the Chit samples, especially those made from pH 13 solutions, after immersion in water for a few seconds. The initially cylindrical gel specimen fell apart to a dispersion of gel flocks with ~ 1 mm in diameter. This degradation was slowed down in gels prepared from pH 9 solutions which were stable in water for up to 4 weeks without altering mechanical properties or integrity.

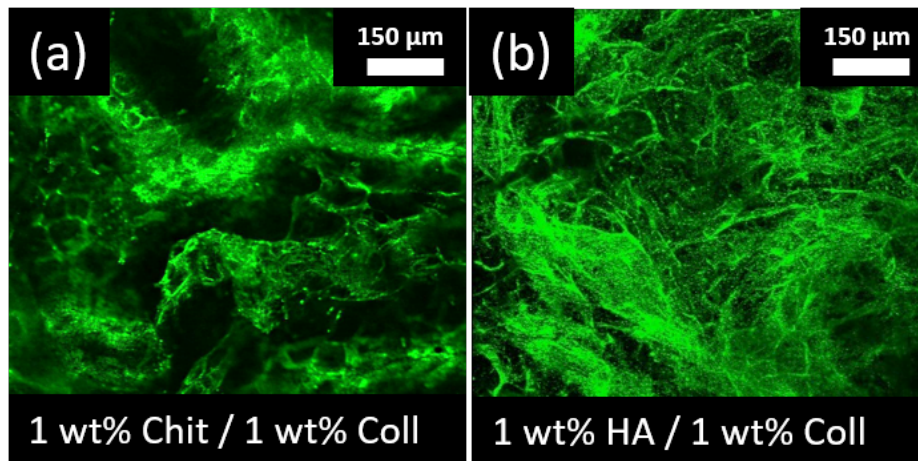


Figure 3.4: Structure of hybrid scaffolds of Chit/Coll and HA/Coll, investigated by LSM

3.3.2 Fabrication and structure of stable hybrid gels

The fabrication of hybrid Chit/Coll scaffolds resulted in cryogels where the properties of Coll dominated. Those gels were not swelling, but stable in water for weeks and relatively stiff, compared to pure Chit scaffolds (see section 3.3.3). Besides the above mentioned fine collagen network that occurred only locally in Chit gel structures (see Fig. 3.3c), denser network areas, consisting of randomly orientated fibers with few irregular pores and besides those two, empty cracks, sort of elongated macro pores, appeared.

HA/Coll mixtures also formed stable hybrid scaffolds. Those showed a lower swelling ratio ($SR(1\%HA/1\%Coll) = 1.2 \pm 0.2$) compared to HA single scaffolds ($SR(2\% HA) = 8 \pm 1.5$) and with Coll content above 2%, swelling ratio was 1. The resulting structures (Fig. 3.4b) showed fibrous networks with irregular shaped pores and the density of those structures varied locally. In conclusion, the three polymer types can be combined to form stable networks with individual structural properties.

3.3.3 Comparison of polymer types

(a) Mechanical properties of single component scaffolds

HA samples behaved highly flexible and elastic and, even under multiple compression cycles were able to retain shape and integrity, while Coll samples were totally rigid and broke after first cycles (data not shown). Coll in general causes rigidity in the samples. Even small amounts of Coll (0.1 wt %) led to cracking of hybrid samples in first cycles with 80% strain. During uniaxial compression, most chitosan samples were fragmented into small gel flocks, even under low loads. However, measured under wet conditions, Chit gels were the most rigid of the 2% scaffold types, though gel properties varied in a broad range in one batch. This was caused by different specimen originating from both phases, so that the Chit was not distributed homogeneously over all specimen and even the different areas in one specimen may have contained different Chit contents. This

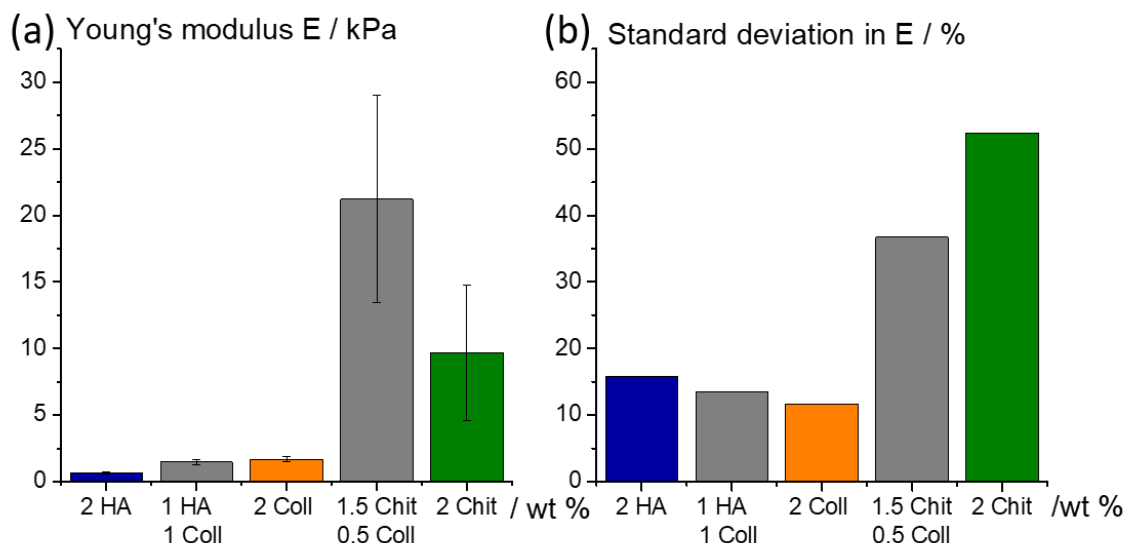


Figure 3.5: Bulk Young's modulus E (a) and standard deviation thereof (b) for pure and hybrid gels with 2 wt % polymer (n=10)

led to the large error bars for bulk mechanical properties, as shown in Fig. 3.5a. Figure 3.5a shows that HA and Coll both were forming reproducible gels. With a polymer content of 2% they both showed low Young's moduli compared to pure Chit. Young's modulus was increased in samples with increased concentration of polymer in case of all polymers (data not shown). Minimum polymer contents required for cryogelation were HA 2%, Coll 1%, Chit 1.5%. The broad variation in case of Chit samples resulted from phase separation and instability of the gels.

(b) Mechanical properties of hybrid scaffolds

Addition of Coll to HA or Chit resulted in irregular pore structure (see Fig. 3.4) and in a significant increase in Young's modulus (Fig. 3.5), when total polymer content was kept constant at 2%. The Young's modulus of Chit/Coll scaffolds was even higher, than the one of pure Chit, which may be related to the Chit network containing randomly oriented elastic Coll fibers additionally or to the improved elasticity of the joint network itself. For all of the three biopolymers as well as all investigated mixtures, there was a slight increase in Young's modulus with increasing crosslinker concentration (data not shown).

(c) Micromechanics of single scaffolds

On microscale, particle movement was most restricted in HA single component samples, leading to high moduli compared to Chit and Coll (see Fig. 3.6). In Coll although the polymer fibers themselves are considered relatively stiff, the measured storage modulus was low. The influence of particles moving through meshes between the Coll fibers in the network has to be further evaluated by variation of particle size in MPT. For the

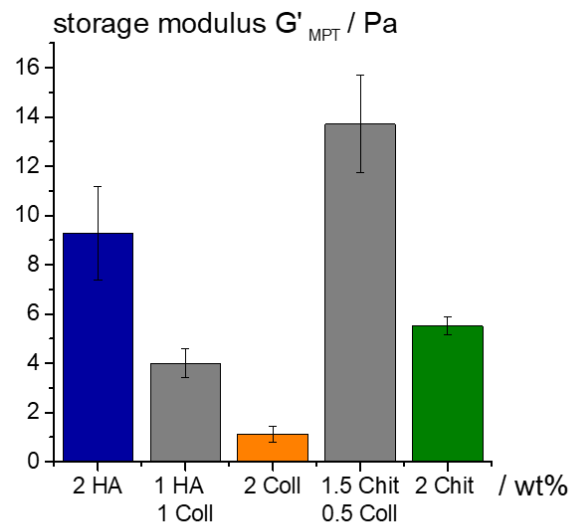


Figure 3.6: Local mechanical properties of single component and hybrid scaffolds

0.19 μm particles, that we have used here, mesh sizes were calculated according to classical theory of rubber elasticity [31]. Compared to $74 \pm 6 \mu\text{m}$ for pure HA and $65 \pm 3 \mu\text{m}$ for pure Chit, Coll mesh size was significantly higher ($149 \pm 18 \mu\text{m}$), allowing the particles to diffuse within meshes. We expect to measure higher entrapment and higher corresponding moduli when particle size is increased [163]. Storage modulus $G'(\text{MPT})$ of 2% Chit lies in between the corresponding values of HA and Coll and the heterogeneity on microscale was in Chit much smaller than on macroscale, which can be seen from the standard deviation of less than 10%. This leads us to conclude, that the areas in Chit samples that were properly crosslinked and originated from the Chit rich phase, formed networks with relatively homogeneous elastic properties and a high density of crosslinks (four per disaccharide possible, HA two per disaccharide, respectively and Coll comparably fewer).

(d) Micromechanics of hybrid scaffolds

In HA/Coll hybrid scaffolds, micro moduli were increased compared to pure Coll scaffolds with same polymer content. The same trend was observed for Chit gels containing small amounts of Coll (see Fig. 3.6). This supports the hypothesis, that both polymers form a joint network with altered mechanical properties and not just the pore geometry is different. At the same time, the non-Gaussian parameter α was increased from 1 ± 0.3 for all types of single scaffolds to 5 in case of HA/Coll and 12 for Chit/Coll respectively. The high degree of heterogeneity, already observed in the irregular pore shape, obviously also had mechanical consequences. The elasticity of the network varied within the field of view for one MPT experiment ($127\mu\text{m} \times 127\mu\text{m}$), but was reproducible for all investigated sample areas. The high variation in bulk mechanical properties of hybrid gels resulted from this heterogeneity in structure.

3.3.4 Influence of fabrication process on mechanical and structural properties of cryogels

Collagen gelation procedure was highly reproducible and stable gels were obtained from 2 wt % Coll with 0.7 to 3.5 wt % crosslinker concentration. The macroscopic properties of those depended on crosslinker concentration, but were independent of freezing method (Fig. 3.7a), whereas the pore structure was not affected by crosslinker concentration, but depended on freezing method (Fig. 3.7c). In contrast, MPT results showed that the network structures had similar local storage moduli, independent of freezing method (Fig. 3.7b) which means the crosslink density was comparable and macroscopic results are explained only by geometric effects like pore size or shape. Needle shaped pores, caused by the accelerated freezing and crystallization in liquid nitrogen and the comparably dense networks were better able to resist mechanical forces. With increasing crosslinker concentration for both freezing methods, G'_{MPT} was increased, which is linked to a higher degree of crosslinking.

3.4 Conclusion

In this study we have investigated the potential of EGDE to crosslink HA, Coll and Chit networks as well as their hybrid forms. Adjusting the preparation protocol allowed us to obtain even chitosan gels with appropriate stability in water. The extensive swelling of HA gels was not found for the other polymers and swelling is hindered by addition of other polymers to HA scaffold. Nevertheless, we were able to obtain porous cryogels, consisting of HA, Chit, Coll, or their mixture. In all cases, increased crosslinker concentration leads to increased Young's modulus, but Coll network architecture is not affected. In case of only partly crosslinked Chit samples, MPT offers the superior potential to analyze just the mechanical properties of crosslinked areas. Using mixtures of the three polymers enables us to independently tailor viscoelastic, structural and biofunctional properties of the macroporous cryogels to fit any application specific needs. Additionally, we have proved the non-cytotoxicity and accessibility of our scaffolds using 3T3 fibroblast cells in live-dead assay. In all investigated scaffolds the cells were able to penetrate into the gel during 2 days and survived for up to 21 days.

Acknowledgements

We greatly acknowledge the support of Prof. Martin Bastmeyer and Sarah Bertels (KIT), who contributed intensively to the cell culture experiments.

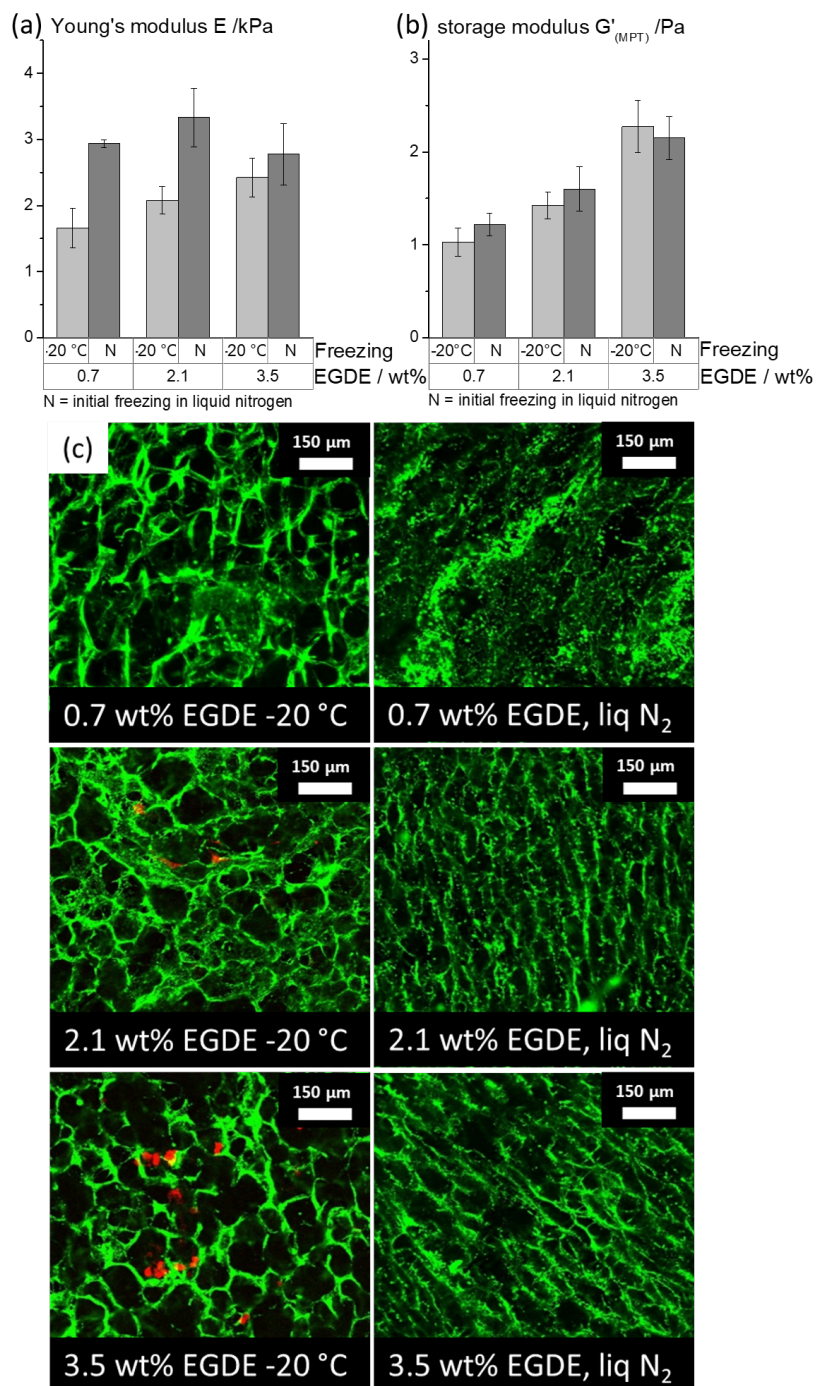


Figure 3.7: Influence of EGDE concentration and freezing condition on (a) bulk Young's modulus (b) local shear modulus $G'_{(MPT)}$ and (c) structure of Coll gels

Chapter 4

Fabrication of non-cytotoxic HA scaffolds

- Full title: Hyaluronic acid cryogels with non-cytotoxic crosslinker genipin
- Authors: J. Roether, C. Oelschlaeger, N. Willenbacher
- Bibliographic information: Materials Letters X, 2590-1508 (2019)
- <https://doi.org/10.1016/j.mlblux.2019.100027>

Abstract

For the first time, macroporous, elastic, three-dimensional hyaluronic acid cryogels were prepared with genipin as non-cytotoxic crosslinking agent. These cryogels are characterized by a lamellar porous structure with a homogeneous pore size of ~ 100 μm , shear elasticity of ~ 2 kPa and a swelling ratio of 2.5 in water. Additionally, multiple particle tracking based microrheology measurements reveal the formation of a heterogeneous network. This novel biomaterial owns great potential as non-cytotoxic alternative for application in drug delivery, as tissue engineering scaffold or wound healing substrate and can help reducing toxicity of artificial skin grafts or tissue equivalents.

4.1 Introduction

For successful tissue engineering, a scaffold must be biofunctional, biodegradable, biocompatible, with a 3D porous architecture and high degree of pore interconnectivity. Furthermore, it should have appropriate mechanical properties to closely mimic mechanical, and ideally also chemical properties of the extracellular matrix. For fabrication of hyaluronic acid (HA) based-scaffolds, phase separation [35] freeze-drying [115] and electrospinning [166] have been established. Therefore, BDDE (1,4-butanediol diglycidyl ether) [124] and glutaraldehyde [35] were used as crosslinkers. The fabrication of one-component HA scaffolds via cryogelation [144] facilitates the formation of homogeneous pores at a relatively low polymer concentration. Crosslinkers that are reactive with HA at low temperatures are ethyleneglycol diglycidylether (EGDE)

[174, 199, 224] and EDC/NHS (carbodiimide/N-hydroxysuccinimide) [89]. Mixed cryogels of HA with collagen, gelatine and chitosan were also crosslinked by EDC/NHS [33] and glutaraldehyde [123, 231]. Most of the crosslinkers and especially their non-reacting residues are cytotoxic [141, 170]. It is consequently desirable to use noncytotoxic crosslinkers to form stable and biocompatible HA based hydrogels. Genipin is a natural product extracted from the gardenia fruit and it was shown that its cytotoxicity is significantly lower than that of common crosslinkers [25, 32, 93, 139, 158, 235]. Genipin has been utilized to crosslink biopolymers, such as chitosan [158] and gelatine [25] or hybrid systems like chitosan/HA [164] but it has never been used to form pure HA gels before. We now proved the suitability of genipin as an alternative crosslinking agent for the fabrication of one component HA porous gels using the cryogelation technique. Thus, we compared the swelling capacity, structural, micro- and macro-viscoelastic properties of HA scaffolds crosslinked with genipin to the corresponding features of such gels crosslinked with commonly used EGDE.

4.2 Materials and methods

4.2.1 Preparation of cryogels and determination of swelling capacity

Macroporous gels were prepared using the cryogelation technique as previously described [199]. Briefly, HA ($M_w = 2.0$ to 2.2 Mio Da, Contipro) was dissolved in 1% NaOH and EGDE was added. For genipin crosslinking, HA was dissolved in PBS and mixed 2:1 with genipin in DMSO (20 mg/ml, considering the maximum solubility). After mixing for 20 min, solutions were frozen at -20°C for 6 days. After thawing, the swelling ratio (SR) was determined by measuring the ratio of the mass of the gel equilibrated in water and un-swollen state.

4.2.2 Rotational rheometry

Gel bulk linear viscoelastic properties were characterized performing oscillatory shear experiments in the linear-viscoelastic regime, using a rotational rheometer Anton Paar MCR 501 (plate/plate, diameter 8 mm, gap 1 mm).

4.2.3 Multiple particle tracking

Local viscoelastic properties of the matrix, namely the pore walls, were investigated using the multiple particle tracking (MPT) technique [68, 252]. In MPT experiments, the thermally driven motion of inert microspheres that are evenly distributed within a sample is monitored. Here, we tracked the Brownian motion of green fluorescent polystyrene microspheres (diameter $0.19\ \mu\text{m}$). For performing measurements exclusively in the matrix, particles were added to the polymer solutions before freezing. The displacements of particle centers were monitored at a rate of 50 frames/s. Movies of the fluctuating microspheres were analyzed using a custom MPT routine, incorporated into the software Image Processing System (Visiometrics iPS) and a self-written

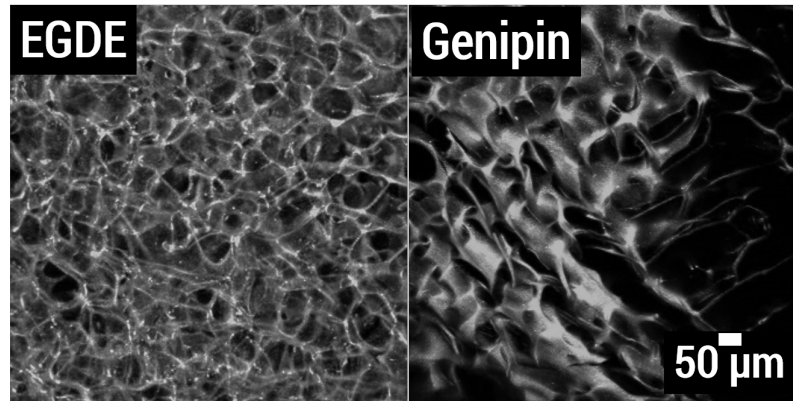


Figure 4.1: LSM images of gels structures, crosslinked with EGDE and genipin, visualized by fluorescence of tracer particles embedded in the pore walls.

Matlab program [120], based on the widely used Crocker and Grier algorithm [39].

4.3 Results and discussion

4.3.1 Cryogels structural properties and swelling capacity

Independent of the crosslinker used, both types of cryogels obtained were spongy, elastic with large pores and they swelled instantaneously when immersed in water. Examples of 3D images of the structure of these cryogels in the wet state, obtained with laser scanning microscopy (LSM 510, Carl Zeiss), are shown in Fig. 4.1. EGDE cryogels show interconnected round pores of size $\sim 100 \mu\text{m}$ and thin matrix wall of $\sim 5\text{--}20 \mu\text{m}$ [199]. For genipin cryogels, the images suggest the formation of a more lamellar porous structure with a pore size almost similar to that of EGDE gels. To our knowledge, this is the first time that pure HA hydrogels have been fabricated with non-cytotoxic crosslinker genipin. Different crosslinking mechanisms are the origin of the formation of these two morphologically different gels. In HA/EGDE gels, epoxy groups of the EGDE are covalently bond to the HA hydroxyl groups under alkaline conditions [224]. Genipin generally reacts with primary amino groups of biopolymers but HA does not have such groups. However, HA has multiple highly reactive hydroxy groups that are able to form e.g. glycosidic bonds, presumably with genipin [212]. The latter are known to be stable as seen in other polycarbohydrates, such as starch. Other gels, based on non-covalent bonds, are known to be stable in water, too [269]. Although the crosslinking mechanism cannot be fully unravelled here, cryogelation of HA and genipin leads to stable intermolecular bonds, that are strong enough to allow for the swelling of HA/genipin gels in water without dissolving. Without genipin, no stable structures can be obtained. Despite the higher molar ratio of crosslinker to polymer, HA/EGDE gels exhibit a higher degree of swelling with $\text{SR} > 7.5$ compared to HA/genipin gels with $\text{SR} \sim 2.5$. This may be due to a heterogeneous gel structure with percolating domains of high crosslink density that limits the swellability of genipin gels. After immersion in water, both compositions show high long-term stability (several months) and shape

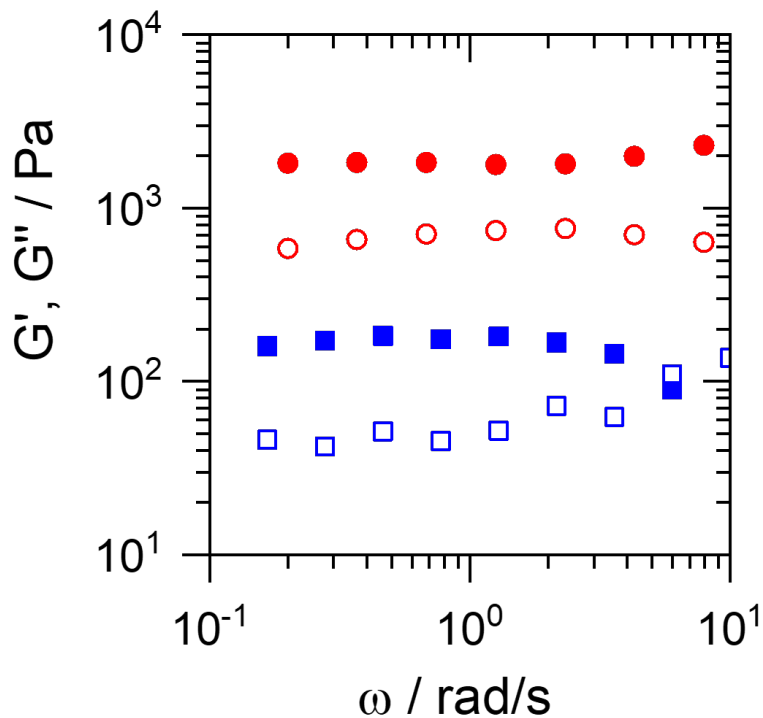


Figure 4.2: Dynamic shear moduli G' (closed symbols) and G'' (open symbols) of 3 wt% HA gels crosslinked with EGDE (blue) and genipin (red). (For interpretation of the references to colour in this figure legend, the reader is referred to the web version of this article.)

Table 4.1: Crosslinker concentrations in a 3 wt% HA hydrogel.

Crosslinker	Concentration /wt%	Reactive groups / mMol/ml	Solvent
EGDE	0.7	40	1 % NaOH
Genipin	0.5	20	PBS with 30% DMSO

fidelity, which can be considered mandatory in tissue engineering applications.

4.3.2 Mechanical properties

In bulk oscillatory shear measurements, gels of both compositions show frequency independent elastic moduli and G' dominates over G'' in the frequency range from 0.1 to 10 rad/s (Fig. 4.2). This is considered as a typical gel-like behavior. Corresponding shear elastic plateau modulus data G_0 (average of G' values obtained in the probed frequency range) show that the less swollen gel made of genipin provides a higher elastic modulus value $G_0 \sim 2000$ Pa compared to the highly swollen EGDE gel where $G_0 \sim 200$ Pa. This is direct evidence of the different crosslink density of the swollen gels. The three-times lower water uptake of the genipin gel outweighs the two-times lower molar ratio of crosslinker to polymer compared to the EGDE gel (see Table 4.1 and see section 4.3.1).

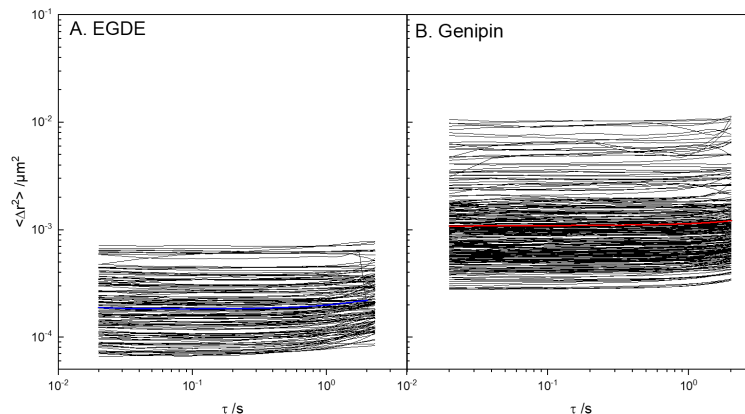


Figure 4.3: MSDs of PS particles ($d = 0.19 \mu\text{m}$) dispersed in the matrix of HA 3 wt% gels crosslinked with EGDE (A) and genipin (B). Blue and red curves are the ensemble-averaged MSD.

In order to characterize the local elasticity of the pore walls, microstructural and local viscoelastic properties of the gels were investigated by means of MPT microrheology. Fig. 4.3 shows the variation of mean square displacements (MSDs) as a function of lag time τ for tracer particles with diameter $0.19 \mu\text{m}$ dispersed in the gel network. In both cases, almost no time dependence of the individual MSDs is found and this result indicates that particles are highly constrained by the surrounding fluid which is consistent with an elastic trapping of particles in a gel-like network. Additionally, for gels crosslinked with genipin (Fig. 4.3B), the range of displacements at a given lag time is much broader than for the gel crosslinked with EGDE (Fig. 4.3A). At $\tau = 0.1$ s, MSDs vary about two orders of magnitude, from $\sim 3 \times 10^{-4}$ to $10^{-2} \mu\text{m}^2$ for genipin gels compared to only one order of magnitude from $\sim 5 \times 10^{-5}$ to $7 \times 10^{-4} \mu\text{m}^2$ for EGDE gels. This indicates a more heterogeneous structure of the HA/genipin network with a non-Gaussian parameter [256] $\alpha = 5.5$, compared to the HA/EGDE gel where $\alpha = 1.4$. As already mentioned above, this might be the reason for the reduced swelling capacity of genipin gels (see 4.3.1). The higher absolute value of the average MSD for genipin gels indicates that particles explore a softer environment than in EGDE gels. The discrepancy between micro- and macrorheology which is more pronounced for genipin than for EGDE hydrogels, is presumably due to densely crosslinked regions in the more heterogeneous genipin hydrogels, that are inaccessible for tracer particles but seem to contribute to the overall mechanical strength of the constructs.

4.4 Conclusion

Genipin can be used as crosslinking agent for producing noncytotoxic macroporous hyaluronic acid cryogels. Bulk elasticity of genipin and conventional EDGE gels are in the same range, whereas the local mechanical properties of genipin gels are more

heterogeneous. Both gels show similar pore sizes in a well-suitable range for cell culture applications. In genipin gels, the pores appear more lamellar, but the major advantage of using genipin as crosslinking agent is its low cytotoxicity that allows the formation of stable cryogels with a broad range of potential applications, e.g. as cell culture scaffold, in drug delivery or wound healing.

Chapter 5

Structure and cell-culture suitability of HA/Coll scaffolds

- Full title: Microstructure, local viscoelasticity and cell culture suitability of 3D hybrid HA/collagen scaffolds
- Authors: J. Roether, S. Bertels, C. Oelschlaeger, M. Bastmeyer, N. Willenbacher
- Bibliographic information: PLoS ONE 13(12): e0207397.
- <https://doi.org/10.1371/journal.pone.0207397>

Abstract

As mechanical properties of cell culture substrates matter, methods for mechanical characterization of scaffolds on a relevant length scale are required. We used multiple particle tracking microrheology to close the gap between elasticity determined from bulk measurements and elastic properties sensed by cells. Structure and elasticity of macroporous, three-dimensional cryogel scaffolds from mixtures of hyaluronic acid (HA) and collagen (Coll) were characterized. Both one-component gels formed homogeneous networks, whereas hybrid gels were heterogeneous in terms of elasticity. Most strikingly, local elastic moduli were significantly lower than bulk moduli presumably due to non-equilibrium chain conformations between crosslinks. This was more pronounced in Coll and hybrid gels than in pure HA gels. Local elastic moduli were similar for all gels, irrespective of their different swelling ratio and bulk moduli. Fibroblast cell culture proved the biocompatibility of all investigated compositions. Coll containing gels enabled cell migration, adhesion and proliferation inside the gels.

5.1 Introduction

Scaffolds for successful tissue engineering must be biodegradable and biocompatible, with an open, macroporous three-dimensional architecture and should have appropriate mechanical properties closely mimicking those of the natural extra cellular matrix (ECM) [95]. Mechanical properties play a fundamental role in resistance

and stability of the gels but also alter cell migration, adhesion, proliferation and metabolism [3, 86, 96, 115, 206, 214, 234, 250]. In the past, mechanical properties of hydrogels were generally characterized using bulk rheological measurements [3, 16, 18, 96, 214, 217, 234], as well as uniaxial compression tests [19, 30, 35, 142, 178]. These latter assess the Young's modulus E which characterizes bulk elasticity of an entire sample on a macroscopic scale. Different moduli are connected to different tissue applications, from soft mucosa with $E \sim \text{kPa}$ to hard bone tissues with $E \sim \text{GPa}$. However, cell behavior is significantly influenced by the elasticity of the direct microenvironment [236], which may not be well characterized by the bulk elastic modulus, particularly, when the gel composition, i.e. the polymer concentration or cross-link density is spatially heterogeneous and/or the gel includes pores. Cells probe the elasticity of their surrounding in the range of up to five times their length (reviewed in [60]) by actively pulling fibers they are adhered to. Whether the displacement of fibers or the corresponding force of the material is sensed, is subject of current discussion [206]. According to the fiber pulling theory, the local properties of pore walls in water filled macroporous scaffolds are more relevant, than bulk elasticity. But pore wall/material thickness should be taken into account, as the force a cell has to apply for buckling of a strut depends on the geometry and elasticity of this object [60]. Some studies exist in the literature where local viscoelastic properties of the surfaces of cell culture substrates were investigated by means of atomic force microscopy (AFM) based nano/micro indentation and cell behavior was said to be affected by the determined matrix elasticity [54, 110, 122, 135, 236]. Here it is important to keep in mind, that cells do not necessarily sense the scaffold surface and that apparent elasticity of soft materials depends on the used measurement method [157]. However, matrix stiffness caused changes in cell morphology, cell differentiation, cell spreading and proliferation [57–59, 149]. Besides that, growing fibroblast cells themselves affect ECM mechanical properties during remodeling, depending on initial scaffold properties [60, 133, 209]. In an iterative process, those altered properties of the remodeled matrix feedback to cell growth. Daviran et al. [45] investigated the degradation of non-porous poly(ethylene glycol)-peptide hydrogels by enzymes secreted from encapsulated cells using a microrheology method and Kuboki et al. [122] showed that the secretion of Coll by seeded cells in addition to the Coll already present increases the matrix stiffness. Additionally, cells increase Coll network density by contraction during remodeling [76]. To our knowledge, for porous hydrogels, only one attempt [268] was made to characterize matrix local viscoelastic properties. Indentation experiments were employed in this case, the new insight, however, was limited due to various drawbacks. A first limitation of this experimental approach is the difficulty to identify the point of zero force. A second one is the softness of the material. Cryogels are considered as soft materials with a Young's modulus $E < 1 \text{ MPa}$ whereas indentation techniques are more adapted for stiff materials with $E > 1 \text{ GPa}$. In conclusion, the study of soft porous hydrated materials still poses various challenges demanding innovative characterization techniques providing accurate information about local viscoelastic properties of soft hydrogels. In this study we used the cryogelation method [174] to fabricate hybrid macroporous scaffolds from hyaluronic acid (HA) and collagen (Coll) mixtures using ethylene glycol diglycidyl ether (EGDE) as chemical crosslinker and we employed multiple particle tracking (MPT) microrheology to determine the local viscoelastic properties of these

soft gels. The goal was to produce cryogels with controlled pore size, wall thickness, and viscoelastic properties for application in cell culture. We wanted to understand how sample composition and local viscoelastic properties of the matrix affect cell behavior. For that, in the first part of the study, we investigated the influence of HA and Coll concentrations on gel swelling capacity, pore size and matrix thickness, as well as macro and micro-mechanical properties. The second part was dedicated to the cultivation of mouse dermal fibroblast cells, incorporated into the macroporous scaffolds. Cell viability, proliferation and morphology were characterized. Finally, the *in vitro* biodegradability of the scaffolds was investigated.

5.2 Materials and Methods

5.2.1 Preparation of HA/Coll cryogels

Macroporous gels were prepared using the cryogelation technique as described in Oelschlaeger et al. [174]. Briefly, sodium hyaluronate (HA), $M_w = 2.2$ Mio Da, Contipro, CZ) was dissolved in a 0.25M sodium hydroxide (Carl Roth, Germany) aqueous solution under constant stirring for 20 min, and this mixture was maintained for 16 h at 4°C until complete dissolution. Coll solutions were prepared following the manufacturers recommendations, by dissolution of Coll (Collagen I, fibrous powder from bovine tendon, AdvancedBioMatrix, USA) in 5 mM hydrochloric acid (Carl Roth, Germany). To ensure appropriate dissolution of Coll and exclude phase separation, the solution had to be mixed for 18 h with magnetic stirrer under ambient temperature, leading to a highly viscous liquid. Rheological properties of solutions of HA, Coll and mixtures are shown as S1 Fig in the supporting information. Hybrid HA/Coll solutions were made of the two solutions by blending them under stirring. After adjusting pH of blended solutions to 13.2 ± 0.2 with concentrated NaOH, 0.7 wt% of crosslinker EGDE (Sigma, USA) were added. By stirring for 30 min, uniform distribution of EGDE was ensured. The solutions were poured into cylindrical PTFE molds (diameter 10 mm, height 3 mm) and tightly sealed. Thereafter molds were placed into an ethylene glycol (Carl Roth, Germany) bath and stored at -20 or -80° C for 6 days. After freezing, gels were allowed to warm up to room temperature for at least 2 h before performing experiments. The repetition of this preparation routine led to five independent batches that were used for characterization. All cylindrical cryogel specimen were immersed in bi-distilled water and all experiments were performed in wet state. The swelling ratio was determined by measuring the ratio of the mass of the gel in the swollen (wet) and un-swollen (dry) state. To ensure sufficient statistical significance, weight was averaged over 10 different of 5 independent batches. In particular, dry gels were weighed directly after fabrication (m_{dry}) and again after being immersed in water for 4 h (m_{wet} , measured in triplicate for each specimen, to take into account the influence of remaining surface water). Swelling ratio is mainly controlled by the interconnectivity of the pores and the water up-taking capacity of the used polymers.

5.2.2 Scaffold pore size and shape, network thickness and topology characterizations

The overall scaffold architecture was investigated firstly using laser scanning microscopy (LSM, LSM 510, Carl Zeiss, Germany). For visualization of the pore walls and for MPT measurements (see 5.2.3), green fluorescent polystyrene particles (diameter 0.19 μm , Bangs Laboratories) were added to the solution before freezing so that particles remained in the polymer phase during gelation and were finally entrapped exclusively in the pore walls. Secondly, swollen specimen were immersed in Rhodamine B solutions for 3 days and after excessive washing in water investigated by a confocal laser scanning microscope (CLSM, TCS SP8, Leica Microsystems, Germany), combined with a 20x multi-immersion objective. A comparison of gels stained with both methods showed a high degree of co-localization, so particles are considered to be distributed all over the polymer network (data not shown).

5.2.3 Multiple particle tracking based optical microrheology

MPT was developed as a microrheological tool that allows for the characterization of microstructural and micromechanical properties of many materials [120] (and references therein). Studying cryogels, we have used this technique to characterize local viscoelastic properties of the matrix and viscous properties of the pore filling liquid. The fluid mechanics of microrheology and especially the principles and applications have been described in detail [68, 252]. The underlying idea of MPT is to monitor the Brownian motion of inert colloidal probe particles embedded in a material and thereby obtain quantitative information about the rheological properties of the surrounding fluid. This technique was introduced in the mid-1990s when Mason and Weitz proposed a quantitative relation between the tracer mean square displacement (MSD) $\langle \Delta r^2(\tau) \rangle$ as a function of lag time τ and the macroscopic complex shear modulus $G^*(\omega)$ as a function of the frequency ω [152]. The Laplace transform of the particle MSD $\langle \Delta \tilde{r}^2(i\omega) \rangle$ is related to the complex modulus G^* of the sample via a generalized Stokes–Einstein equation (GSE, general form for 3D, see Eq. 1) [153]:

$$G^*(\omega) = \frac{k_B T}{\pi a i \omega \langle \Delta \tilde{r}^2(i\omega) \rangle} = G'(\omega) + iG''(\omega) \quad (5.1)$$

a stands for the radius of the embedded beads, k_B for the Boltzmann constant and T for the temperature. This GSE relation is valid only under the assumption that the material surrounding the sphere can be treated as an isotropic and homogeneous continuum, i.e. that the particle size is larger than the structural length scales of the probed material. For the cryogels investigated here, the mesh size calculated from macrorheological measurements ranged from 4–17 nm (see section 4.2.2), which is much smaller than the size of the particles we used (diameter 200 nm). Furthermore, probe particle and fluid inertia can be neglected, Reynolds number Re and Stokes number Stk both are well below 1. For 2D tracking of beads suspended in an ideal elastic material, Eq. 5.1 reduces to Eq. 5.2 [262] including a prefactor of 2/3 for the numbers

of dimensions [98]:

$$G_0 = \frac{2k_B T}{3\pi a \langle \Delta r^2(\tau) \rangle} \quad (5.2)$$

Where G_0 is the shear modulus of the material independent of ω . All cryogels investigated here, behave like elastic solids, as confirmed by the time-independence of the MSD at times < 0.3 s, independent of the matrix composition. Therefore, we used Eq. 5.2 to determine local matrix elasticity, G_0 hereinafter referred to as $G_{0,\text{MPT}}$. Our setup is based on an inverted fluorescence microscope (Axio Observer D1, Carl Zeiss, Germany) equipped with a Fluar 100x objective (numerical aperture 1.3, 100x magnification, oil immersion lens, Carl Zeiss). We tracked the Brownian motion of green fluorescent polystyrene microspheres of $0.19 \mu\text{m}$ diameter in two dimensions. In isotropic materials, no additional information is obtained from 3D tracking and by reducing the measurement to 2D, the performance of the system is enhanced. For performing MPT measurements exclusively in the matrix, particles were added to the polymer solutions before freezing. In order to exclude protein absorption on the particle surface, which would affect the measured diffusivity, we compared measurements with native polystyrene (PS) particles to PS particles functionalized with Polyethylene glycol (donated by Xabier Murgia, Department of drug delivery, Helmholtz Institute for Pharmaceutical Research Saarland). Particle diffusion was similar for both particle types confirming that the effect of adhering protein or HA on the particle surface is negligible. To perform MPT experiments in the pore liquid, tracer particles of $0.5 \mu\text{m}$ diameter were locally added to pores of polymerized swollen samples using a syringe. Images of these fluorescent beads were recorded via a sCMOS camera Zyla X (Andor Technology, Ireland: 21.8 mm diagonal sensor size, 2160×2160 square pixels). The displacements of particle centers were monitored in a $127 \times 127 \mu\text{m}$ field of view at a rate of 50 frames/sec. This latter value is the maximum rate of image capture that our camera can achieve, so that the temporal resolution at short timescales is limited to 0.02s. Movies of the fluctuating microspheres were analyzed using a custom MPT routine, including the software Image Processing System (Visiometrics iPS) and a self-written Matlab code [120], based on the widely used Crocker and Grier tracking algorithm [39]. We examined the distribution of displacements, known as the Van Hove correlation function [241] and calculated the non-Gaussian parameter α according to Eq. 5.3 [256].

$$\alpha = \frac{\langle x^4(\tau) \rangle}{3\langle x^2(\tau) \rangle^2} - 1 \quad (5.3)$$

This parameter describes the derivation of the MSD values from a Gaussian distribution expected for a homogeneous uniform sample and characterizes the heterogeneity of the sample on a 0.1–1 μm length scale.

5.2.4 Bulk mechanical properties

Compression test

Uniaxial unconfined compression tests were performed at room temperature using the commercial tensile testing machine Texture Analyzer TA.XTplus (Stable Micro System, UK) equipped with a 5 kg load cell. Tests were performed on cylindrically shaped gels (diameter \ll plate size) of different height and diameter, depending on the degree of swelling. Samples were compressed up to 80% strain at a compression speed of 0.5 mm/s. The strain η was calculated as the ratio of the change in length during compression Δl and initial height of the sample l_0 . Using this, Young's modulus E was determined as the slope of the initially linear stress-strain curve in the strain region $< 5\%$, (see Fig. 5.8 and 5.9).

Oscillatory Shear

In shear, the gels were characterized through their storage modulus G' and loss modulus G'' as a function of frequency. Measurements were performed using a rotational rheometer (Physica MCR501, Anton Paar) with a plate-plate geometry (diameter 8 mm). Gap height was adjusted between 1 and 2 mm depending on the height of the swollen samples to obtain a normal force of 0.15 ± 0.05 N. For all compositions, frequency sweeps were performed in the linear regime at a stress amplitude of $\tau = 0.5$ Pa, covering the frequency range of 0.1 to 10 rad/s.

5.2.5 Degradation Kinetics

Disk-shaped gels (initial diameter: 10 mm, height: 3 mm) of different composition were placed in beakers filled with water (ten times the initial weight of the individual specimen). Individual specimens were used for compression tests or MPT measurements after different periods of time, from one day to 500 days.

5.2.6 In vitro assessment of biocompatibility

The thawed gels were swollen in water and washed with PBS (Phosphate Buffered Saline, PAN Biotech). Afterwards they were placed in 12-well plates and immersed in DMEM (Dulbecco's Modified Eagles Medium, PAN Biotech), supplemented with 10% FCS (Fetal Calves Serum, PAN Biotech). Cells were passaged according to a routine protocol and cultivated under standard conditions (37°C, 5% CO₂, 90% rel. humidity). NIH-3T3 fibroblast cells were detached using 0.25% trypsin/EDTA (ethylenediaminetetraacetic acid) in PBS and suspended in supplemented medium. Cells were seeded onto the gels at a density of 75 000 cells per gel (235 mm³). Initially, they were allowed to settle without additional medium for 30 min at 37°C. Later, 2 ml medium were added and the cells were cultivated for 8 days. Medium was exchanged every second day. For each independent experiment, gels from a newly synthesized batch were used. Live/dead assay was performed after 1, 3 and 8 days by addition of 0.5 μ l Calcein (Thermo Fischer Scientific, 4mM in DMSO (dimethyl sulfoxide)) and 2 μ l Ethidium homodimer (Thermo Fischer Scientific, 2 mM in DMSO/water) directly into the 2

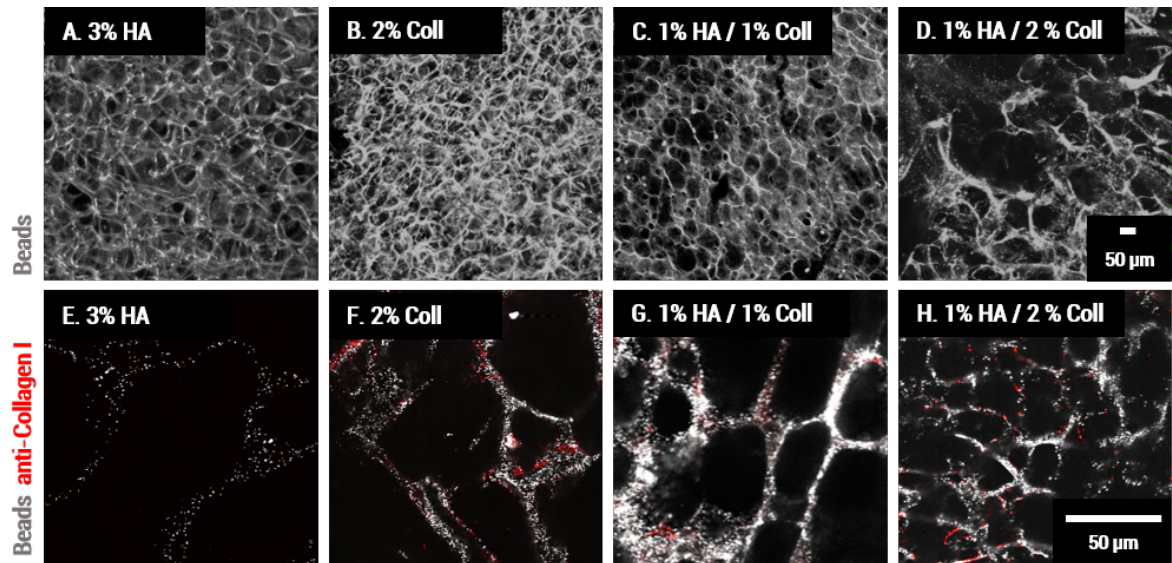


Figure 5.1: Morphology of swollen cryogels. LSM images of fluorescent tracer particles localized in the gel network. 3D stack (A-D) and corresponding 2D image, 40x magnification, with anti-Coll staining shown in red (E- H).

ml nutrient medium in each well. Resulting concentrations were $0.25 \mu\text{l}$ Calcein/ml medium and $1 \mu\text{l}$ Ethidium homodimer/ml medium. After incubation for 15 min, at least 5 LSM images were recorded during 15 min. In all images, living and dead cells were counted and the count was averaged for all images. For characterization of cell morphology, the gels were first fixed with 4% para-formaldehyde (30 min, 20°C), then washed twice with PBS and permeabilized with Triton X-100 in PBS for 20 min. Cell division events were investigated after 1, 3, and 8 days in culture by EdU-labeling. The labeling procedure was performed with the Click-itTM EdU Alexa FluorTM 594 Imaging kit according to the manufacturer's instructions. Scaffolds were washed with 1% BSA (bovine serum albumin in PBS) after fixation and permeabilization. Anti-Actin and DAPI staining was performed subsequently. Therefore, scaffolds were immersed in primary antibody solution (anti-actin, Sigma Aldrich, A2066 1:200 in 1% BSA) for 6h. After washing with PBS twice, scaffolds were placed in secondary antibody solution (goat-anti-rabbit Alexa FluorTM 647, Jackson Immuno Research, 1:250 and DAPI, Carl Roth, 1:1000 in 1% BSA) over night at -4°C . Prior to imaging, scaffolds were washed with PBS twice. At least 5 images per scaffold were taken and ratio of number of EdU positive cells to total cell count was averaged. All experiments were done in triplicate. For each independent run, new gels were produced.

5.3 Results and Discussion

5.3.1 Structural properties of HA, Coll and hybrid cryogels

Pore size and shape of cell-free gels of different compositions were qualitatively determined from LSM images. For visualization of the network structure, the fluorescence signal of embedded tracer particles was recorded. Fig 1.1 shows images of hydrated

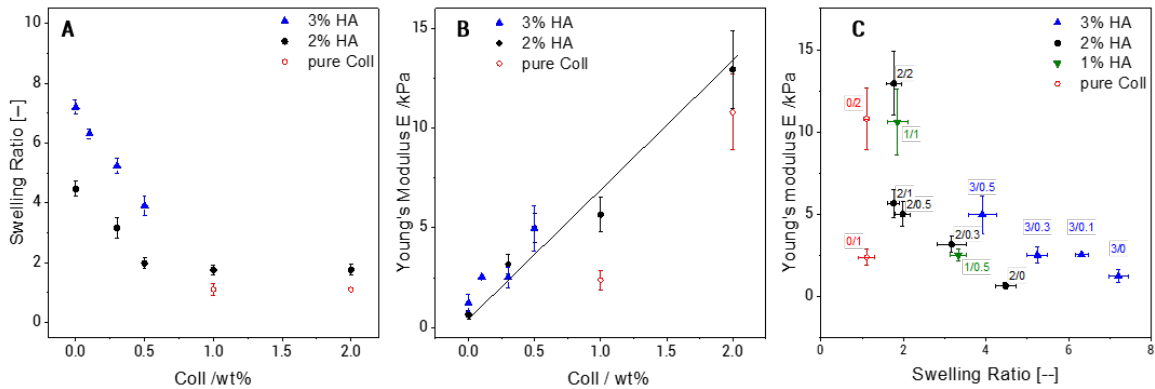


Figure 5.2: Influence of swelling behavior on bulk elasticity of cryogels. Swelling ratio (A) and Young’s modulus measured in uniaxial compression (B) over Coll concentration, and influence of degree of swelling on Young’s modulus for samples with different HA/Coll content in wt% (C). Young’s modulus values represents average and standard deviation obtained from at least 25 specimens of each composition.

cryogels with a total polymer concentration of 2–3 wt% composed of 3% HA (Fig 5.1A and 5.1E), 2% Coll (Fig 5.1B and 5.1F) as well as a mixtures of HA and Coll (Fig 5.1C, 5.1D, 5.1G and 5.1H). The 3%HA, 2%Coll and 1%HA/1%Coll gels all exhibit a fairly roundish pore shape in the swollen state, but pore size varies. Pure HA gels have larger pores $\sim 100 - 120\mu\text{m}$ in diameter (Fig 5.1A and 5.1E) compared to $\sim 50\mu\text{m}$ pores in pure Coll (Figs. 5.1B and F) and $\sim 50\mu\text{m}$ pores in 1% HA/1% Coll gels (Fig 5.1C and 5.1G). The matrix thickness and variation of pore size are similar in these gels. However, the gel consisting of 1%HA/2%Coll (Fig 5.1D and 5.1H), shows a strong local variation in pore size. In some areas, pores were narrower than $20\mu\text{m}$, elsewhere big cracks disturbed the continuous network. To get more information about the Coll distribution in the hybrid matrix, we stained Coll I (shown in red) using polyclonal α -Coll I (rabbit) primary antibody in combination with Cy3-labeled (goat) secondary antibody (Fig 5.1E–H). As expected, no Coll is present in pure HA gel (Fig 5.1E), while in pure Coll (Fig 5.1F), interconnected Coll fibers are visible along all pore wall structures. In both hybrid scaffolds (Fig 5.1G and H), the Coll network is interrupted by unstained sections, where only tracer particles are visible indicating a non-homogeneous Coll distribution in the matrix.

5.3.2 Swelling and bulk mechanical properties

Swelling

As mentioned previously, one of the distinctive properties of macroporous HA gels is to swell instantaneously when immersed in water or in a standard cell culture medium [254]. The excessive swelling of HA gels seems to be related to the ability of glycosaminoglycans with their large number of hydrophilic groups and flexible three-dimensional structure, to bind lots of water [146]. Swelling capacity of Coll free gels

increased from 4.35 ± 0.37 for 2%HA gels to 7.21 ± 0.24 for 3%HA gels (see Fig 5.2A). As the total amount of crosslinker was kept constant (0.7 wt %) this increased swelling capacity is related to the lower crosslinker/ polymer ratio, i.e. decreased crosslink density. An increase in swelling ratio with lower crosslinker/polymer ratio at constant HA content was observed before [174]. Furthermore, Fig 5.2A shows the effect of the Coll concentration on swelling ratio in water. For both HA concentrations, we observed a linear decrease of swelling capacity when the Coll content was increased to 0.5 wt %. For the gel with 2 wt % HA, the swelling ratio decreased from 4.35 ± 0.37 to 1.98 ± 0.18 when the Coll concentration was increased from 0 to 0.5 wt % and levelled off at a constant swelling ratio upon further increase of Coll concentration. This decrease in swelling capacity, also seen elsewhere [127, 202], can be related to a reduction of the HA/Coll network flexibility due to the rigidity of Coll fibers. These latter serve as a cage, hindering the expansion of the flexible HA polymer coils. Finally, for cryogels composed only of Coll, swelling ratio was close to one, i.e. these gels essentially do not swell. Similar observations have been reported for natural cartilage, where Coll can also take-up water, but due to the dense rigid fibrous structure, swelling is limited [56]. The Coll network is apparently so stiff that it cannot expand and swelling is not possible.

Cryogel bulk elasticity in uniaxial compression and shear

Fig 5.2B shows that Young's modulus E in the wet state, increases almost linearly from 0.5 to 13 kPa, when the Coll content in 2 wt % HA gels is increased from 0 to 2 wt %. A reinforcement of the matrix with increasing Coll concentration is expected in the dry state due to the formation of strong Coll fibers randomly distributed within the network. These fibers made of polypeptide chains are known to form stable helical structures in alkaline solutions at room temperature [115]. However, in the wet state, the effect of swelling is dominating. Less swollen, especially Coll containing gels show higher elastic moduli compared to highly swollen gels (see Fig 5.2C). As seen in Fig 5.3B, the Young's modulus of 2%HA ($E = 0.65 \pm 0.21$ kPa) is similar to the one of 3%HA ($E = 1.1 \pm 0.5$ kPa), though the swelling ratio is substantially higher for 3%HA gels (7.2 ± 0.2 , compared to 4.5 ± 0.3 for 2% HA). This is consistent keeping in mind that the crosslinker concentration is the same in both cases but more polymer between network junctions is available to preserve the shape of the swollen gel including 3%HA. The lower crosslinker to polymer ratio in the 3%HA gel leads to an increased swelling ratio for the 3%HA gel, but the Young's modulus is similar as for 2%HA, because due to the increased total polymer content, the density of entanglements among polymer chains is higher than in 2%HA gel and this contributes to the elasticity of the gel, too. The contribution of entanglements to the modulus is on the same order of magnitude as that of the crosslinks [174]. Finally, we observed that the Young's modulus of the cryogel composed of only Coll was higher by a factor of 15 compared to the one obtained for HA (both 2 wt %), while swelling is four times lower compared to pure HA gels. Even at a concentration of 1%Coll the modulus is five times higher than that of 2%HA gel. This confirms the high compressive strength of Coll networks and the strong influence of the degree of swelling. As seen in Fig 5.3A, the pure 3%HA gel ($E = 1.1 \pm 0.5$ kPa) is weaker in uniaxial compression, compared to pure 2%Coll

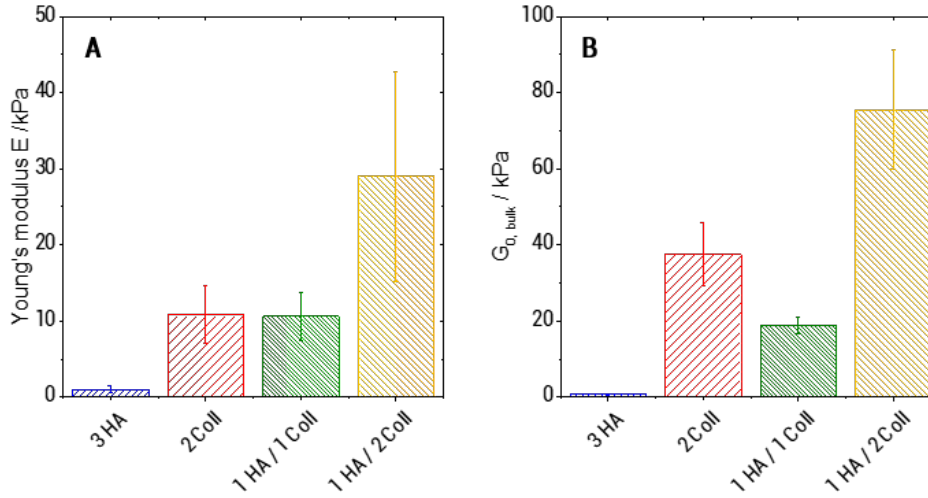


Figure 5.3: Bulk mechanics of cryogels. Young's modulus determined in uniaxial compression (A) and shear modulus obtained from small amplitude oscillatory shear (B).

gels ($E = 11 \pm 4$ kPa) or hybrids (11 ± 3 kPa for 1%HA/1%Coll and 29 ± 14 kPa for 1 %HA/ 2%Coll). Bulk elasticity values of 1%HA/2%Coll scatter strongly which might be related to the heterogeneous structure seen in Fig 1. This latter gel exhibits the highest modulus despite its higher degree of swelling compared to the pure 2%Coll sample. However, an increased modulus for heterogeneous structures was observed in various other polymer systems before, e.g. acrylic thickeners [121, 177] or methacrylate copolymers [265]. Uniaxial compression of a macroscopic, swollen specimen, is not only determined by the matrix elasticity. Besides the degree of swelling (see section 5.3.2), structural properties, such as pore size, pore shape, pore interconnectivity and wall thickness may also affect Young's modulus. In oscillatory shear, samples of all compositions show frequency independent elastic moduli and G' dominates over G'' in the frequency range from 0.1 to 100 rad/s (see Fig 5.7). This is considered typical gel-like behavior. Corresponding shear modulus data $G_{0,bulk}$ (average of G' values obtained in the probed frequency range) are shown in 5.3B. As in uniaxial compression, the highly swollen pure HA samples appear weaker ($G_{0,bulk} = 0.8 \pm 0.2$ kPa) than Coll containing samples. Pure Coll ($G_{0,bulk} = 38 \pm 8$ kPa) exhibits a higher modulus than the 1% HA/1%Coll mixture ($G_{0,bulk} = 19 \pm 2$ kPa). The highest shear modulus was found for the 1%HA/2%Coll mixture ($G_{0,bulk} = 76 \pm 16$ kPa). In conclusion, the bulk shear and compression moduli are on the same order of magnitude and a similar ranking within the series of investigated samples is found. However, the $G_{0,bulk}$ values are somewhat higher than corresponding Young's modulus values. This is in contrast to the $E = 3 \cdot G_0$ relationship expected for uniform, isotropic bodies and may be attributed to the heterogeneous porous structure of the gels investigated here. Finally, from above $G_{0,bulk}$ values, we can directly determine the mesh size ξ_{bulk} of the scaffold network according to the classical theory of rubber elasticity assuming thermal

equilibrium (Eq. 5.4) [203]:

$$G_{0,bulk} = \frac{k_B T}{\xi_{MPT}^3} \quad (5.4)$$

In all cases, ξ_{bulk} varied between 17 ± 2 nm (pure HA) and 4 ± 0.2 nm (1% HA / 2% Coll). These values are significantly smaller than the diameter of the embedded tracer particles (diameter = 200 nm) we used for MPT measurements. Consequently, this result confirms the validity of Eq. 5.2, namely that the material can be treated as a continuum on the length scale that is sensed by the particles.

5.3.3 Local viscoelastic properties from multiple particle tracking microrheology

We employed multiple particle tracking (MPT) microrheology for characterization of local viscoelastic properties of the HA/Coll matrix as well as viscous properties of the pores. Independent of the sample composition, we observed purely diffusive motion of the tracer particles dispersed in the pores, i.e. the microenvironment surrounding the particles responded like a viscous liquid (data not shown). The obtained viscosity was close to that of water and in all cases these pore filling solutions were homogeneous as indicated by the value of the non-Gaussian parameter $\alpha \cong 0$ (see Eq. 5.3). The motion of particles dispersed in the cryogel network (Fig 5.4A) was significantly different from diffusion in the pores. For both, single component HA (Fig 5.4A1) and single component Coll (Fig 5.4A2) scaffolds, MSD curves were time independent ($d\Delta r^2/d\tau \approx 0$) throughout all probed time scales and showed an average MSD (red curve) value of $2.7 \pm 0.2 \times 10^{-4} \mu\text{m}^2$ and $4.6 \pm 0.3 \times 10^{-4} \mu\text{m}^2$, respectively. This indicates that particles were highly constrained by their surrounding which is consistent with an elastic trapping of tracer particles in a gel-like network. In contrast, HA/Coll mixtures (Fig 5.4A3 and 5.4A4) showed viscoelastic behavior, as the corresponding MSD plots exhibited an upward curvature at long lag times ($\tau > 1$ s), indicating slow viscous diffusion of the beads corresponding to a transition into the terminal flow regime. Furthermore, the analysis of the MSD distribution provides information about the degree of heterogeneity of the matrix and the local variation of viscoelastic properties with microscale resolution. For the pure HA gel (Fig 5.4A1), the range of displacement at a given lag time was quite narrow. At $\tau = 0.1$ s, MSDs varied within one order of magnitude, from 10^{-4} to $10^{-3} \mu\text{m}^2$. For pure Coll gel (Fig 5.4A2), the range of displacement was slightly broader, MSDs covered a range of almost 1.5 decades from 10^{-4} to $3 \times 10^{-3} \mu\text{m}^2$. Corresponding values of the non-Gaussian parameter α were $\alpha = 1.4 \pm 1.2$ and $\alpha = 3.1 \pm 1.7$ for pure HA and Coll gel, respectively (see Fig 5.4C). This result indicates that both, pure HA and pure Coll network, were essentially homogeneous. Higher α -values were found for the hybrid gels ($\alpha = 6.0 \pm 3.0$ for 1%HA/1%Coll and $\alpha = 4.6 \pm 3.1$ for 1%HA/2%Coll gels). Despite the large uncertainty in determination of the α values due to a strong variation of MSD distributions obtained in different regions of a sample, it is obvious that the matrix heterogeneity was more pronounced for these hybrid gels with a variation of the absolute MSD values within 2.5 orders of magnitude (Fig 5.4A3 and 5.4A4). Distribution and length scale of heterogeneities were mapped by plotting all particle positions in the plane of observation (Fig 5.4B) and coloring each

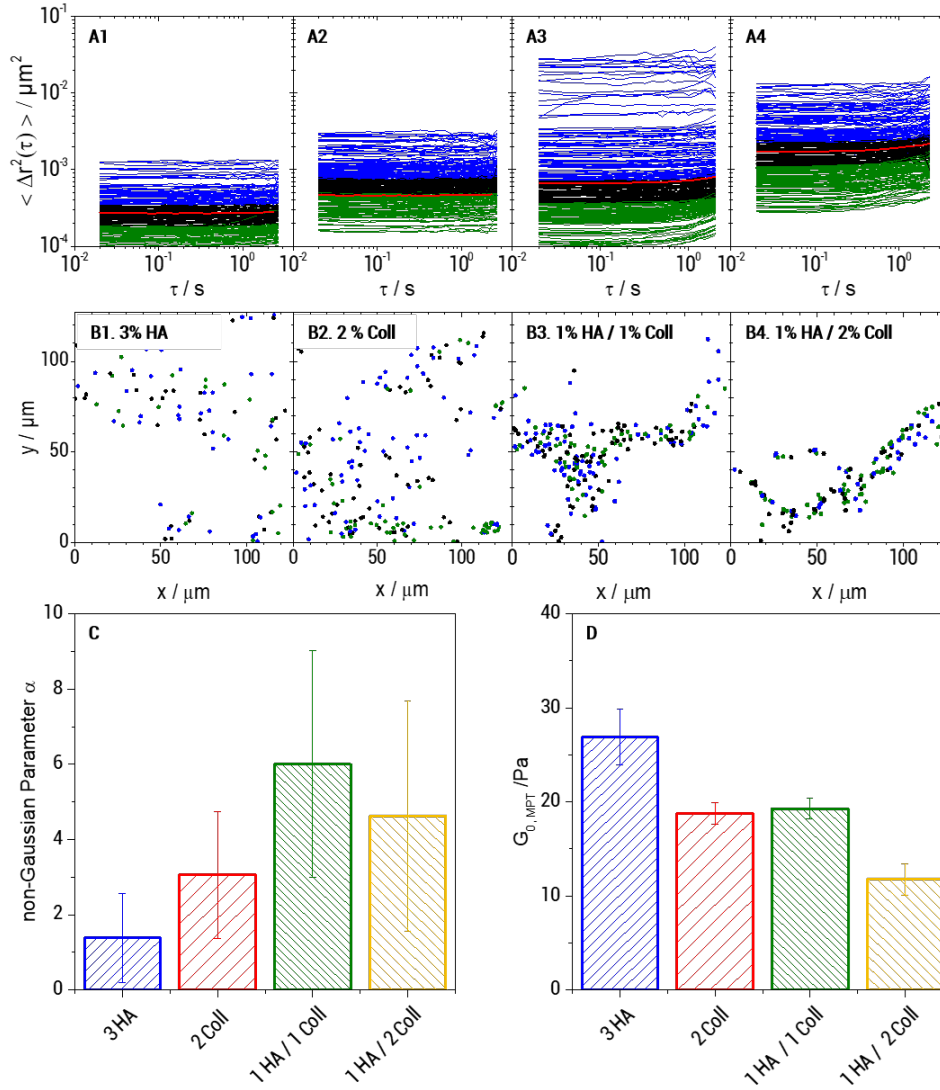


Figure 5.4: Local characterization of HA and Coll scaffolds. MSD plots from MPT measurements (A), corresponding trajectories (B), (color code: blue refers to highly mobile particles (highest third of MSD values), green corresponds to the almost immobile ones (lowest third of MSD values) and black is used for the middle third of MSD values), local heterogeneity characterized in terms of the non-Gaussian parameter α ($\tau = 0.1\text{s}$) calculated for the ensemble of MSDs according to Eq. 5.3 (C): α values were obtained averaging data from 4 videos (~ 200 particles /frame) that were recorded at different localizations of at least two samples of each batch. The given error bars show the standard deviation of corresponding evaluated material parameters, and local storage modulus (D).

Table 5.1: Numerical values of E , $G_{0,bulk}$, $G_{0,MPT}$ and α as for different gel compositions. Values are shown as mean and standard deviation.

	3% HA	2% Coll	1% HA / 1% Coll	1% HA / 2% Coll
E / kPa	1 ± 0.5	11 ± 4	11 ± 3	29 ± 14
$G_{0,bulk}$ / kPa	0.7 ± 0.2	37 ± 8	19 ± 2	75 ± 16
$G_{0,MPT}$ / Pa	27 ± 3	19 ± 1	19 ± 1	12 ± 2
α / [-]	1.4 ± 1.2	3.1 ± 1.7	6.0 ± 3.0	4.6 ± 3.1

individual trajectory according to the MSD's absolute value. Blue color corresponds to highly mobile particles (highest third of MSD values), green color corresponds to the almost immobile ones (lowest third of MSD values) and black is used the middle third of MSD values. Independent of the matrix composition, mobile and immobile particles were homogeneously distributed all over the sample without any pattern and the length scale of heterogeneity was shorter than the mean distance between particles. Finally, we determined the localelastic plateau modulus $G_{0,MPT}$ from the time-independent average MSD ($\tau < 0.3s$) using Eq. 5.2. We found $G_{0,MPT}$ values ranging from 26.9 ± 3.0 Pa for pure HA to 11.7 ± 1.7 Pa for 1% HA/2% Coll. (Fig 5.4D) leading to apparent mesh size ξ_{MPT} values varying between 53 ± 4 nm (pure HA) and 70 ± 7 nm (1% HA / 2% Coll). Note, calculation of $G_{0,MPT}$ is less affected by the strong variation of MSDs than the determination of the heterogeneity parameter α as visible from the smaller relative standard deviations for the former quantity. Most strikingly, the local elastic moduli $G_{0,MPT}$ were much lower (and naturally mesh sizes calculated from these were higher) than the corresponding bulk shear moduli $G_{0,bulk}$ shown in Fig 5.3 consistent with results previously reported for pure HA gels [174]. This might be due to a pronounced contribution of stretched out of equilibrium chain segments between network junctions as observed earlier for keratin networks [182] or due to densely crosslinked areas not accessible for the tracer particles and thus not contributing to $G_{0,MPT}$ but showing up in the bulk modulus. Exposing Collagen to an acidic environment during our sample preparation can lead to a loss of telopeptides [91] resulting in a decrease of the number of ligand binding sites relevant for the molecular packing structure of the Collagen. This might explain the existence of such densely packed molecular structures. This latter hypothesis, however is not consistent with the uniform distribution of tracer particles visible in Fig 1 and in [174]. The ratio $G_{0,bulk}/G_{0,MPT}$ is about 30 times larger for the 2%Coll gel ($G_{0,bulk}/G_{0,MPT} \approx 2000$) than for the 3%HA gel ($G_{0,bulk}/G_{0,MPT} \approx 65$) suggesting that out of equilibrium network strands formed during cryogelation are more important for the stiffer Coll chains than for the highly flexible HA polymers. This effect is even more pronounced for the mixed gels for which $G_{0,bulk}/G_{0,MPT}$ values of 4000 (1% HA/2% Coll) and 700 (1%HA/1%Coll) are found, similar findings were reported for other biomaterials before but not specifically addressed [207]. Table 5.1 summarizes the numerical values of the different mechanical parameters obtained for all investigated gel compositions.

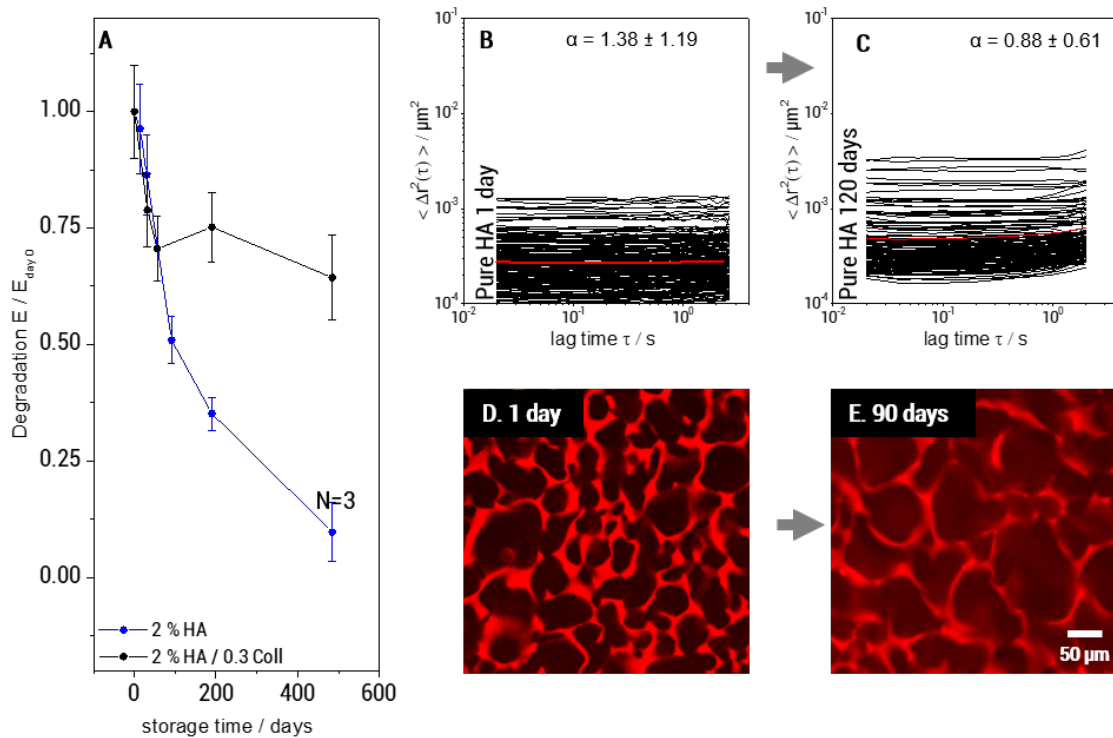


Figure 5.5: Degradation of cryogels. Decrease in Young's modulus over storage time (A), Changes in MSD plots after 1 day (B) and after 120 days (C) and corresponding LSM images of pure HA gels stained with Rhodamine B after 1 day (D) and 90 days (E). The resulting Young's moduli were averaged over three to five samples at each specific point in time. The shown error bars represent the corresponding standard deviation.

5.3.4 Degradability

Scaffolds used for culturing cells should initially support and stabilize the growing tissue. Then they should gradually degrade when the regenerated tissue starts to develop its own mechanical integrity and strength. Information about scaffold degradation kinetics is thus important for a targeted tissue engineering. Fig 5.5A shows the degradation of one component HA and hybrid HA/Coll scaffolds in water at 20°C, expressed in terms of Young's modulus. HA scaffolds degraded almost linearly in time, and after 500 days, E was only 10% of the initial value. For the hybrid scaffold, including additionally 0.3% Coll, the modulus decreases during the first 100 days until it reaches 70% of its initial value. Afterwards it remains constant for up to 500 days, indicating that Coll fibers are less sensitive to degradation by water, than HA polymer networks. Degradation was also investigated using MPT. Fig 5.5B and 5.5C show the variation of MSDs as a function of lag time τ for a 2%HA scaffold after one day and 120 days

immersed in water, respectively. The local plateau modulus $G_{0,\text{MPT}}$, deduced from the average MSD curve decreased by 60% of the initial value from 29 ± 8 Pa to 10 ± 2 after 120 days. Similar experiments on a mixed gel (2% HA / 0.3% Coll) revealed a decrease by only 20% of the initial value from 6.8 ± 3 to 5.4 ± 2 Pa. The strong decrease in $G_{0,\text{MPT}}$, i.e. increase in particle mobility, in the pure HA network is due to the degradation of HA chains and a corresponding decrease in crosslink density. In the presence of Coll, this degradation was much weaker. Apparently, Coll fibers are less sensitive to chain scission. Additionally for aged gels, a slight upward curvature of the MSD plots at high lag times was observed (Fig 5.5C). This viscoelastic response indicates defects in the degraded network. Besides the decrease in gel elasticity, degradation resulted in an increase of the pore size, as shown in Fig 5.5D and 5.5E. The pores of pure HA scaffolds grew from 100 to 300 μm within 90 days in water. In contrast, for the mixed gel (2% HA / 0.3% Coll) no increase in pore size was observed and bulk elasticity was not further affected after 60 days of storage.

5.3.5 Biocompatibility of HA/Coll cryogels

All tested compositions appeared suitable for cell culture. During cultivation of 3T3 fibroblasts for 8 days, viability and cell division rate were both on a high level. As shown in Fig 5.6A, viability investigated after 8 days was slightly higher in HA containing gels ($79 \pm 8\%$ for pure HA gel, $80 \pm 14\%$ for 1%HA/1%Coll and $87 \pm 4\%$ for 1%HA/2%Coll) compared to pure Coll ($66 \pm 2\%$). However, in 1%HA/2%Coll, only few cell division events were observed ($14 \pm 8\%$ EdU positive cells at day 8, see Fig 5.6B). This might be related to insufficient nutrient supply in the denser areas of these heterogeneous gels and this was further supported by the fact that cells settle preferentially close to cracks, because here flow of nutrient media is facilitated. Additionally, as shown in Fig 1, this gel possessed comparably thick pore walls. As cells are said to probe their environment by sensing the force needed to deform structures [60], they might prefer the more homogeneously distributed pores and thinner pore walls in 1%HA/1%Coll mixtures or pure Coll gels. In fact, in pure Coll gel and 1%HA/1%Coll mixtures, investigation of cell morphology (Fig 5.6C, 5.6D and 5.6E) showed that cells spread and adhered well forming confluent layers all over the network structures. Whether the broader pore size distribution (see Fig 5.1) or the increase in heterogeneity of local matrix elasticity (see Fig 5.4E) was responsible for this change, needs to be further investigated. Interestingly, after 3 days of cell culture, pure Coll ($95 \pm 3\%$ live cells, $93 \pm 3\%$ cell division rate) was superior in terms of cell division and viability, compared to all other samples. In pure HA viability and cell division rate ($48 \pm 12\%$ EdU positive cells) were surprisingly high after 8 days. However, overall cell numbers were low, since active cell migration into the pure HA gel was impeded by the lack of adhesive protein patterns. But obviously, appropriate cultivation conditions were available for the few cells that were transported into the gels passively. Those were, as expected because of lacking adhesive structures, not able to spread and stayed in aggregates of up to 50 cells (see Fig 5.6C1, 5.6D1 and 5.6E1). However, the variation in micro- and macro-elasticity of the gels investigated here is too small to explain differences in cell behavior by aspects of mechanotransduction. On macro scale, as well as on microscale, moduli of all tested compositions are in the same range. But the ratio of macro to micro modulus

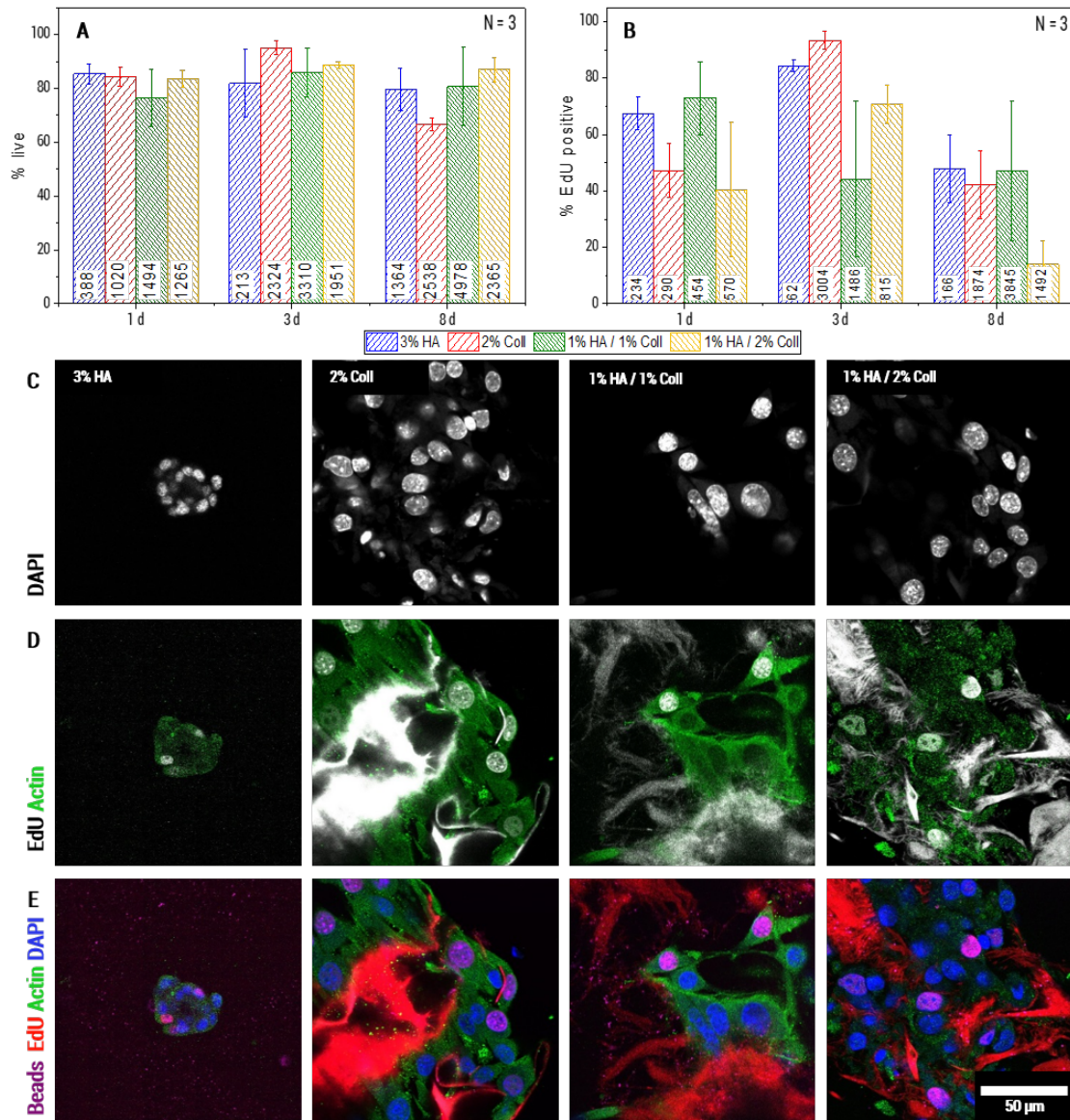


Figure 5.6: Biocompatibility of cryogel scaffolds. Survival rate (A), proliferation rate (B), presented as mean of $N = 3$ independent experiments with standard deviation. Morphology of 3T3 cells cultivated in cryogels for 8d: Cell cores stained with DAPI (C), Actin (green) and EdU positive cells and EdU stained network (gray). Coll I network showed bright fluorescence signal, when stained by the EdU assay used here. In HA only light background fluorescence was observed. (D) and merge of all channels (E).

is significantly different for pure HA gels and Coll containing gels (see section 5.3.3). In order to clarify whether cell behavior is affected by this elasticity ratio, i.e. cells can sense the free energy of their environment or the number of stretched out of equilibrium chain segments between network junctions, additional tests with separate variation of composition and elasticity ratio will be necessary. To conclude, our scaffolds have a high degree of biocompatibility. Coll is, as already known, necessary for cell adhesion and 1% Coll/1% HA is the most attractive gel for cell growth. In terms of long-time proliferation, it might be even more favorable than pure Coll, which is currently used commonly.

5.4 Conclusions

We investigated the influence of Coll concentration on material properties and cell culture suitability of HA based cryogel scaffolds. Firstly, we were able to show that increasing Coll concentrations reduces swelling of porous HA gels, while pure Coll gels do not swell at all, though they are porous as well. The elastic properties of the gels are mainly depending on the degree of swelling, which makes pure Coll gels to appear stiffer compared to pure HA gels with the same overall polymer content. All different types of scaffolds were proven to be suitable for long term culture of fibroblasts and the introduction of Coll improves mimicry of natural ECM and enables cells to adhere to the scaffolds. In 1%HA/2%Coll gels, cells were able to migrate deep into the scaffold and viability as well as proliferation were both satisfying during 8 days of cell culture. Biodegradability of cryogels is drastically reduced when small fractions of Coll are incorporated into HA gels (in vitro, immersed in water). We are able to tailor the mechanical, chemical and degradation properties of macroporous, biobased, bio-functional cryogel scaffolds and their function over persistence time in a wide range by varying the amounts of HA and Coll, crosslinker concentration and process parameters. On microscale, HA and Coll single component gels are both relatively homogeneous, whereas HA/Coll mixtures showed heterogeneity in network elasticity and pore shape. The local elasticities measured by MPT were significantly lower, compared to bulk elastic moduli, which might be related to a contribution of stretched out of equilibrium chain segments between network junctions. Whether cell survival and proliferation are affected by the enthalpic energy density of the surrounding gel mainly contributing to the bulk modulus or by the local thermally excited network response has to be addressed in future research. However, with the results presented in this study, we were able to show, that MPT can help for accurate microscale characterization of complex biomaterials. In order to study the material properties that are sensed by cells, geometrical and micromechanical characterization has to be brought together.

Supporting information

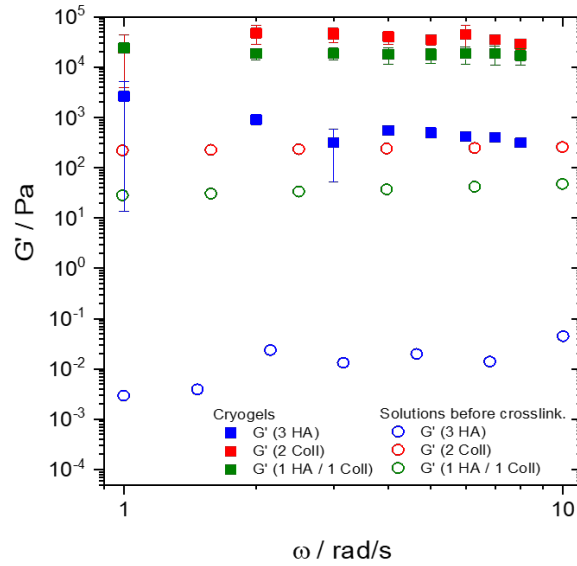


Figure 5.7: Bulk rheological measurements of precursor solutions and cryogels. Frequency sweeps were measured with CP20 (solutions) and PP08 (gels) in the linear viscoelastic regime.

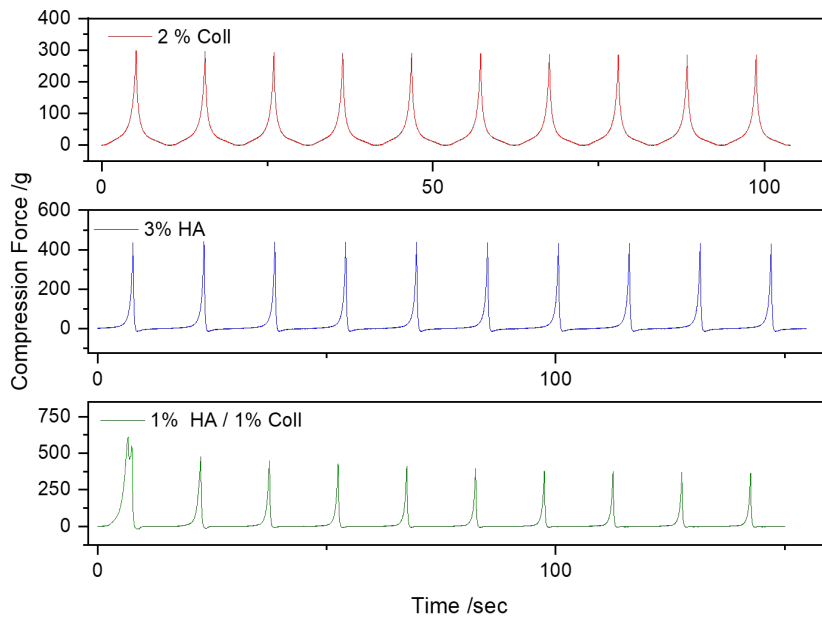


Figure 5.8: Exemplary force vs time plots of multiple strain cycles.

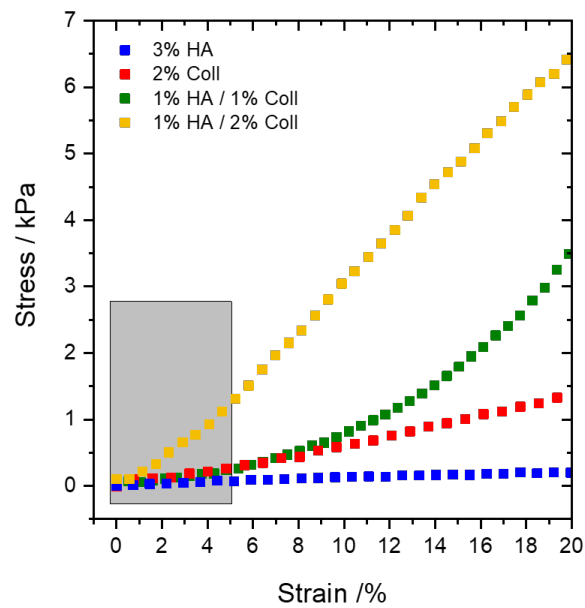


Figure 5.9: Exemplary stress-strain plots resulting from one-time uniaxial compression of cryogel cylinders. Young's moduli were calculated from data on the strain region $< 5\%$, which is highlighted in grey.

Chapter 6

Local elasticity of natural and synthetic ECM

- Full title: Monitoring matrix remodelling in the cellular microenvironment using microrheology for complex cellular systems
- Authors: J. Hafner, D. Grijalva, A. Ludwig-Husemann, S. Bertels, L. Bensinger, A. Raic, J. Gebauer, C. Oelschlaeger, M. Bastmeyer, K. Bieback, C. Lee-The-dieck, N. Willenbacher
- Bibliographic information: Acta Biomaterialia, 115(2020) 254-266
- <https://doi.org/10.1016/j.actbio.2020.04.053>

Abstract

Multiple particle tracking (MPT) microrheology was employed for monitoring the development of extracellular matrix (ECM) mechanical properties in the direct microenvironment of living cells. A customized setup enabled us to overcome current limitations: (i) Continuous measurements were enabled using a cell culture chamber, with this, matrix remodelling by fibroblasts in the heterogeneous environment of macroporous scaffolds was monitored continuously. (ii) Employing tracer laden porous scaffolds for seeding human mesenchymal stem cells (hMSCs), we followed conventional differentiation protocols. Thus, we were, for the first time able to study the massive alterations in ECM elasticity during hMSC differentiation. (iii) MPT measurements in 2D cell cultures were enabled using a long distance objective. Exemplarily, local mechanical properties of the ECM in human umbilical vein endothelial cell (HUVEC) cultures, that naturally form 2D layers, were investigated scaffold-free. Using our advanced setup, we measured local, apparent elastic moduli $G_{0,\text{app}}$ in a range between 0.08 and 60 Pa. For fibroblasts grown in collagen-based scaffolds, a continuous decrease of local matrix elasticity resulted during the first 10 hours after seeding. The osteogenic differentiation of hMSC cells cultivated in similar scaffolds, led to an increase of $G_{0,\text{app}}$ by 100 %, whereas after adipogenic differentiation it was reduced by 80 %. The local elasticity of ECM that was newly secreted by HUVECs increased significantly upon addition of

protease inhibitor and in high glucose conditions even a twofold increase in $G_{0,app}$ was observed. The combination of these advanced methods opens up new avenues for a broad range of investigations regarding cell-matrix interactions and the propagation of ECM mechanical properties in complex biological systems.

6.1 Introduction

Many cellular processes, such as motility, differentiation, adhesion, proliferation and metabolism of cells depend on the mechanical properties of the extracellular matrix (ECM) [38, 55, 57, 58, 86, 96, 135, 149, 206, 234], making a sound mechanical characterization of the cellular surrounding indispensable to ultimately understand and control these cellular processes. However, mechanical properties of artificial ECM substitutes and cell-secreted ECM, such as stiffness and elasticity, may alter continuously due to the impact of the cells, that live within the ECM and constantly control their environment by secreting, organizing, and remodelling matrix molecules. Thus, mechanical properties of the ECM cannot be characterized by one single value. However, knowing the complex alteration of ECM mechanics is crucial for development of artificial ECM substitutes. Furthermore, a better understanding of cell-matrix interactions in artificial and cell-secreted ECM helps us to describe biological processes, such as wound healing, angiogenesis and cancer metastasis. E.g. tumors were shown to be highly sensitive towards mechanical stimuli from their environment and additionally cause rigorous changes in the ECM elasticity [223]. This better understanding can be achieved by monitoring the development of local mechanical properties while cells remodel their surrounding.

Traditionally, the elasticity of ECM substitutes including all types of biobased gels, was characterized in bulk experiments, such as compression and tension tests [19, 30, 35, 142, 198] and oscillatory shear rheometry [3, 17, 18, 96, 214, 217, 234], performed on centimeter sized specimen. These methods characterize cell-laden, potentially porous scaffolds, in some cases even flooded with liquid media with their given heterogeneity as a homogeneous material on a continuum mechanical level. This limits the explanatory power of such methods and neglects cells' sensitivity to the mechanical properties in their direct proximity that raises the need for mechanical characterization on a much shorter length-scale, i.e. less than 200 μm [60, 236].

One potential approach to realize local characterization of mechanical properties is using quartz crystal microbalances, which characterize the elasticity of a nanometer thick surface layer on oscillating gold surfaces by measuring the energy dissipation [151]. Despite the high spatial resolution in vertical direction, horizontally, still the whole sensor surface, including adhering cells, ECM, and surface modifications, is considered or cells need to be removed. The latter can result in altered ECM properties. More precise localization can be achieved by using atomic force microscopy (AFM) and other indentation experiments for the characterization of the local mechanical and structural properties of biomaterials [54, 110, 122, 157, 236, 259, 268] and delicate natural ECM [147, 220, 248]. However, due to the indentation of a small probe, this technique is limited to probing exclusively the surface of a sample.

To circumvent these limitations, microrheology methods, in particular active mi-

rorheology methods, were employed for studying ECM substitutes. In such experiments, micrometer-sized single tracer particles or particle ensembles were placed in the cellular surrounding and their motion was actively triggered by external forces. The resulting displacement was measured, allowing for the characterization of local elasticity. For example optical tweezers were employed for studying the elasticity of ECM substitutes laden with breast cancer cells [223, 228] and for the characterization of ECM elasticity in sprouting angiogenesis [105]. This latter technique has also been used to characterize changes in elastic properties of natural collagen ECM due to cellular contractility [111] and of actin filament networks due to the presence of active motors in the system [161]. It also allowed for the characterization of the heterogeneous microstructure of fibrin-based ECM [119]. Li et al. [137] used magnetic twisting beads that were conjugated to the collagen fibers of the adventitial layer of porcine aortas for studying ECM local elasticity. Another promising optical tweezers based method is nonlinear stress inference microscopy. Using $\sim 5 \mu\text{m}$ particles, this technique was successfully implemented for studying cell-generated stresses capable of buckling filaments in a 3D polymer matrix [80].

A gentler method to study local mechanical properties of delicate biomaterials with respect to heterogeneities on shorter length scales is passive microrheology. In contrast to active microrheology, the driving force is the Brownian motion of the tracer particles themselves and smaller tracer particles can be used. Gambini et al. [67] used such a passive single particle tracking method for studying mechanical properties of jellyfish ECM by microscopying the jellyfish as a whole and Nijenhuis et al. [168] examined the elasticity of the pericellular matrix of chondrocytes by a combined approach of positioning the tracer particle with an optical trap and studying Brownian motion for rheological measurements.

MPT is an advanced passive microrheology technique, which allows for the characterization of the viscoelastic properties sensed by an entire particle collective ($n > 100$). Based on this, local distributions in viscoelasticity and local heterogeneity can be characterized. MPT was initially used for characterization of intracellular elasticity [40, 238] and pericellular matrix layers [242]. To our knowledge, MPT was never used for studying natural macroporous ECM, but in several studies, ECM substitutes were characterized, including the local elasticity of artificial ECM in tumors [102] or in another approach tumor cells were encapsulated in collagen I gels, doped with particles for MPT measurements [103].

A series of MPT measurements at different time-points was used for monitoring the elasticity of special proteinase-cleavable, PEG-based ECM substitutes during several days of cell culture and revealed a decreasing matrix elasticity in the direct surrounding of encapsulated MSCs [45, 208]. The decreasing matrix elasticity was explained with matrix degradation caused mainly by matrix metalloproteinases (MMPs) that were secreted by the cells. Although these approaches delivered a spatially resolved elasticity profile for defined homogeneous materials they possess limitations in terms of the cell surrounding: Cells need to be encapsulated in highly homogeneous PEG-based gels and the number of analyzed particles is still limited.

To overcome these restrictions, we developed a MPT protocol using macroporous collagen scaffolds of pore size $\sim 50 \mu\text{m}$ and pore wall thickness $\sim 5\text{-}10 \mu\text{m}$ [199] on which cells can be seeded conventionally. Cells migrate into the pores until they adhere

to a pore wall and settle there. MPT measurements are thus performed in the narrow pore wall, directly in the surrounding of cells' anchoring sites. Tracer particles of very small diameter, $\sim 0.2 \mu\text{m}$, are used in order to avoid wall effects and not to disturb the gel formation. Furthermore, due to the 3D porous architecture and narrow pore wall thickness, we expect no variation of ECM mechanical properties with distance from the cell surface as well as no disturbing effect of cells contractility. For the gels investigated here, however, MPT does not yield the true bulk modulus of the gel but an apparent modulus. Values calculated from the mean square displacement of tracer particles on the basis of the generalized Stokes-Einstein (GSE) equation are much lower than bulk values (bulk results not shown here, compare [199]). This discrepancy may be due to densely crosslinked areas inaccessible for the tracer particles and thus not contributing to the MPT elasticity, or due to a pronounced contribution of stretched out of equilibrium chain segments between network junctions as observed earlier for keratin networks [182]. However, changes during cell cultivation in the apparent moduli obtained from MPT reflect changes in the mechanical properties of the ECM. Furthermore, we combined the MPT setup with a cell culture chamber, so that continuous measurements could be performed to study the change of ECM elasticity in direct cell surrounding over time.

To validate this setup, 3T3 fibroblasts served as well characterized model system. They appear especially interesting, because maintenance of ECM properties is one key function of fibroblast cells. They are responsible for the production of ECM and its integrity, i.e. they synthesize and secrete ECM components, grouped into (i) proteoglycans and glycosaminoglycans and (ii) structural proteins, e.g. collagens and fibronectin [251]. Additionally, fibroblasts produce several classes of proteases, for example MMPs, which cleave peptide bonds in the ECM [162], as well as the corresponding inhibitors, called tissue inhibitors of metalloproteinase (TIMP) [42]. The balance of both, together with the matrix secretion, regulates ECM composition and its mechanical properties. The underlying metabolism is further regulated by the complex interplay of cell-cell and cell-matrix interactions [155].

While undifferentiated MSCs are expected to maintain and remodel the ECM properties similar to fibroblasts, differentiated MSCs change ECM mechanical properties dramatically.

During osteogenic differentiation, the expression level of collagen I and osteocalcin is increased [255]. With progressive differentiation, the formation of hydroxyapatite and mineralisation of the ECM takes place [48, 189]. In contrast, adipogenic differentiation is characterized by an extensive remodeling of the ECM by proteases [22, 138] and is accompanied by losing cell-matrix adhesion [145]. Enzymatic degradability of the MSC's microenvironment constitutes a prerequisite for adipogenesis as well as osteogenesis [113]. Therefore cell-matrix engineering demands a thorough understanding of cell-matrix interactions and corresponding cellular traction force change over time.

Surprisingly, the effect of cell differentiation on local matrix elasticity was never studied before, although studying the local mechanical properties of ECM substitutes and of the ECM itself appears as a very urgent question, not only in biomaterials design and cell biology, but also to uncover new therapeutic strategies. Thus, we employed MPT to study the effect of chemically induced MSC differentiation on ECM mechanical properties in 3D scaffolds.

In contrast to stromal cells forming 3D tissues, endothelial cells (ECs) are known to naturally form continuous monolayers lining the interior surface of blood vessels. For understanding their matrix elasticity, 2D models appear much more relevant than 3D studies. Consequently, we used HUVEC cells as an easily accessible model for ECs to show that MPT is even suitable to study the local elasticity of newly secreted ECM in scaffold-free 2D cell cultures.

ECs maintain a non-thrombogenic surface to facilitate blood flow and besides, they regulate the exchange of gases, nutrients, and metabolic waste between the plasma, and the interstitial spaces. In microvessels, endothelial cells can be mobilized to proliferate and migrate in response to angiogenic signals, including mechanical cues generated by the sub-endothelial ECM [75, 151, 211, 225]. The remodelling of endothelial ECM is regulated by MMP activity. Hence, we verified this novel 2D approach by investigating the local elasticity of ECM, newly secreted by HUVECs with and without additional protease inhibitor.

In this study, we present a proof of principle for applying MPT to study local ECM elasticity. We were able to determine local shear moduli in the direct proximity of living cells and on a length scale that is relevant for cells mechanosensing. We showed the suitability and biocompatibility of the method for three different applications, namely continuous remodelling of ECM in 3D by fibroblasts, change of ECM elasticity during differentiation of hMSCs in 3D and elasticity of newly secreted HUVEC ECM in 2D.

6.2 Materials and Methods

6.2.1 2D and 3D cell culture and differentiation

Scaffold preparation for 3D cell cultures

3D scaffolds were prepared as described previously [199]. In brief, 2 wt% HA (Hyaluronic acid; Contipro, Czech Republic) were dissolved in 1 % NaOH and stored for 16 h at 4°C; 4 wt% Coll (Collagen I; fibrous powder from bovine tendon, Advanced Biomatrix, USA) were dissolved in 5 mM acetic acid by continuous stirring for 24 h. Blending this with the same amount of 1 % NaOH yielded a 2 wt % Coll solution. For hybrid scaffolds (1 wt% HA and 1 wt% Coll), 2 wt% HA and 2 wt% Coll precursor solutions were blended 1:1. In both compositions, 0.7 wt% Ethylene glycol diglycidyl ether (EGDE) was added as chemical crosslinker. The resulting solutions were poured into cylindrical molds and frozen at -20°C for 6 days to allow cryogelation. The resulting microporous gels were thawed, subsequently swollen in water and washed with PBS (Phosphate Buffered Saline, PAN Biotech).

3T3 fibroblast cells for monitoring ECM degradation and viability in 3D gels

After washing the gels, they were placed in 12-well plates, washed with DMEM (Dulbecco's Modified Eagles Medium, PAN Biotech), supplemented with 10 % FCS (Fetal calf serum, PAN Biotech) and immersed in DMEM/FCS. Cells were passaged according to a routine protocol and cultivated under standard conditions (37°C , 5 % CO_2 ,

90 % rel. humidity).

NIH-3T3 fibroblasts were transfected with LifeAct RFP using an electroporation protocol. In brief, the pellet was washed twice and resuspended in ice-cold electroporation buffer (consisting of 120 mM KCl, 10 mM K_2HPO_4/KH_2PO_4 , pH 7.6, 2 mM $MgCl_2$, 25 mM HEPES pH 7.6 and 0,5 % Ficoll 400 in ddH₂O). The electroporation was performed in a 0.4 cm cuvette according to the experimental protocol (250 V/ 950 μ F) with a BioRad electroporator. The cells were recovered on ice and subsequently seeded in supplemented culture medium.

For seeding, cells were detached using 0.25 % trypsin/EDTA (ethylenediaminetetraacetic acid) in PBS and suspended in supplemented medium. Cells were seeded onto the gels at a density of 75 000 cells per gel (235 mm³). Initially, they were allowed to settle without additional medium for 30 min at 37°C. Later, 2 ml medium were added and the cells were cultivated for 8 days. All supernatant medium was exchanged every second day. Live/dead assay was performed with non-transfected cells to avoid interference of the fluorescence signals. After 1, 4 and 8 days of cultivation, 0.5 μ l Calcein (Thermo Fischer Scientific, 4 mM in DMSO (dimethyl sulfoxide) and 2 μ l Ethidium homodimer (Thermo Fischer Scientific, 2 mM in DMSO/water) were added directly into the 2 ml nutrient medium in separate wells for each time point. Calcein and Ethidium homodimer were applied at a final concentration of 0.25 and 1 μ l/ ml medium, respectively. After incubation for 15 min, at least 5 Laser Scanning Microscope (LSM; LSM 500, Zeiss) images were recorded during 15 min. In all images, living and dead cells were counted and the count was averaged for all images corresponding to one time point. All experiments were done in triplicate. For each biological replicate, gels from a newly synthesized batch were used.

hMSC culture for monitoring ECM remodeling during differentiation in 2D and 3D

Human bone marrow-derived MSCs (kindly provided by Prof. Dr. Karen Bieback, German Red Cross Blood Service Baden-Wuerttemberg/Hessen, Mannheim) were seeded in a density of 2000 cells/cm² on TCP (tissue culture plastic) and cultured in DMEM high glucose (Sigma-Aldrich) with 5 % human platelet lysate (PL; PL Bioscience, Aachen) and 2 U/ml heparin (PL Bioscience) under standard cell culture conditions (37°C, 5 % CO₂). Cells were subcultured at \approx 80 % confluency and passages 2 to 6 were used for the experiments. For seeding hMSCs into 3D scaffolds, cells were washed with PBS and detached using trypsin/EDTA solution (0.05/0.02 wt%, Sigma-Aldrich). After 5 min at 37°C, the trypsinization was stopped by addition of DMEM with 10 % FCS (Sigma-Aldrich). The cells were then centrifuged and resuspended in DMEM with 5 % PL and 2 U/ml heparin. Finally, the highly concentrated cell suspensions were seeded onto 3D scaffolds (1 wt% HA / 1 wt% Coll) to final densities of 32×10^4 and 16×10^4 cells/118 mm³ for adipogenic and osteogenic differentiation, respectively. After allowing settlement of the cells in the gels for 15 min at 37°C, the total amount of medium was adjusted with DMEM, supplemented with 5 % PL, 2 U/ml heparin and 100 U/ml penicillin and 100 μ g/ml streptomycin (Sigma-Aldrich) to 500 μ l/well.

Adipogenic and osteogenic differentiation of hMSCs

After the initial 24 h of cell cultivation, the medium was removed and replaced by 500 μl adipogenic induction medium (MSC Adipogenic Differentiation Medium 2, Promocell) with 100 U/ml penicillin and 100 $\mu\text{g}/\text{ml}$ streptomycin (Sigma-Aldrich) to induce adipogenic differentiation. Osteogenic differentiation, hence, was induced by 500 μl osteogenic induction medium (MSC Osteogenic Differentiation Medium, Promocell) with 100 U/ml penicillin and 100 $\mu\text{g}/\text{ml}$ streptomycin (Sigma-Aldrich) per well. Control samples with the respective cell count were further on cultured in DMEM with 5 % PL, 2 U/ml heparin and 100 U/ml penicillin and 100 $\mu\text{g}/\text{ml}$ streptomycin (Sigma-Aldrich). For all conditions, the medium was changed twice per week and cells were cultured for 21 days.

HUVEC cell culture for monitoring ECM remodeling in 2D

HUVECs were isolated as described previously [21] after having obtained informed consent and transfected with a lentiviral vector to express dTomato. The cells were cultured using Endothelial Cell Growth Medium 2 (Promocell) supplemented with penicillin/streptomycin. For MPT measurements HUVEC were seeded in 24-well plates (Nunc, Thermo Fischer Scientific) with a density of 7500 cells/cm². Every second day, medium was changed completely. For the protease inhibitor conditions, the medium was supplemented with 1 $\mu\text{l}/\text{ml}$ or 5 $\mu\text{l}/\text{ml}$ Halt protease inhibitor cocktail (Thermo Fischer Scientific). The control condition was kept in culture medium. For the high glucose condition, simulating high blood glucose in diabetes, the medium used for the whole cultivation, was supplemented with 100 mmol/l glucose, according to WHO's diagnostic criteria for diabetes ≥ 7.0 mmol/l fasting plasma glucose [260]. After 48h the culture medium was aspirated and replaced with PBS containing MPT particles.

6.2.2 Characterization of local viscoelastic matrix properties using MPT

MPT in general

The underlying principles and fluid mechanics of MPT microrheology have been described in detail [68, 252]. In brief, the Brownian motion of inert colloidal probe particles embedded in a material is monitored. Thereby, quantitative information about the rheological properties of the surrounding fluid is obtained [154] based on a fundamental relationship between tracer mean square displacement (MSD) as a function of lag time τ and the complex shear modulus $G^*(\omega)$ as a function of the frequency. The Laplace transform of the particle MSD is related to the complex modulus G^* of the sample via a generalized Stokes-Einstein equation (GSE, general form, see Eq 1) [153, 262]:

$$G^* = \frac{2k_B T}{3\pi a i \omega \langle \Delta r^2(i\omega) \rangle} \quad (6.1)$$

a stands for the radius of the embedded beads, k_B for the Boltzmann constant and T for the temperature. This GSE relation is valid in 2D under the assumption that

the material surrounding the tracer particles can be treated as an isotropic and homogeneous continuum, i.e. that the particle size is larger than the structural length scales of the probed material. Furthermore, tracer particle and fluid inertia need to be neglectable, which is appropriate here, since Reynolds number and Stokes number both are well below 1. For 2D tracking of beads suspended in an ideal elastic material, Eq 6.1 reduces to Eq 6.2 [98, 262]

$$G_0 = \frac{2k_B T}{3\pi a \langle \Delta r^2(\tau) \rangle} \quad (6.2)$$

where G_0 stands for the frequency independent shear modulus of the material. As confirmed by the time independency of the MSDs (at $\tau = 0.1$ s, all materials investigated here, behave like elastic solids. As the collagen gels considered here are heterogeneous materials, MPT does not yield the true bulk modulus, thus G_0 is termed apparent modulus $G_{0,\text{app}}$ in the following. In the first step of MPT evaluation procedure, all particle trajectories are represented in a trajectory plot. Trajectories of freely diffusing particles cover a larger area compared to trajectories of elastically trapped particles, that are more restricted in their motion. Furthermore, areas in which no particles were present throughout the whole measurement can be identified. Then from these trajectories, the coordinates of the particle centroids were transformed into MSD traces. Time independent MSDs correspond to elastically trapped particles, whereas for freely diffusing particles, a linear increase over lag time τ is expected. Complex polymer materials often yield ensembles of MSDs including tracers of both limiting cases, and often also curved MSDs representing diffusion in a viscoelastic environment. Thus, the variation of obtained MSDs in one measurement provides insight into the heterogeneity of the material within the field of view ($127 \times 127 \mu\text{m}$). In order to characterize the material heterogeneity often the Van Hove correlation function [241] is used and the non-Gaussian parameter α is calculated [256]. This parameter describes the derivation of the MSD values from a Gaussian distribution expected for an ideal homogeneous uniform sample ($\alpha = 0$) at a fixed lag time τ . Real fluids with $\alpha \leq 1$ are considered homogeneous on the probed length scale typically ranging from 0.1 to 1 μm . For image analysis, the software Image Processing System (Visiometrics iPS, Visiometrics GbR, Germany) was used and the calculation of MSDs and moduli was performed using a self-written Matlab code [98, 241, 256, 262]. The evaluation routine is described in more detail in [113].

MPT in 3D scaffolds and 2D cell culture

For MPT in porous gels, the inverted fluorescence microscope (Axio Observer, Carl Zeiss, Germany, see Fig. 6.1A) was equipped with a high precision objective (Fluar 100x, N.A. 1.3, working distance 0.17 mm, Carl Zeiss). Images were recorded using a sCMOS camera Zyla X (Andor Technology, Ireland: 21.8 mm diagonal sensor size, 2160×2160 square pixels). We have also determined the so-called static error χ as described by Savin et al. [204] for our experimental setup. This quantity corresponds to the apparent random motion of particles due to the noise of the camera and digitization effects. It has been evaluated by fixing tracer particles on a substrate, and by

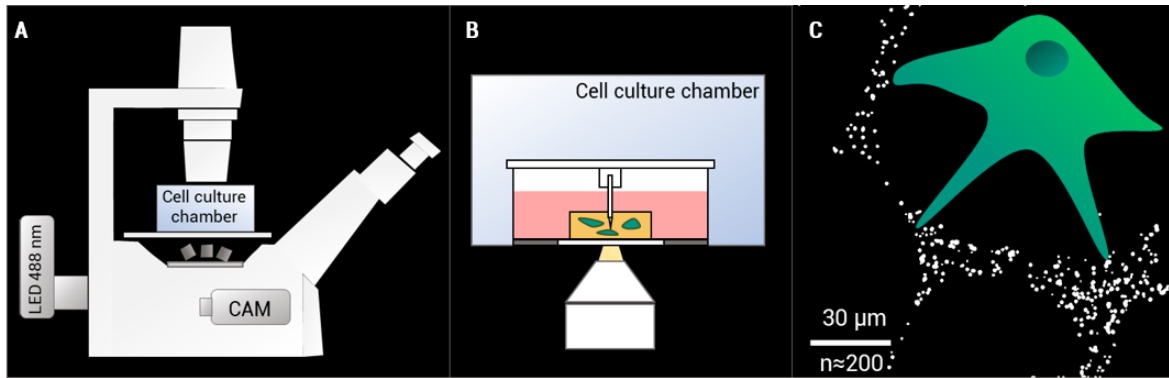


Figure 6.1: Schematic of our Live Cell MPT setup used to monitor the change in ECM viscoelasticity in the surrounding of 3T3 fibroblasts cultured in porous 2 wt% Coll scaffolds: A) Sketch of the used experimental setup consisting of an inverted fluorescence microscope, equipped with a colored light source (LED), a high speed camera (CAM) and a high magnification objective. B) close-up of the cell-culture chamber, in which cell-laden gels are investigated in a glass-bottom petri dish. The needle avoids motion of the scaffold, while it is immersed in fluid. C) Resulting field of view showing a cell in the porous scaffold with tracer particles embedded in the pore walls.

performing measurements under similar noise and signal conditions as for the rest of the experiments. The static error for the experimental setup and tracer particles used here was $\chi \sim 10^{-4} \mu\text{m}^2$ and defined the lower limit of accessible MSD. Non-functionalized, surfactant stabilized polystyrene microspheres of diameter $0.2 \mu\text{m}$ (Bangs Laboratories, USA) were added together with EGDE during gel preparation [199] and the gels were placed in glass bottom petri dishes (Cell E&G, #GBD00004-200) or on conventional glass slides (Carl Roth, #1) see Fig. 6.1B).

Fibroblasts and HUVECs were located by their actin cytoskeleton which showed red fluorescence after transfection with LifeAct RFP. For the localization of MSCs, a cell plasma membrane staining kit (orange fluorescence Cytopainter, Abcam) was used. This allowed us to localize the spatial expansion of the cells without fixation. In Fig. 6.1C, an exemplary field of view with a cell (scheme) and particles embedded in the surrounding pore walls of a hydrogel is shown. With our setup the thermal motion of tracer particles in the vicinity of cells located in a depth of about $20 \mu\text{m}$ within the porous scaffolds was investigated. The depth of focus was $0.3 \mu\text{m}$ according to the specifications of the objective given by the manufacturer, i.e. we essentially performed a 2D tracking. In our so called LiveCell MPT experiments (see Fig. 6.1), only tracer particles in the direct environment of single living cells, well embedded in the scaffolds, were considered. We used this setup for two different experiments:

(i) A series of discontinuous measurements was performed at room temperature. For each point of time and each condition, at least 6 sets, corresponding to 6 different locations in the scaffold, were recorded within 5 min operating time and analyzed subsequently. For each experiment, 3 biological replicates were investigated.

(ii) Continuous measurements were performed monitoring the same field of view/the same living cell at all time points. The seeded scaffold was therefore kept in cell culture

conditions using a cell culture chamber (Pecon CTI controller 3700). The measurement was started after adding the final amount of medium during the seeding protocol, the subsequent measurements were performed hourly for the first 8 hours after seeding. The shown values are thus single values determined in the surrounding of one and the same single cell.

In 2D cell cultures, MPT measurements were performed directly in the well plates, using a long distance objective (LD EC Epiplan neofluar 100x0.75 DIC, N.A. 0.75, working distance 4 mm, Carl Zeiss). To enhance the fluorescence signal, tracer particles with diameter $0.96\ \mu\text{m}$ were used and these were added to the media 15 min prior to the measurement, yielding a final particle concentration of 0.017 wt%. All measured values are shown as mean of 3 independent biological replicates with standard deviation. Differences between groups were tested with one-way ANOVA (performed in Origin(Pro), Version 2019b, OriginLab Corporation, Northampton, USA) and considered significant if $p \leq 0.05$.

The section below summarizes the statistical analysis of the MPT experiments. For gels with fibroblasts (section 6.3.1, Fig. 6.2C), MPT experiments were performed in triplicate and for each measurement, at least 6 sets of images corresponding to 6 different locations in the gel were considered. Results shown in Fig. 6.3 refer to a single MPT experiment for each point in time. For gels including hMSC cells (section 6.3.2, Fig. 6.4A), all values are shown as mean of 3 independent biological replicates with standard deviation. For ECM secreted by HUVECs (section 6.3.3, Fig. 6.5C), averaged apparent moduli resulting from 2 biological replicates with 6 sets each, are shown as function of frequency. Error bars indicate standard deviation.

Rotational rheometry

The bulk viscoelastic properties of cell-laden gels and cell-free controls were characterized through their storage modulus G' and loss modulus G'' as a function of frequency. Measurements were performed using a rotational rheometer (Physica MCR501, Anton Paar) with a plate-plate geometry (diameter 8 mm). Gap height was adjusted between 1 and 2 mm depending on the height of the samples, swollen in DMEM/FCS, to adjust the normal force to $0.15 \pm 0.05\ \text{N}$. For all conditions, frequency sweeps were performed in the linear regime at a stress amplitude of $\tau = 0.5\ \text{Pa}$, covering the frequency range of 0.1 to 10 rad/s. No evidence of wall slip was found in preliminary experiments performed at different gap heights. Modulus data provided below are a mean of two independent measurements.

6.2.3 Proof of hMSC differentiation by staining

Von Kossa staining

Osteogenic differentiation was visualized by von Kossa stain. Hereby, the phosphate ions in mineralic components, characteristic for the ECM in osteogenic differentiation, are precipitated with silver ions, so that hydroxyapatite and calciumphosphate depositions appear black. After being cultured for 3 weeks, 2D cell cultures were fixed with 10 vol% formaldehyde (Applichem) for 15 min, subsequently washed with ddH₂O

and stained with 5 wt% silver nitrate solution (Merck, Darmstadt) for 15 min. Thereafter, samples were washed with ddH₂O and incubated in 1 wt% Pyrogallol (Merck) in dark for 2 min. The staining was then washed with ddH₂O and fixed with 5 wt% sodium thiosulfate for 5 min followed by a last washing step with ddH₂O. Optical images were obtained using an inverse fluorescence microscope (Axio Vert A1, Carl Zeiss, Oberkochen) and a camera (Axiocam Cc1 60N-C1“1.0x camera, Carl Zeiss).

Oil Red staining

For the visualization of adipogenic differentiation in 2D after 3 weeks of culture, fat vacuoles were stained by Oil Red. After cell fixation in 10 vol% formaldehyde and washing with ddH₂O, 60 vol% isopropanol (VWR) were added and incubated for 2 min. Oil Red O (Sigma-Aldrich) working solution was prepared from a 0.3 % (wt/vol) Oil Red stock in isopropanol by diluting this 3:2 with ddH₂O. The final concentration was 0.18 % (wt/vol) and remaining solids were removed by centrifugation. 250 μ l of the staining solution were added per well and incubated for 5 min. Subsequently, the samples were washed with tap water, until clear supernatant was obtained. Cell nuclei were stained purple with hematoxylin solution, Harris modified (Sigma-Aldrich) for 2 min. After a final washing with tap water, images were taken using an inverted fluorescence microscope (Axio Vert A1, Carl Zeiss, Oberkochen) and a camera (Axiocam Cc1 60N-C1“1.0x camera, Carl Zeiss).

6.3 Results and Discussion

6.3.1 Continuous monitoring of matrix degradation by fibroblasts

Fibroblasts are known to remodel their environment extensively by secreting proteinases that degrade collagen-rich matrix structures. We used for the first time MPT to characterize the effect of fibroblast growth on the local viscoelastic properties of a HA/Coll scaffold in the direct cell surrounding. In a first approach, this effect was monitored during 8 days of cell culture by investigation of the scaffolds local mechanical properties with MPT experiments directly after cell seeding and after 1, 4 and 8 days of cell cultivation. Per time point, 9 experiments were performed, i.e 9 fields of view were investigated. Thus, the mechanical properties were characterized on a length scale of one field of view ($127 \times 127 \mu\text{m}$) for the setup shown in Fig. 6.1) and the $G_{0,\text{app}}$ values for all cells in a cell population were averaged. Fig. 6.2A and B show the variation of MSDs as a function of lag time for tracer particles (diameter = $0.19 \mu\text{m}$), dispersed in the matrix of 1 wt% HA / 1 wt% Coll cryogel scaffolds directly after cell seeding and after 4 days of culture, respectively. In both cases, all MSD traces exhibit almost no time dependence in the investigated lag times (τ in s) and their absolute values show a narrow distribution within 1.5 decades. Consequently, the non-Gaussian parameter α is ≤ 1 . These results indicate that the tracer particles are at all time points (culture time in days) trapped elastically in a homogeneous, gel-like network. However, the mean MSD (shown as colored line in Fig. 6.2A and B) increased from

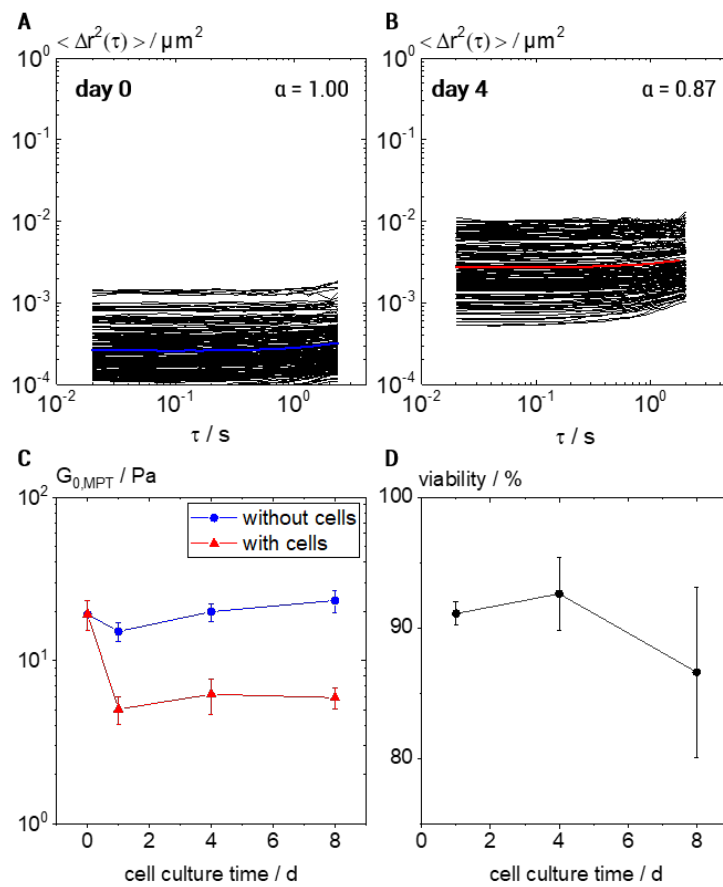


Figure 6.2: Degradation of 1 wt% HA / 1 wt% Coll scaffolds by 3T3 cells: A) MSD plots resulting from MPT video sequences, recorded directly after seeding (day 0) B) and after 4 days of cell culture. C) Plateau modulus $G_{0,\text{app}}$ over cell culture time for scaffolds with and without cells, determined from at least 6 independent measurements per condition and D) Cell viability, measured from 10 images per time point

$\approx 2.5 \times 10^{-5}$ directly after seeding to $\approx 3 \times 10^{-3} \mu\text{m}^2$ after 4 days of cell cultivation. This indicates a reduction in matrix stiffness, corresponding to a decrease of the elastic plateau modulus.

Fig. 6.2C shows the evolution of the matrix stiffness over the entire 8 days of cell cultivation. The elastic plateau values obtained from MPT measurements after 0, 1, 4 and 8 days with (red) and without cells (blue) are shown. In the cell-laden scaffolds, a strong decrease of the scaffolds' stiffness was observed within the first day. $G_{0,\text{app}}$ decreased from 19.2 ± 4.0 to 5.2 ± 1.3 Pa (see Fig. 6.2C) as calculated from the average value of the resolved lines in Fig. 6.2A and B according to Eq 6.2. This decrease in matrix stiffness in the direct cell surrounding results presumably from the fibroblasts remodelling the ECM by upregulating proteinase activity to design matrix elasticity according to their current needs [1]. A disturbing effect of cells contractility on MPT measurements of ECM mechanical properties can be excluded here since similar elasticity values were obtained for scaffolds with and without cells (see Fig. 6.2C, cell culture time 0 h). During the following days, $G_{0,\text{app}}$ remained constant at a value of 6 ± 2 Pa till day 8. In contrast, the elasticity of cell-free scaffolds was almost constant during the entire experiment with $G_{0,\text{app}}$ ranging between 18 and 22 Pa which indicates that no degradation took place. This confirms furthermore, that the decrease in matrix stiffness is not related to any chemical modification or enzymatic degradation due to the reaction with cell culture media components, but caused by the metabolic actions of the cultured cells.

This change in local viscoelasticity near the embedded cells does not show up in bulk shear modulus measurements. $G_{0,\text{bulk}} \approx 21$ kPa remains constant for the entire duration of the experiments and no difference between gels with or without cells can be detected. It should be noticed that the bulk modulus $G_{0,\text{bulk}}$ is about three orders of magnitude higher than $G_{0,\text{app}}$. This was observed for various other biomaterials [182, 207]. For the scaffolds used here, it is discussed in [199] in more detail.

MPT resolves the mechanical properties locally on a length scale that is relevant for cells' mechanosensing [60, 220]. The viability of the fibroblasts (see Fig. 6.2D) is > 85 % during the whole experiment, i.e. the observed changes in the matrix elasticity are related to the metabolic activity of a healthy population of fibroblasts. A high number of apoptotic cells might cause additional weakening of the matrix due to secretion of large amounts of intracellular enzymes, but this is not the case here.

As we have seen in Fig. 6.2C, the degradation of the scaffold mainly takes place within the first day. This important initial period of time was further investigated in a second approach, using a novel MPT setup including a cell-culture chamber (see Fig. 6.1). Using this, we were able to monitor the matrix elasticity in the direct surrounding of one single cell during the first 9 h after seeding. Fig. 6.3A shows the overlay of the fluorescence signal resulting from the actin cytoskeleton (red) and from the tracer particles embedded in the surrounding pore walls (green). The images were obtained by using the inverted fluorescence microscope of the MPT setup, where background fluorescence and blur, especially in the red channel, cause large shadows and the resolution in depth is limited. For verifying characteristic, healthy fibroblast morphology, a 3D image obtained from LSM is shown in Fig. 6.3B. In MPT experiments, the red fluorescent cytoskeleton still helps to localize the cells in the 3D scaffold. LSM is, however, not suitable for MPT experiments, due to the long scanning times. For

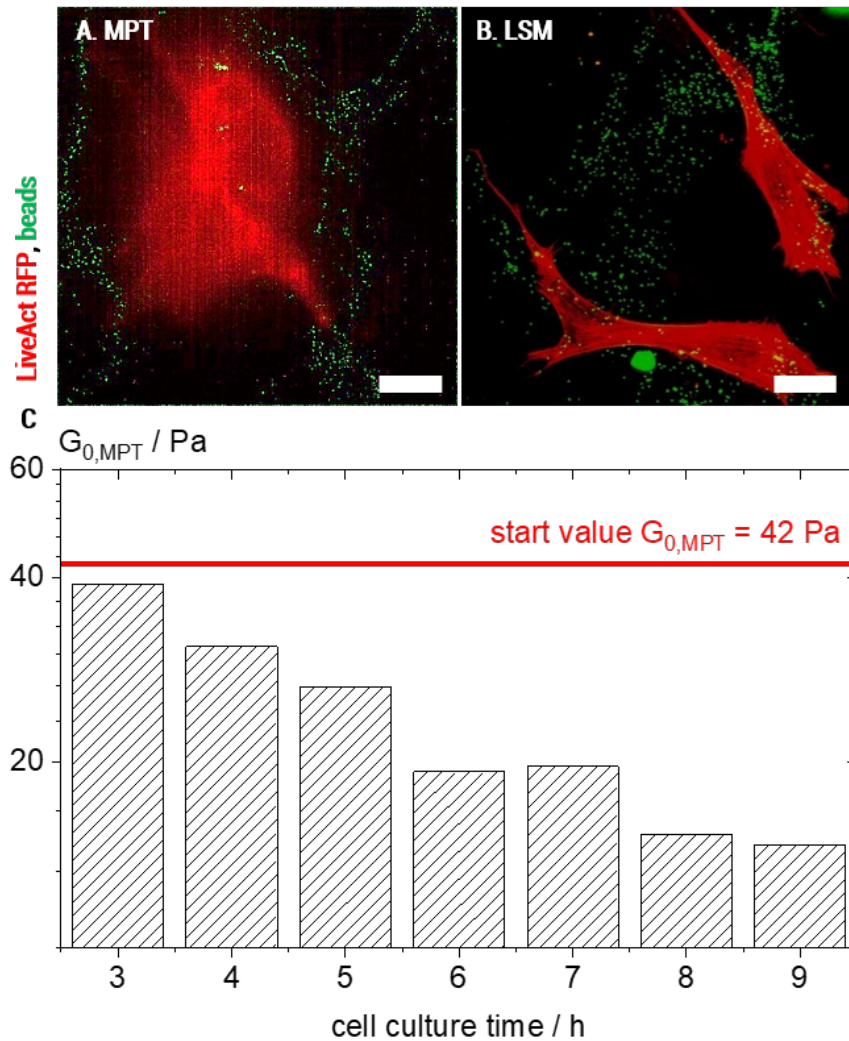


Figure 6.3: Continuous LiveCell MPT: A) Microscope image, taken with the inverted fluorescence microscope (555 and 488 nm colored LED) and high speed camera of the MPT setup, showing MPT tracers distributed in the 2 wt% Coll scaffold matrix (green) and the actin cytoskeleton of the imaged 3T3 cell (transfected with LifeAct RFP, red) and B) same scaffold visualized using LSM and C) time evolution of $G_{0,app}$ in the direct cell surrounding of an individual living 3T3 cell.

evaluating mechanical properties, the Brownian motion of the tracer particles is in focus and therefore, after recording the 555 nm signal initially, MPT videos for data evaluation are taken with the 488 nm light source only, to reduce noise. Between the single video recordings, cells were kept in the dark and only for the measurement, the light source was switched on. Fig. 6.3C shows the gradual reduction of matrix stiffness in the direct environment of the investigated single cell through the variation of the plateau modulus $G_{0,\text{app}}$. Starting from 42 Pa, measured immediately after seeding, a continuous decrease in $G_{0,\text{app}}$ is observed within the following 9 h, yielding a final value of 15 Pa. This ratio of final to initial modulus is in good accordance with the averaged results obtained for a whole population of fibroblasts, shown in Fig. 6.2. Consequently, this single cell, as well as all other cells considered in the aforementioned experiments, continuously decreased the elasticity of the scaffold in their direct surrounding, most likely by upregulating MMP activity [66]. These enzymes are known to cleave peptide bonds in e.g. collagen structures. *In vivo*, the enzymatic activity of MMPs underlies a complex regulation cycle, including the availability of MMP inhibitors, which helps the cells to maintain the mechanical properties of their ECM [66]. In 3D scaffolds, however, cells need to remodel the scaffolds provided to them. Most likely, the observed continuous decrease is driven by the discrepancy between the stiff scaffolds provided and the desired softer ECM the cells try to achieve by degrading the artificial ECM. Followingly, upregulating MMP expression in cells seeded on stiffer scaffolds is already shown in other studies [82, 263] and could be one explaining mechanism to adjust the given scaffold by the cells in our study. Processes like this can be elucidated in more detail and on shorter time scales, referring to one single cell by combining the MPT setup with a cell culture chamber.

6.3.2 ECM mechanics after adipogenic and osteogenic differentiation in 3D

In vivo, MSCs differentiate according to current needs, e.g. responding to exercise or regenerating connective tissue in order to compensate lacking cells [28]. During differentiation either into the osteoblast or the adipocyte lineage, their phenotype is completely changed, including metabolic function and the ability to build up completely different tissues [28, 114]. The mechanical properties of such tissues depend on the stiffness of the cells and, especially in ECM rich tissues, on the mechanical properties of the ECM connecting the cells [220, 249].

Using adipogenic and osteogenic differentiation inducing media in 3D hMSC cultures based on 1 wt% HA / 1 wt% Coll scaffolds, we studied the mechanical properties in the cells' environment after terminal differentiation into adipocytes and osteoblasts, respectively. In Fig. 6.4, the local plateau modulus, obtained from MPT measurements in the scaffold-network, is shown for cell-laden and cell-free samples. After 21 days of cell culture, in the adipogenic differentiation medium (Adip), a difference in $G_{0,\text{app}}$ of ≈ 19 Pa was found between cell-laden (3.8 ± 0.8 Pa) and cell-free scaffolds (22 ± 4 Pa). The same initial cell count in MSC maintenance medium (DMEM, control) yielded a similar decrease of ≈ 22 Pa in the cell-laden scaffold (10.1 ± 0.9 Pa) compared to the cell-free control (32 ± 13 Pa). Under both conditions, the scaffold elasticity is

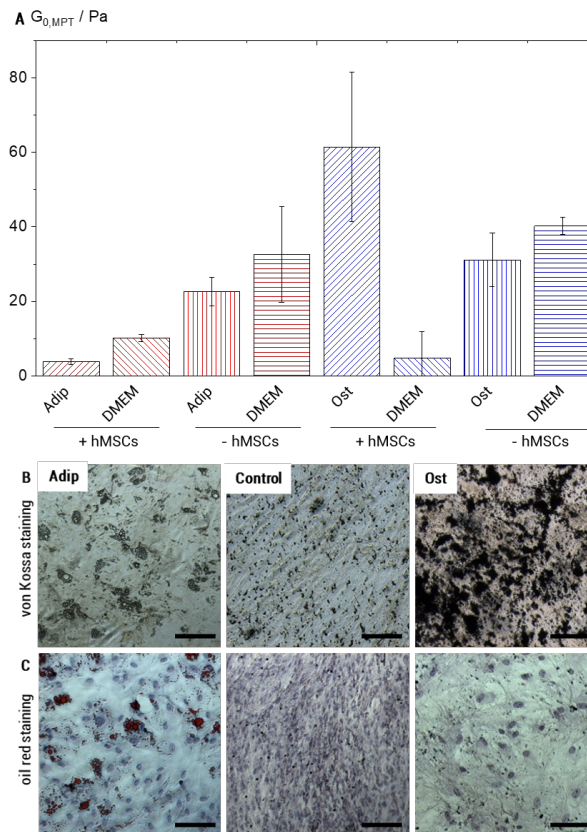


Figure 6.4: MPT as versatile tool to monitor matrix mechanics during cell differentiation in 3D scaffolds: A) $G_{0,app}$ in the direct cell environment, measured for MSCs cultured for 21 days in adipogenic differentiation medium (Adip), osteogenic differentiation medium (Ost) and respective cell densities cultivated in control medium (DMEM). Corresponding data for empty gels (- hMSCs) are shown for comparison and cell-laden scaffolds are labeled accordingly (+ hMSCs). All measured values are shown as mean of 3 independent biological replicates with standard deviation. B) Visualization of hydroxyapatite formation in the ECM during osteogenic differentiation by von Kossa staining (black) of adipogenic, control and osteogenic condition and C) Visualization of oil vesicles (red) by Oil Red staining of adipogenic, control and osteogenic condition. Nuclei are stained in blue. Images are obtained in 2D, all scale bars represent 100 μm .

reduced by the cells, but it is worth considering the difference in cell numbers. Continuous proliferation in DMEM should result in much higher cell numbers compared to low proliferation rates during adipogenic differentiation. Thus, the decrease of G_0 in adipogenic condition is caused by a presumably much smaller number of cells than in the control condition, so that the scaffold-softening effect per cell can be considered to be stronger during adipogenic differentiation. In the case of osteogenic differentiation (Ost), a significant increase of ≈ 30 Pa in $G_{0,app}$ is observed for the cell-laden scaffold (61 ± 20 Pa) compared to the cell-free counterpart (31 ± 7 Pa). In contrast, in DMEM, a decrease by almost a factor of 10 was found when comparing cell-free (40 ± 2 Pa) to cell-laden scaffolds (5 ± 5 Pa).

As commonly assumed, the osteoblasts that result from the osteogenic differentiation do not only secrete collagen and other ECM compounds, but also contribute to the calcification of the existing ECM [48, 189]. Our tracer particles are embedded in the scaffold matrix, so that their motion is more restricted by the stiffening network. Thus, higher values for $G_{0,app}$ are obtained, showing MPT's unique capability to quantify the differences in matrix elasticity, which result from differentiation here. Comparing adipogenic and osteogenic conditions, we see a total difference of about 60 Pa in the local elasticity of both cell laden scaffolds, reflecting the extreme difference in mechanical properties in the corresponding tissue types *in vivo* - bone and adipose tissue, whose tissue E modulus differ in more than four orders of magnitude [81].

To proof that the measured effects on local matrix elasticity were derived from successful differentiation of hMSCs, we employed von Kossa and Oil Red staining protocols. Von Kossa (see Fig. 6.4B) makes mineralization in the ECM visible, large mineralized areas are clearly visible in the osteogenic induced sample (right), whereas in control (middle) and adipogenic (left) condition, only some unspecific grey shades occurred. Oil Red (see Fig. 6.4C) stains fat vacuoles in adipocytes. In adipogenic induced differentiation (first row), lots of fat vacuoles are seen in red, whereas in control (middle) and osteogenic (right) condition, only purple nuclei are visible. To summarize, the induced differentiation was successful and the specific metabolic activity of osteoblasts and adipocytes resulted in a measurable difference in local ECM elasticity.

6.3.3 ECM mechanics in 2D

Seeded on conventional TCP without any scaffold, cells live in ECM that is exclusively secreted by themselves. This ECM is supposed to match their actual needs and is thus constantly remodelled by secretion of additional matrix components and degrading enzymes[66]. However, the total amount of newly secreted material in such a scaffold-free approach is much less than the amount of synthetic material provided in scaffold-based systems. Furthermore, the material is located on TCP and cannot be moved to glass slides without damaging it. Consequently, the use of a long distance objective is required and still, resolution and fluorescence intensity are reduced, compared to measurements on glass slides. Thus, the minimum particle size allowing for reliable tracking is $1 \mu\text{m}$. Additionally, the natural ECM cannot be doped with particles during fabrication, so that for MPT, the particles need to be added later on. Thus, such 2D experiments work by adding tracer particles to the nutrient media surrounding a 2D cell layer after a few minutes waiting time some tracers are entrapped in the network

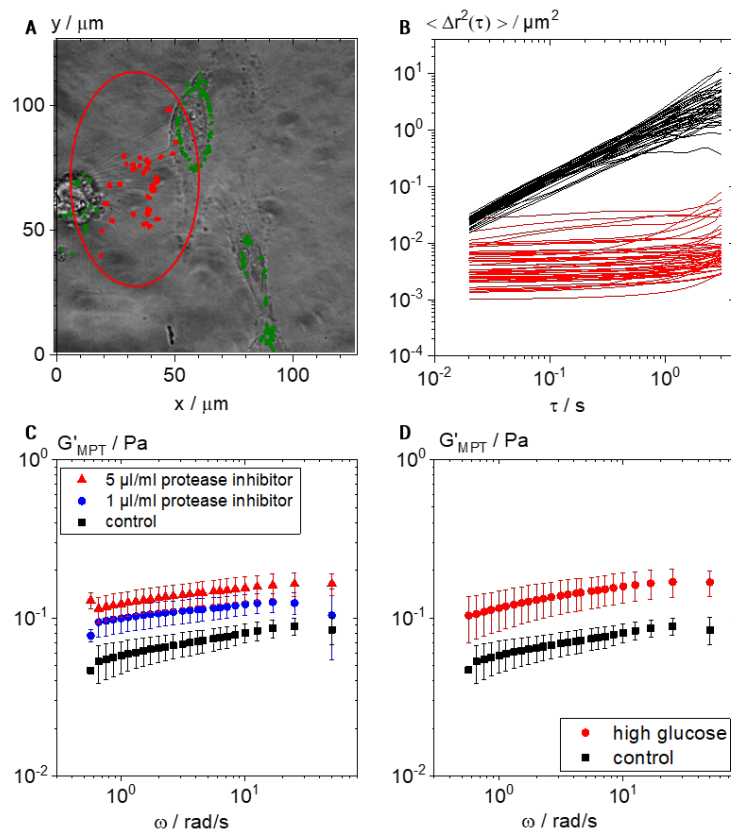


Figure 6.5: MPT allows for characterization of newly secreted ECM in scaffold-free 2D cell culture of HUVECs: A) Light microscopy image showing 3 cells and thin fibers connecting them, in overlay with trajectories of $0.96 \mu\text{m}$ MPT tracers, sensing elastic environment (slope of the MSD < 0.5) used for characterization of the inter-cellular network / ECM (red). Those that were excluded from the analysis, because they might be sticking to the cell surface are shown in green. B) resulting MSD plots for a typical experiment with the cellular layer in PBS showing the two populations for the elastic ECM (red) and viscous PBS (black). C) Effect of protease inhibitor on the ECM elasticity. Control (black) is compared to two inhibitor concentrations, $1 \mu\text{l/ml}$ (blue) and $5 \mu\text{l/ml}$ (red). D) Comparison of the elasticity of secreted ECM under high glucose (100 mmol/l glucose) and control (5.6 mmol/l glucose) conditions.

built around the cells.

As this entrapment happens randomly, always two populations of tracer particles are found in such MPT experiments. Some particles are trapped in the newly secreted network (shown in red in Fig. 6.5A and B) and sense the local elasticity of the ECM. The other fraction continues to diffuse freely, sensing the viscosity of the solvent/media (shown in black in Fig. 6.5B). The viscosity calculated from these MSDs agrees very well with the data for the viscosity of pure PBS. For the characterization of the mechanical properties of the ECM we use only the elastically trapped fraction of tracer particles and corresponding data is further processed to eliminate particles, that are sticking to cellular surfaces (shown in green), because we aimed at characterizing the ECM and not the mechanical properties of cells or their membranes. We use the generalized Stoke-Einstein equation (GSE, Eq 6.1) to calculate the complex shear modulus $G^*(\omega) = G' + iG''$. We do not know, whether the probed material is homogeneous and in thermal equilibrium, and accordingly we are not sure whether Eq 6.1 is fulfilled here. Thus we have to treat the calculated moduli as apparent values. Nevertheless, their variation indicates changes in the viscoelastic properties of the ECM. For calculation of local apparent moduli, corresponding data is further processed to eliminate particles, that are sticking to cellular surfaces (shown in green), because we aimed at characterizing the ECM and not the mechanical properties of cells or their membranes.

Averaged apparent moduli resulting from 6 independent sets, measured in HUVEC cultures, are shown as function of frequency in Fig. 6.5C (black curve). Here we also show the effect of the concentration of additionally supplemented Halt protease inhibitor cocktail. This inhibitor cocktail is supposed to down-regulate the activity of the MMPs secreted by the cells during remodeling. The resulting matrix elasticity is shown in red (5 $\mu\text{l/ml}$ inhibitor) and blue (1 $\mu\text{l/ml}$ inhibitor) and compared to the control without inhibitor. In all cases, G' is essentially frequency independent. This indicates a gel-like behaviour of the ECM, independent of the inhibitor concentration. However, the absolute values of $G'_{0,\text{app}}$ (taken at $\omega = 10$ rad/s) increased significantly with increasing inhibitor concentration from 0.08 ± 0.01 (no inhibitor) to 0.122 ± 0.02 Pa (5 $\mu\text{l/ml}$). This proves the high sensitivity of MPT in the low elasticity range and is in good agreement with the reduced matrix degradation activity expected for high inhibitor concentration.

One potential application for studying mechanical properties of ECM is tissue re-organisation associated with diabetes. Diabetes mellitus is characterized by a chronic hyperglycemia due to severe insulin resistance and/or insufficiency. Up to date there are various ECM modifications which are assumed to be involved in the pathomechanisms of diabetic complications. The most prominent mechanism is the formation of Advanced glycation endproducts (AGE), which are formed by non-enzymatic glycation of proteins [5, 258]. The effect of AGE ranges from inflammatory activation [229] and modification of cellular migration [140] to alteration of mechanical properties of ECM caused by crosslinking of ECM molecules [43]. Collagen is one prominent ECM protein which is affected by the formation of abnormal, stable intermolecular cross-links in a hyperglycemic context [7, 130, 218]. Another important mechanism is altered MMP/TIMP related ECM remodeling [9] as a cellular response in a diabetic environment. The mechanical alteration in glycated matrix components alone [43] as well as changes of cell stiffness were investigated using AFM and MPT after endocytosis of

tracer particles, respectively [159].

Especially vascular endothelial cells are exposed in first order to an elevated blood glucose level and it has been reported that hyperglycemia induces a complex dysfunction of endothelial cells [179, 233] with the consequence of diverse micro- and macrovascular pathologies of diabetes [23, 74, 193].

Thus, we studied local elasticity of the ECM at very high glucose concentrations. For 100 mmol/l glucose, we found $G_{0,\text{app}} = 0.15 \pm 0.03$ Pa, which is almost twice the value obtained under normal conditions (0.08 ± 0.01 Pa, both measured at 10 rad/s). This alteration is presumably more related to osmosis and densification of the gel due to reduced water activity or chemical modification of the ECM by glucose itself (protein glycation), than related to alterations in cell metabolism.

6.4 Conclusion

Multiple particle tracking microrheology was successfully used to monitor the matrix remodelling of single fibroblast cells in 3D scaffolds continuously. During the first 9 h after seeding, a monotonic decrease in $G_{0,\text{app}}$ from 42 to 15 Pa was observed for a single cell and after 24 h, 5 ± 1 Pa were measured in the discontinuous experiment averaging over multiple cells per time point. In contrast, no effect of growing cells showed up in conventional bulk shear experiments.

Furthermore, we characterized the ECM elasticity in hMSC cultures, where adipogenic and osteogenic differentiation was induced using specific differentiation media. We were able to prove that the osteogenic differentiation leads to a significant increase in local elastic modulus $G_{0,\text{app}}$ to ≈ 60 Pa of the HA / Coll based scaffolds with initial $G_{0,\text{app}} \approx 30$ Pa. This is related to the densification of the matrix by additional secretion of ECM components and the mineralization of the ECM during osteogenesis. In contrast, during adipogenic differentiation, the homeostasis is shifted towards softer ECM and $G_{0,\text{app}}$ is consequently decreased significantly to ≈ 5 Pa.

Finally, we studied the secretion of new ECM in a scaffold-free 2D HUVEC culture with different concentrations of Halt protease inhibitor cocktail. Increased inhibitor concentration showed the expected increase of ECM elasticity from $G_{0,\text{app}} = 0.08 \pm 0.01$ Pa for control condition to 0.12 ± 0.02 Pa for the highest inhibitor concentration. Upon cultivation in high glucose concentration, a twofold increase in $G_{0,\text{app}}$ compared to the control was observed. The resolution of our setup can consequently be considered sufficient to characterize the remodelling of even very soft ECM in 2D.

The techniques shown here and their combination provide great potential for studying cell-matrix interactions and their continuous effect on matrix elasticity in 2D cultures and in near-natural 3D scaffolds. Providing deeper insight in the remodelling of artificial ECM substitutes can support the design of biomaterials with appropriate properties for cell culture. Furthermore, having a tool to investigate ECM elasticity can help us to understand diseases and perhaps unravel pathways for potential therapies modulating ECM mechanics.

6.5 Acknowledgements

ALH, AR and CLT have received funding from the European Research Council (ERC) under the European Union’s Horizon 2020 research and innovation programme (grant agreement No 757490) and from the BMBF NanoMatFutur programme (FKZ 13N 12968).

MB and SB acknowledge support by the Helmholtz Association via the program “BioInterfaces in Technology and Medicine” (BIFTM); the Deutsche Forschungsgemeinschaft (DFG, German Research Foundation) under Germany’s Excellence Strategy – 2082/1 – 390761711, Cluster of Excellence “3D Matter Made to Order” (3DMM2O) and by the Carl Zeiss Foundation.

JG acknowledges support by the International Research Training Group 1874/2 DIAMICOM and the Deutsche Diabetes Gesellschaft.

Chapter 7

Summary and outlook

Unraveling microstructural and local mechanical properties of porous biopolymer based cryogel scaffolds and the corresponding precursor solutions, the fabrication of cell culture scaffolds was improved, so that we could use them as substrates for studying ECM mechanical properties in the direct surrounding of living cells.

A sound microstructural characterization of the precursor solutions based on lyophilized Coll helped us to better understand the later network formation during cryogelation. Overlaying subsequent images of MPT video sequences taken in acidic Coll solutions, allowed for the first time for a direct visualization of the Coll fiber network. For all concentrations in the range from 0.05 to 1 wt%, some tracer particles diffused freely, while we found at the same time a relevant fraction of elastically trapped tracer particles. These particles were found in the Coll structures, suggesting a structure presumably comprising multiple dense bundles not permeable for the 0.2 μm particles. These were embedded in a swollen surrounding layer accessible by the 0.2 μm tracer particles but with largely varying stiffness according to the broad variation in absolute values of the corresponding time-independent MSDs.

Our experimental procedure allowed for the first time the in-situ analysis of the supramolecular structure and local viscoelasticity of dissolved Coll and enabled the real-time monitoring of structure formation. This powerful microrheology imaging tool possesses great potential for the in-situ characterization of other fibers dispersed in continuous phases with similar optical properties or intransparent suspensions, where light microscopy imaging fails. Furthermore, this gentle method does not require any chemical modification by stains or fluorophores and is thus perfectly suitable for delicate biopolymers, such as proteins and carbohydrates, but also more novel bio-engineered materials based on DNA [92, 160]. The low amount of sample needed for MPT further advances the suitability in terms of investigating precious biological samples. In terms of fundamental research, such in-situ local elasticity data for dispersed objects can help gaining more adequate parameters for simulating two-phasic systems. To date, simulations dealing with the mechanical behavior of dispersions are in most cases based on the elastic modulus of the full material [10, 247]. However the dispersion of polymer fibers is often accompanied by swelling, partial dissolution or other interaction with the continuous phase, that cannot be considered in bulk characterization of the non-dispersed material.

The impact of the elasticity of dispersed fibers on the viscoelastic properties of

the resulting dispersion was to date investigated only for very reduced model systems [190, 201]. However, in terms of storage, transportation and processing of precise, complex (bio-)polymer dispersions comprising of delicate fiber networks, this knowledge is crucial.

Knowing microstructural and local mechanical properties of HA[173] and Coll (see chapter 2) allowed us to develop an appropriate formulation process for cryogels based on HA [174], Coll [199] and mixtures thereof. Keeping potential commercial applications in mind, biomaterials based on cost-effective, easily available materials are favoured by the emerging tissue engineering industry. Thus, chitosan owns great potential, due to its structural similarity to HA and low cost production from crustaceans' shells. Adjusting the former preparation protocol we were able to obtain even chitosan gels with appropriate stability in water.

Using HA, Chit, Coll, or their mixtures, enabled us to independently tailor viscoelastic, structural and biofunctional properties of the macroporous cryogels to fit application specific needs. Additionally, we have proved the non-cytotoxicity and accessibility of our scaffolds using 3T3 fibroblast cells as a model. Live-dead assays revealed that in all investigated scaffolds the cells were able to penetrate into the gels during the first 48 h and survived for up to 21 days.

Despite the high degree of biocompatibility of EGDE-crosslinked cryogels, medical applications seek for biomaterials based on officially approved chemicals. The requirements for such an approval by e.g. the Food and Drug Administration (FDA; mainly US) are more extensive and more complex, including genotoxicity and second reproduction toxicity, together with long-term impact on patients and following generations. Thus, for commercialization of biomedical products, the usage of approved chemicals is beneficial. Genipin, a plant based crosslinking agent is considered a non-hazardous chemical and was used in traditional Chinese medicine. Genipin was used as crosslinking agent for producing noncytotoxic macroporous cryogels based on gelatin and other biomaterials before. However, we were for the first time able to produce HA based cryogels crosslinked with genipin.

Resulting bulk elasticity of genipin and conventional EDGE gels were in the same range. Both gels show similar pore sizes in a well suitable range for cell culture applications. The range of potential applications for such stable biogels, including the use as cell culture scaffolds, in drug delivery or wound healing substrates, is large. The further advantages, including tuneable stiffness and non-animal origin (using HA from microbial fermentation), together with the comparatively low polymer consumption make it an attractive option for cosmetic surgery. In latter, the high shape fidelity, low biodegradability and non-cytotoxic degradation products are additional benefits of this novel material. Nevertheless, detailed biocompatibility studies *in vitro* and *in vivo* need to be performed together with up-scaling experiments for realizing a preparation process in industrial scale and appropriate sterile conditions.

In contrast to cell-free implants in aesthetic surgery, for cell-laden scaffolds and the near-natural ingrowth of mammalian cells into the provided scaffolds, protein structures are necessary. Thus, we investigated the influence of Coll concentration on material properties and cell culture suitability of HA based cryogel scaffolds. The elastic properties of the resulting gels were mainly depending on the degree of swelling, which makes pure Coll gels to appear stiffer compared to pure HA gels with the same overall

polymer content.

Most importantly, all different types of scaffolds were proven to be suitable for long term culture of fibroblasts and the introduction of Coll enabled cells to adhere to the scaffolds. Viability and proliferation were both satisfying during 8 days of cell culture in mixed HA/Coll gels. However, biodegradability of cryogels is drastically reduced when small fractions of Coll are incorporated into HA gels (*in vitro*, immersed in water).

These well-characterized porous scaffolds with their high biofunctionality and biocompatibility were chosen as platform for performing MPT measurements in the direct surrounding of living cells. Using an advanced setup, MPT microrheology was successfully used to monitor the matrix remodelling of single fibroblast cells continuously in the aforementioned 3D scaffolds. In contrast to the continuous decrease, yielding a final reduction of 50 % after the first 8 h after seeding, no effect of growing cells showed up in conventional oscillatory shear experiments.

Using similar cryogel scaffolds, we characterized the ECM elasticity in hMSC cultures, where adipogenic and osteogenic differentiation was induced using specific differentiation media. We were able to prove that the osteogenic differentiation leads to a significant increase in local elastic modulus $G_{0,MPT}$ to ~ 60 Pa of the scaffolds with initial $G_{0,MPT} \sim 30$ Pa. This is related to the densification of the matrix by additional secretion of ECM components and the mineralization of the ECM during osteogenesis. In contrast, during adipogenic differentiation, the homeostasis is shifted towards softer ECM and $G_{0,MPT}$ is consequently decreased significantly to ~ 5 Pa.

As described in [57–59] not only ECM mechanical properties are affected by cells' metabolic activity, but at the same time, cell fate and metabolism can be altered by mechanical stimuli from the ECM, including elasticity [60, 220], geometry [60, 206] and topography [78, 122, 197]. Thus, a reasonable expansion of our experiments with chemically induced stem cell differentiation might be the investigation of stem cell fate directed by scaffold mechanical properties and the feed-back on the propagation of ECM local elastic properties. The thereby generated understanding of cell-matrix interactions and their complex time course could help to better understand important biological processes, such as wound healing, tumor metastasis and ageing. The direct application of this knowledge might open-up a novel class of therapeutic approaches, based on mechanical stimuli.

For further validating the suitability of MPT to characterize local mechanical properties of ECM, the discrepancy between moduli determined from MPT and conventional shear experiments needs to be fully understood. For all our cryogels and various other biomaterials, the local elastic moduli, measured by MPT were significantly lower, compared to bulk elastic moduli, which might be related to a contribution of stretched out of equilibrium chain segments between network junctions of HA or caused by inaccessible sites in heterogeneous materials, that contribute to bulk elasticity, but are not probed in MPT measurements. Thus, a simple, tuneable model system with properties similar to semi-solid biomaterials, needs to be characterized with other referencing methods on multiple length scales.

In a final, scaffold-free approach, we studied the elastic properties of newly secreted ECM in 2D HUVEC cultures with different concentrations of Halt protease inhibitor cocktail. Increased inhibitor concentration showed the expected increase of ECM elasticity from $G_{0,MPT} = 0.08 \pm 0.01$ Pa for control condition to 0.12 ± 0.02 Pa

for the highest inhibitor concentration. Upon cultivation in high glucose concentration, a twofold increase in $G_{0,\text{MPT}}$ compared to the control was observed. The resolution of our setup can consequently be considered sufficient for characterization of ECM remodelling in 2D. However, the biological relevance of this phenomenon needs to be further investigated. To date, several potential explanations, including chemical modifications of the ECM by glucose itself, changed osmotic activity or altered metabolic behaviour of cells in diabetic conditions, are discussed. However, to better understand the impact of glucose concentration on ECM mechanical properties, sound MPT studies comprising different washing protocols for the produced ECM and nutrition protocols during cell culture with altered glucose concentrations in the medium need to be performed. The correlation with genetic studies might further help to prove metabolic effects. In general, MPT provides great potential for studying cell-matrix interactions and their continuous effect on matrix elasticity in 2D cultures and in near-natural 3D scaffolds. Providing deeper insight in the remodelling of artificial ECM substitutes can help designing biomaterials with suitable properties for cell culture.

Bibliography

- [1] V. F. Achterberg, L. Buscemi, H. Diekmann, J. Smith-Clerc, H. Schwengler, J.-J. Meister, H. Wenck, S. Gallinat, and B. Hinz. The nano-scale mechanical properties of the extracellular matrix regulate dermal fibroblast function. *Journal of Investigative Dermatology*, 134(7):1862 – 1872, 2014. ISSN 0022-202X. doi: <https://doi.org/10.1038/jid.2014.90>.
- [2] G. Agoda-Tandjawa, S. Durand, S. Berot, C. Blassel, C. Gaillard, C. Garnier, and J.-L. Doublier. Rheological characterization of microfibrillated cellulose suspensions after freezing. *Carbohydrate Polymers*, 80(3):677–686, 2010.
- [3] M. Ahearne. Introduction to cell-hydrogel mechanosensing. *Interface focus*, 4(2): 20130038, 2014. ISSN 2042-8898. doi: 10.1098/rsfs.2013.0038.
- [4] E. J. Amis, C. J. Carriere, J. D. Ferry, and A. Veis. Effect of ph on collagen flexibility determined from dilute solution viscoelastic measurements. *International Journal of Biological Macromolecules*, 7(3):130–134, 1985.
- [5] N. A. Ansari and Z. Rasheed. Non-enzymatic glycation of proteins: From diabetes to cancer. *Biochemistry (Moscow) Supplement Series B: Biomedical Chemistry*, 3(4):335–342, 2009. ISSN 1990-7508. doi: 10.1134/S1990750809040027.
- [6] J. Apgar, Y. Tseng, E. Fedorov, M. B. Herwig, S. C. Almo, and D. Wirtz. Multiple-particle tracking measurements of heterogeneities in solutions of actin filaments and actin bundles. *Biophysical journal*, 79(2):1095–1106, 2000.
- [7] N. C. Avery and A. J. Bailey. The effects of the maillard reaction on the physical properties and cell interactions of collagen. *Pathologie-biologie*, 54(7):387–395, 2006. ISSN 0369-8114. doi: 10.1016/j.patbio.2006.07.005.
- [8] E. A. Balazs. Therapeutic use of hyaluronan. *Structural Chemistry*, 20(2):341–349, 2009. ISSN 1040-0400. doi: 10.1007/s11224-009-9435-y.
- [9] D. Baltzis, I. Eleftheriadou, and A. Veves. Pathogenesis and treatment of impaired wound healing in diabetes mellitus: new insights. *Advances in therapy*, 31(8):817–836, 2014.
- [10] A. A. Banaei. *Simulation of deformable objects transported in fluid flow*. PhD thesis, KTH Royal Institute of Technology, 2019.

- [11] A. Banerjee, M. Arha, S. Choudhary, R. S. Ashton, S. R. Bhatia, D. V. Schaffer, and R. S. Kane. The influence of hydrogel modulus on the proliferation and differentiation of encapsulated neural stem cells. *Biomaterials*, 30(27):4695–4699, 2009. ISSN 01429612. doi: 10.1016/j.biomaterials.2009.05.050.
- [12] R. Bansil, J. P. Celli, J. M. Hardcastle, and B. S. Turner. The influence of mucus microstructure and rheology in helicobacter pylori infection. *Frontiers in immunology*, 4:310, 2013. ISSN 1664-3224. doi: 10.3389/fimmu.2013.00310.
- [13] A. Barbetta, A. Carrino, M. Costantini, and M. Dentini. Polysaccharide based scaffolds obtained by freezing the external phase of gas-in-liquid foams. *Soft Matter*, 6(20):5213, 2010. ISSN 1744-683X. doi: 10.1039/c0sm00616e.
- [14] G. K. Batchelor. The stress generated in a non-dilute suspension of elongated particles by pure straining motion. *Journal of Fluid Mechanics*, 46(4):813–829, 1971. ISSN 0022-1120. doi: 10.1017/S0022112071000879.
- [15] S. Battista, D. Guarnieri, C. Borselli, S. Zeppetelli, A. Borzacchiello, L. Mayol, D. Gerbasio, D. R. Keene, L. Ambrosio, and P. A. Netti. The effect of matrix composition of 3d constructs on embryonic stem cell differentiation. *Biomaterials*, 26(31):6194–6207, 2005. ISSN 01429612. doi: 10.1016/j.biomaterials.2005.04.003.
- [16] D. Berillo, B. Mattiasson, I. Y. Galaev, and H. Kirsebom. Formation of macroporous self-assembled hydrogels through cryogelation of fmoc-phe-phe. *Journal of colloid and interface science*, 368(1):226–230, 2012. ISSN 0021-9797. doi: 10.1016/j.jcis.2011.11.006.
- [17] D. Berillo, B. Mattiasson, I. Y. Galaev, and H. Kirsebom. Formation of macroporous self-assembled hydrogels through cryogelation of fmoc-phe-phe. *Journal of colloid and interface science*, 368(1):226–230, 2012.
- [18] S. Bhat and A. Kumar. Cell proliferation on three-dimensional chitosan-agarose-gelatin cryogel scaffolds for tissue engineering applications. *Journal of bioscience and bioengineering*, 114(6):663–670, 2012. ISSN 1347-4421. doi: 10.1016/j.jbiosc.2012.07.005.
- [19] S. Bhat, A. Tripathi, and A. Kumar. Supermacroporous chitosan-agarose-gelatin cryogels: in vitro characterization and in vivo assessment for cartilage tissue engineering. *Journal of the Royal Society, Interface*, 8(57):540–554, 2011. ISSN 1742-5662. doi: 10.1098/rsif.2010.0455.
- [20] M. A. Bibbo, S. M. Dinh, and R. C. Armstrong. Shear flow properties of semi-concentrated fiber suspensions. *Journal of Rheology*, 29(6):905–929, 1985. ISSN 01486055. doi: 10.1122/1.549836.
- [21] K. Bieback, M. Vinci, S. Elvers-Hornung, A. Bartol, T. Gloe, M. Czabanka, H. Klüter, H. Augustin, and P. Vajkoczy. Recruitment of human cord blood-derived endothelial colony-forming cells to sites of tumor angiogenesis. *Cytotherapy*, 15(6):726–739, 2013.

-
- [22] A. Bouloumié, C. Sengenès, G. Portolan, J. Galitzky, and M. Lafontan. Adipocyte produces matrix metalloproteinases 2 and 9: Involvement in adipose differentiation. *Diabetes*, 50(9):2080–2086, 2001. ISSN 0012-1797. doi: 10.2337/diabetes.50.9.2080.
- [23] M. Brownlee. The pathobiology of diabetic complications: A unifying mechanism. *Diabetes*, 54(6):1615–1625, 2005. ISSN 0012-1797. doi: 10.2337/diabetes.54.6.1615.
- [24] M. J. Buehler. Nature designs tough collagen: explaining the nanostructure of collagen fibrils. *Proceedings of the National Academy of Sciences of the United States of America*, 103(33):12285–12290, 2006. doi: 10.1073/pnas.0603216103.
- [25] M. F. Butler, Y.-F. Ng, and P. D. Pudney. Mechanism and kinetics of the crosslinking reaction between biopolymers containing primary amine groups and genipin. *Journal of Polymer Science Part A: Polymer Chemistry*, 41(24):3941–3953, 2003.
- [26] M. Caggioni, P. T. Spicer, D. L. Blair, S. E. Lindberg, and D. A. Weitz. Rheology and microrheology of a microstructured fluid: The gellan gum case. *Journal of Rheology*, 51(5):851–865, 2007. ISSN 01486055. doi: 10.1122/1.2751385.
- [27] Y. Cai and D. K. Schwartz. Mapping the functional tortuosity and spatiotemporal heterogeneity of porous polymer membranes with super-resolution nanoparticle tracking. *ACS applied materials & interfaces*, 9(49):43258–43266, 2017.
- [28] A. I. Caplan. Mesenchymal stem cells. *Journal of Orthopaedic Research*, 9(5):641–650, 1991. doi: 10.1002/jor.1100090504.
- [29] J. Celli, B. Gregor, B. Turner, N. H. Afdhal, R. Bansil, and S. Erramilli. Viscoelastic properties and dynamics of porcine gastric mucin. *Biomacromolecules*, 6(3):1329–1333, 2005. ISSN 1525-7797.
- [30] K.-H. Chang, H.-T. Liao, and J.-P. Chen. Preparation and characterization of gelatin/hyaluronic acid cryogels for adipose tissue engineering: In vitro and in vivo studies. *Acta Biomaterialia*, 9(11):9012–9026, 2013. ISSN 1742-7061. doi: 10.1016/j.actbio.2013.06.046.
- [31] R. Chang, J. Nam, and W. Sun. Effects of dispensing pressure and nozzle diameter on cell survival from solid freeform fabrication-based direct cell writing. *Tissue engineering. Part A*, 14(1):41–48, 2008. ISSN 1937-335X. doi: 10.1089/ten.a.2007.0004.
- [32] Y. Chang, C.-C. Tsai, H.-C. Liang, and H.-W. Sung. In vivo evaluation of cellular and acellular bovine pericardium fixed with a naturally occurring crosslinking agent (genipin). *Biomaterials*, 23(12):2447–2457, 2002.
- [33] C.-H. Chen, C.-Y. Kuo, Y.-J. Wang, and J.-P. Chen. Dual function of glucosamine in gelatin/hyaluronic acid cryogel to modulate scaffold mechanical properties and to maintain chondrogenic phenotype for cartilage tissue engineering.

- International journal of molecular sciences*, 17(11), 2016. ISSN 1422-0067. doi: 10.3390/ijms17111957.
- [34] E. A. G. Chernoff and D. A. Chernoff. Atomic force microscope images of collagen fibers. *Journal of Vacuum Science & Technology A: Vacuum, Surfaces, and Films*, 10(4):596–599, 1992. ISSN 0734-2101.
- [35] M. N. Collins and C. Birkinshaw. Morphology of crosslinked hyaluronic acid porous hydrogels. *Journal of Applied Polymer Science*, 120(2):1040–1049, 2011. ISSN 00218995. doi: 10.1002/app.33241.
- [36] X. Cong, S.-M. Zhang, L. Batty, and J. Luo. Application of human induced pluripotent stem cells in generating tissue-engineered blood vessels as vascular grafts. *Stem Cells and Development*, 28(24):1581–1594, 2019.
- [37] K. G. Cornwell, A. Landsman, and K. S. James. Extracellular matrix biomaterials for soft tissue repair. *Advances in Wound and Bone Healing*, 26(4):507–523, 2009. ISSN 0891-8422. doi: 10.1016/j.cpm.2009.08.001.
- [38] B. D. Cosgrove, K. L. Mui, T. P. Driscoll, S. R. Caliarì, K. D. Mehta, R. K. Assoian, J. A. Burdick, and R. L. Mauck. N-cadherin adhesive interactions modulate matrix mechanosensing and fate commitment of mesenchymal stem cells. *Nature materials*, 15(12):1297–1306, 2016. ISSN 1476-1122. doi: 10.1038/nmat4725.
- [39] J. C. Crocker and David G. Grier. Methods of digital video microscopy for colloidal studies. *Journal of colloid and interface science*, 179(1):298–310, 1996. ISSN 0021-9797. doi: 10.1006/jcis.1996.0217.
- [40] J. C. Crocker and B. D. Hoffman. Multiple-particle tracking and two-point microrheology in cells. In *Cell Mechanics*, volume 83 of *Methods in Cell Biology*, pages 141 – 178. Academic Press, 2007. doi: [https://doi.org/10.1016/S0091-679X\(07\)83007-X](https://doi.org/10.1016/S0091-679X(07)83007-X).
- [41] J. C. Crocker and B. D. Hoffman. Multiple-particle tracking and two-point microrheology in cells. In *Methods in Cell Biology : Cell Mechanics*, volume 83, pages 141–178. Academic Press, 2007. ISBN 0091-679X. doi: 10.1016/S0091-679X(07)83007-X.
- [42] W. Cruz-Munoz and R. Khokha. The role of tissue inhibitors of metalloproteinases in tumorigenesis and metastasis. *Critical reviews in clinical laboratory sciences*, 45(3):291–338, 2008. doi: 10.1080/10408360801973244.
- [43] H. Dandia, K. Makkad, and P. Tayalia. Glycated collagen—a 3d matrix system to study pathological cell behavior. *Biomaterials Science*, 2019.
- [44] M. Daviran, H. S. Caram, and K. M. Schultz. Role of cell-mediated enzymatic degradation and cytoskeletal tension on dynamic changes in the rheology of the pericellular region prior to human mesenchymal stem cell motility. *ACS*

-
- biomaterials science & engineering*, 4(2):468–472, 2018. ISSN 2373-9878. doi: 10.1021/acsbiomaterials.7b01005.
- [45] M. Daviran, S. M. Longwill, J. F. Casella, and K. M. Schultz. Rheological characterization of dynamic remodeling of the pericellular region by human mesenchymal stem cell-secreted enzymes in well-defined synthetic hydrogel scaffolds. *Soft Matter*, 2018. ISSN 1744-683X. doi: 10.1039/c8sm00408k.
- [46] D. W. de Kort, T. Nikolaeva, and J. A. Dijksman. Rheo-nmr: Applications to food. *Modern Magnetic Resonance*, pages 1–21, 2017. ISSN 33192827.
- [47] D. W. de Kort, T. Nikolaeva, and J. A. Dijksman. Rheo-nmr: Applications to food. In *Modern Magnetic Resonance*, pages 1589–1608. Springer International Publishing, 2018.
- [48] H. A. Declercq, R. M. Verbeeck, L. I. D. Ridder, E. H. Schacht, and M. J. Cornelissen. Calcification as an indicator of osteoinductive capacity of biomaterials in osteoblastic cell cultures. *Biomaterials*, 26(24):4964 – 4974, 2005. ISSN 0142-9612. doi: <https://doi.org/10.1016/j.biomaterials.2005.01.025>.
- [49] C. J. Dibble, M. Kogan, and M. J. Solomon. Structure and dynamics of colloidal depletion gels: Coincidence of transitions and heterogeneity. *Physical Review E*, 74(4):041403, 2006.
- [50] B. O. Diekman, N. Christoforou, V. P. Willard, H. Sun, J. Sanchez-Adams, K. W. Leong, and F. Guilak. Cartilage tissue engineering using differentiated and purified induced pluripotent stem cells. *Proceedings of the National Academy of Sciences*, 109(47):19172–19177, 2012.
- [51] S. M. Dinh and R. C. Armstrong. A rheological equation of state for semiconcentrated fiber suspensions. *Journal of Rheology*, 28(3):207–227, 1984. ISSN 01486055. doi: 10.1122/1.549748.
- [52] D. E. Discher, P. Janmey, and Y.-l. Wang. Tissue cells feel and respond to the stiffness of their substrate. *Science*, 310(5751):1139–1143, 2005. doi: 10.1126/science.1116995.
- [53] X. Duan and H. Sheardown. Dendrimer crosslinked collagen as a corneal tissue engineering scaffold: mechanical properties and corneal epithelial cell interactions. *Biomaterials*, 27(26):4608–4617, 2006. ISSN 01429612. doi: 10.1016/j.biomaterials.2006.04.022.
- [54] D. M. Ebenstein and L. A. Pruitt. Nanoindentation of soft hydrated materials for application to vascular tissues. *Journal of biomedical materials research. Part A*, 69(2):222–232, 2004. ISSN 1552-4965. doi: 10.1002/jbm.a.20096.
- [55] J. A. Eble and S. Niland. The extracellular matrix in tumor progression and metastasis. *Clinical & experimental metastasis*, 36(3):171–198, 2019. doi: 10.1007/s10585-019-09966-1.

- [56] S. R. Eisenberg and Alan J. Grodzinsky. The kinetics of chemically induced nonequilibrium swelling of articular cartilage and corneal stroma. *Journal of Biomechanical Engineering*, 109(1):79–89, 1987. ISSN 0148-0731. doi: 10.1115/1.3138647.
- [57] A. J. Engler, M. A. Griffin, S. Sen, C. G. Bonnemann, H. L. Sweeney, and D. E. Discher. Myotubes differentiate optimally on substrates with tissue-like stiffness: pathological implications for soft or stiff microenvironments. *The Journal of Cell Biology*, 166(6):877–887, 2004. ISSN 0021-9525. doi: 10.1083/jcb.200405004.
- [58] A. J. Engler, S. Sen, H. L. Sweeney, and D. E. Discher. Matrix elasticity directs stem cell lineage specification. *Cell*, 126(4):677–689, 2006. ISSN 0092-8674. doi: 10.1016/j.cell.2006.06.044.
- [59] A. J. Engler, F. Rehfeldt, S. Sen, and D. E. Discher. Microtissue elasticity: Measurements by atomic force microscopy and its influence on cell differentiation. In Y.-l. Wang and D. E. Discher, editors, *Cell mechanics*, volume 83 of *Methods in Cell Biology*, pages 521–545. Elsevier, Amsterdam, 2007. ISBN 9780123705006. doi: 10.1016/S0091-679X(07)83022-6.
- [60] N. D. Evans and E. Gentleman. The role of material structure and mechanical properties in cell–matrix interactions. *Journal of Materials Chemistry B*, 2(17):2345, 2014. ISSN 2050-750X. doi: 10.1039/c3tb21604g.
- [61] M. Flaibani and N. Elvassore. Gas anti-solvent precipitation assisted salt leaching for generation of micro- and nano-porous wall in bio-polymeric 3d scaffolds. *Materials science & engineering. C, Materials for biological applications*, 32(6):1632–1639, 2012. ISSN 0928-4931. doi: 10.1016/j.msec.2012.04.054.
- [62] A. C. Fonseca, P. Ferreira, R. A. Cordeiro, P. V. Mendonça, J. R. Góis, M. H. Gil, and J. F. J. Coelho. Drug delivery systems for predictive medicine: Polymers as tools for advanced applications. In M. S. Mozaffari, editor, *New Strategies to Advance Pre/Diabetes Care: Integrative Approach by PPPM*, volume 3 of *Advances in Predictive, Preventive and Personalised Medicine*, pages 399–455. Springer, Dordrecht, 2013. ISBN 978-94-007-5970-1. doi: 10.1007/978-94-007-5971-8{\textunderscore}16.
- [63] P. Fratzl, editor. *Collagen: Structure and Mechanics*. Springer Science+Business Media LLC, Boston, MA, 2008. ISBN 9780387739052. doi: 10.1007/978-0-387-73906-9.
- [64] W. Friess. Collagen – biomaterial for drug delivery: Dedicated to professor dr. eberhard nürnberg, friedrich-alexander-universität erlangen-nürnberg, on the occasion of his 70th birthday. *European Journal of Pharmaceutics and Biopharmaceutics*, 45(2):113–136, 1998. doi: 10.1016/S0939-6411(98)00017-4.
- [65] W. Friess and G. Lee. Basic thermoanalytical studies of insoluble collagen matrices. *Biomaterials*, 17(23):2289–2294, 1996. ISSN 01429612.

-
- [66] J. Gaffney, I. Solomonov, E. Zehorai, and I. Sagi. Multilevel regulation of matrix metalloproteinases in tissue homeostasis indicates their molecular specificity in vivo. *Matrix Biology*, 44-46:191 – 199, 2015. ISSN 0945-053X. doi: <https://doi.org/10.1016/j.matbio.2015.01.012>.
- [67] C. Gambini, B. Abou, A. Ponton, and A. J. M. Cornelissen. Micro- and macrorheology of jellyfish extracellular matrix. *Biophysical Journal*, 102(1):1–9, 2012. ISSN 00063495. doi: 10.1016/j.bpj.2011.11.4004.
- [68] M. L. Gardel, M. T. Valentine, and D. A. Weitz. Microrheology. In K. S. Breuer, editor, *Microscale diagnostic techniques*, pages 1–49. Springer, 2005.
- [69] I. Gatej, M. Popa, and M. Rinaudo. Role of the pH on hyaluronan behavior in aqueous solution. *Biomacromolecules*, 6(1):61–67, 2005. ISSN 1525-7797. doi: 10.1021/bm040050m.
- [70] A. Gautieri, S. Vesentini, A. Redaelli, and M. J. Buehler. Hierarchical structure and nanomechanics of collagen microfibrils from the atomistic scale up. *Nano letters*, 11(2):757–766, 2011. doi: 10.1021/nl103943u.
- [71] E. Gentleman, A. N. Lay, D. A. Dickerson, E. A. Nauman, G. A. Livesay, and K. C. Dee. Mechanical characterization of collagen fibers and scaffolds for tissue engineering. *Biomaterials*, 24(21):3805–3813, 2003. ISSN 01429612.
- [72] P. C. Georges and P. A. Janmey. Cell type-specific response to growth on soft materials. *Journal of applied physiology (Bethesda, Md. : 1985)*, 98(4):1547–1553, 2005. ISSN 8750-7587. doi: 10.1152/jappphysiol.01121.2004.
- [73] F. Gobeaux, E. Belamie, G. Mosser, P. Davidson, and S. Asnacios. Power law rheology and strain-induced yielding in acidic solutions of type I-collagen. *Soft Matter*, 6(16):3769–3777, 2010. ISSN 1744-683X.
- [74] S.-Y. Goh and M. E. Cooper. Clinical review: The role of advanced glycation end products in progression and complications of diabetes. *The Journal of clinical endocrinology and metabolism*, 93(4):1143–1152, 2008. doi: 10.1210/jc.2007-1817.
- [75] D. Gospodarowicz and C. Ill. Extracellular matrix and control of proliferation of vascular endothelial cells. *The Journal of Clinical Investigation*, 65(6):1351–1364, 6 1980. doi: 10.1172/JCI109799.
- [76] F. Grinnell. Fibroblast biology in three-dimensional collagen matrices. *Trends in Cell Biology*, 13(5):264–269, 2003. ISSN 09628924. doi: 10.1016/S0962-8924(03)00057-6.
- [77] A. Gross, A. Torge, U. F. Schaefer, M. Schneider, C.-M. Lehr, and C. Wagner. A foam model highlights the differences of the macro- and microrheology of respiratory horse mucus. *Journal of the mechanical behavior of biomedical materials*, 71:216–222, 2017. ISSN 1878-0180. doi: 10.1016/j.jmbbm.2017.03.009.

- [78] F. Guilak, D. M. Cohen, B. T. Estes, J. M. Gimble, W. Liedtke, and C. S. Chen. Control of stem cell fate by physical interactions with the extracellular matrix. *Cell stem cell*, 5(1):17–26, 2009. ISSN 1875-9777. doi: 10.1016/j.stem.2009.06.016.
- [79] C. M. Hale, S. X. Sun, and D. Wirtz. Resolving the role of actomyosin contractility in cell microrheology. *PloS one*, 4(9), 2009.
- [80] Y. L. Han, P. Ronceray, G. Xu, A. Mandalino, R. D. Kamm, M. Lenz, C. P. Broedersz, and M. Guo. Cell contraction induces long-ranged stress stiffening in the extracellular matrix. *Proceedings of the National Academy of Sciences*, 115(16):4075–4080, 2018.
- [81] A. M. Handorf, Y. Zhou, M. A. Halanski, and W.-J. Li. Tissue stiffness dictates development, homeostasis, and disease progression. *Organogenesis*, 11(1):1–15, 2015.
- [82] D. Hanjaya-Putra, J. Yee, D. Ceci, R. Truitt, D. Yee, and S. Gerecht. Vascular endothelial growth factor and substrate mechanics regulate in vitro tubulogenesis of endothelial progenitor cells. *Journal of Cellular and Molecular Medicine*, 14(10):2436–2447, 2010. doi: 10.1111/j.1582-4934.2009.00981.x.
- [83] C. T. Hanks, J. C. Wataha, and Z. Sun. In vitro models of biocompatibility: A review. *Dental Materials*, 12(3):186–193, 1996. ISSN 0109-5641. doi: 10.1016/S0109-5641(96)80020-0.
- [84] A. K. Harvey, M. S. Thompson, Le Cochlin, P. A. Raju, Z. Cui, H. Cornell, P. A. Hulley, and J. M. Brady. Functional imaging of tendon. *Ann. Brit. Machine Vision Assoc*, 2009.
- [85] V. C. Hascall, A. K. Majors, de la Motte, Carol A, S. P. Evanko, A. Wang, J. A. Drazba, S. A. Strong, and T. N. Wight. Intracellular hyaluronan: a new frontier for inflammation? *Biochimica et Biophysica Acta (BBA)-General Subjects*, 1673(1):3–12, 2004. ISSN 0304-4165.
- [86] M. G. Haugh. *The development of novel scaffolds for tissue engineering with a range of structural and mechanical properties*. Doctoral thesis, University of Dublin, Trinity College Dublin, 01.02.2009.
- [87] R. Henderson. The potential and limitations of neutrons, electrons and x-rays for atomic resolution microscopy of unstained biological molecules. *Quarterly reviews of biophysics*, 28(2):171–193, 1995.
- [88] T. M. A. Henderson, K. Ladewig, D. N. Haylock, K. M. McLean, and A. J. O’Connor. Cryogels for biomedical applications. *Journal of Materials Chemistry B*, 1(21):2682, 2013. ISSN 2050-750X. doi: 10.1039/c3tb20280a.
- [89] T. M. A. Henderson, K. Ladewig, D. N. Haylock, K. M. McLean, and A. J. O’Connor. Formation and characterisation of a modifiable soft macro-porous

-
- hyaluronic acid cryogel platform. *Journal of biomaterials science. Polymer edition*, 26(13):881–897, 2015. ISSN 1568-5624. doi: 10.1080/09205063.2015.1065597.
- [90] V. Herle, P. Fischer, and E. J. Windhab. Stress driven shear bands and the effect of confinement on their structures a rheological, flow visualization, and rheo-sals study. *Langmuir*, 21(20):9051–9057, 2005. ISSN 0743-7463.
- [91] R. Holmes, S. Kirk, G. Tronci, X. Yang, and D. Wood. Influence of telopeptides on the structural and physical properties of polymeric and monomeric acid-soluble type i collagen. *Materials science & engineering. C, Materials for biological applications*, 77:823–827, 2017. ISSN 0928-4931. doi: 10.1016/j.msec.2017.03.267.
- [92] Y. Hu, C. M. Domínguez, J. Bauer, S. Weigel, A. Schipperges, C. Oelschlaeger, N. Willenbacher, S. Keppler, M. Bastmeyer, S. Heißler, et al. Carbon-nanotube reinforcement of dna-silica nanocomposites yields programmable and cell-instructive biocoatings. *Nature Communications*, 10(1):1–14, 2019.
- [93] L. L. Huang, H.-W. Sung, C.-C. Tsai, and D.-M. Huang. Biocompatibility study of a biological tissue fixed with a naturally occurring crosslinking reagent. *Journal of Biomedical Materials Research: An Official Journal of The Society for Biomaterials, The Japanese Society for Biomaterials, and the Australian Society for Biomaterials*, 42(4):568–576, 1998.
- [94] J. A. Hubbell. Biomaterials in tissue engineering. *Bio/technology*, 13(6):565–576, 1995.
- [95] D. W. Hutmacher. Scaffold design and fabrication technologies for engineering tissues — state of the art and future perspectives. *Journal of Biomaterials Science, Polymer Edition*, 12(1):107–124, 2001. ISSN 0920-5063. doi: 10.1163/156856201744489.
- [96] H.-D. Hwang, H.-J. Cho, P. Balakrishnan, C.-W. Chung, I.-S. Yoon, Y.-K. Oh, Y. Byun, and D.-D. Kim. Cross-linked hyaluronic acid-based flexible cell delivery system: application for chondrogenic differentiation. *Colloids and surfaces. B, Biointerfaces*, 91:106–113, 2012. ISSN 1873-4367. doi: 10.1016/j.colsurfb.2011.10.052.
- [97] Y. Hwang, N. Sangaj, and S. Varghese. Interconnected macroporous poly(ethylene glycol) cryogels as a cell scaffold for cartilage tissue engineering. *Tissue Engineering Part A*, 16(10):3033–3041, 2010. ISSN 1937-3341. doi: 10.1089/ten.tea.2010.0045.
- [98] T. Indei, J. D. Schieber, A. Córdoba, and E. Pilyugina. Treating inertia in passive microbead rheology. *Physical review. E, Statistical, nonlinear, and soft matter physics*, 85(2 Pt 1):021504, 2012. ISSN 1539-3755. doi: 10.1103/PhysRevE.85.021504.

- [99] J F Kennedy, Glyn O. Phillips, P A Williams, V C Hascall, editor. *Hyaluronan: Proceedings of an International Meeting, September 2000, North East Wales Institute, UK*. Woodhead Publishing, 2002. ISBN 978-1-85573-570-5.
- [100] S. Ji and J. Ding. The wetting process of a dry polymeric hydrogel. *Polymer journal*, 34(4):267–270, 2002. ISSN 0032-3896.
- [101] J. Jiang, S. B. Nicoll, and H. H. Lu. Co-culture of osteoblasts and chondrocytes modulates cellular differentiation in vitro. *Biochemical and biophysical research communications*, 338(2):762–770, 2005.
- [102] D. P. Jones, W. Hanna, and J. P. Celli. Mapping dynamic mechanical remodeling in 3d tumor models via particle tracking microrheology. In K. V. Larin and D. D. Sampson, editors, *Optical Elastography and Tissue Biomechanics II*, SPIE Proceedings, page 93270L. SPIE, 2015. doi: 10.1117/12.2084282.
- [103] D. P. Jones, W. Hanna, G. M. Cramer, and J. P. Celli. In situ measurement of ecm rheology and microheterogeneity in embedded and overlaid 3d pancreatic tumor stroma co-cultures via passive particle tracking. *Journal of Innovative Optical Health Sciences*, 10(06):1742003, 2017. ISSN 1793-5458. doi: 10.1142/S1793545817420032.
- [104] C. G. Joung, N. Phan-Thien, and X. J. Fan. Direct simulation of flexible fibers. *Journal of Non-Newtonian Fluid Mechanics*, 99(1):1–36, 2001. ISSN 0377-0257. doi: 10.1016/S0377-0257(01)00113-6. URL <http://www.sciencedirect.com/science/article/pii/S0377025701001136>.
- [105] B. A. Juliar, M. T. Keating, Y. P. Kong, E. L. Botvinick, and A. J. Putnam. Sprouting angiogenesis induces significant mechanical heterogeneities and ecm stiffening across length scales in fibrin hydrogels. *Biomaterials*, 162:99–108, 2018. ISSN 01429612. doi: 10.1016/j.biomaterials.2018.02.012.
- [106] Y. Jung, G. Bauer, and J. A. Nolte. Concise review: induced pluripotent stem cell-derived mesenchymal stem cells: progress toward safe clinical products. *Stem cells*, 30(1):42–47, 2012.
- [107] S.-W. Kang, J.-S. Kim, K.-S. Park, B.-H. Cha, J.-H. Shim, J. Y. Kim, D.-W. Cho, J.-W. Rhie, and S.-H. Lee. Surface modification with fibrin/hyaluronic acid hydrogel on solid-free form-based scaffolds followed by bmp-2 loading to enhance bone regeneration. *Bone*, 48(2):298–306, 2011. ISSN 1873-2763. doi: 10.1016/j.bone.2010.09.029.
- [108] P. Kannus. Structure of the tendon connective tissue. *Scandinavian Journal of Medicine and Science in Sports*, 10(6):312–320, 2000. ISSN 0905-7188. doi: 10.1034/j.1600-0838.2000.010006312.x.
- [109] K. Kato, G. Bar, and H.-J. Cantow. The interplay between surface microtopography and-mechanics of type i collagen fibrils in air and aqueous media: an atomic force microscopy study. *The European physical journal. E, Soft matter*, 6(1):7–14, 2001. ISSN 1292-8941.

-
- [110] J. D. Kaufman, G. J. Miller, E. F. Morgan, and C. M. Klapperich. Time-dependent mechanical characterization of poly(2-hydroxyethyl methacrylate) hydrogels using nanoindentation and unconfined compression. *Journal of materials research*, 23(5):1472–1481, 2008. ISSN 0884-1616. doi: 10.1557/JMR.2008.0185.
- [111] M. Keating, A. Kurup, M. Alvarez-Elizondo, A. Levine, and E. Botvinick. Spatial distributions of pericellular stiffness in natural extracellular matrices are dependent on cell-mediated proteolysis and contractility. *Acta biomaterialia*, 57:304–312, 2017.
- [112] M. Keshtkar, M.-C. Heuzey, P. J. Carreau, M. Rajabian, and C. Dubois. Rheological properties and microstructural evolution of semi-flexible fiber suspensions under shear flow. *Journal of Rheology*, 54(2):197, 2010. ISSN 0148-6055. doi: 10.1122/1.3301245. URL <https://sor.scitation.org/doi/pdf/10.1122/1.3301245>.
- [113] S. Khetan, M. Guvendiren, W. R. Legant, D. M. Cohen, C. S. Chen, and J. A. Burdick. Degradation-mediated cellular traction directs stem cell fate in covalently crosslinked three-dimensional hydrogels. *Nature materials*, 12(5):458–465, 2013. ISSN 1476-1122. doi: 10.1038/nmat3586.
- [114] K. A. Kilian, B. Bugarija, B. T. Lahn, and M. Mrksich. Geometric cues for directing the differentiation of mesenchymal stem cells. *Proceedings of the National Academy of Sciences*, 107(11):4872–4877, 2010. ISSN 0027-8424. doi: 10.1073/pnas.0903269107.
- [115] H. J. Kim, K. K. Kim, I. K. Park, B. S. Choi, J. H. Kim, and M. S. Kim. Hybrid scaffolds composed of hyaluronic acid and collagen for cartilage regeneration. *Tissue Engineering and Regenerative Medicine*, 9(2):57–62, 2012. ISSN 1738-2696. doi: 10.1007/s13770-012-0007-7.
- [116] I. L. Kim, S. Khetan, B. M. Baker, C. S. Chen, and J. A. Burdick. Fibrous hyaluronic acid hydrogels that direct msc chondrogenesis through mechanical and adhesive cues. *Biomaterials*, 34(22):5571–5580, 2013. ISSN 01429612. doi: 10.1016/j.biomaterials.2013.04.004.
- [117] M. Y. Kim and J. Lee. Chitosan fibrous 3d networks prepared by freeze drying. *Carbohydrate polymers*, 84(4):1329–1336, 2011.
- [118] H. K. Kleinman. Role of collagenous matrices in the adhesion and growth of cells. *The Journal of Cell Biology*, 88(3):473–485, 1981. ISSN 0021-9525. doi: 10.1083/jcb.88.3.473.
- [119] M. Kotlarchyk, E. Botvinick, and A. Putnam. Characterization of hydrogel microstructure using laser tweezers particle tracking and confocal reflection imaging. *Journal of Physics: Condensed Matter*, 22(19):194121, 2010.
- [120] A. Kowalczyk, C. Oelschlaeger, and N. Willenbacher. Visualization of micro-scale inhomogeneities in acrylic thickener solutions: A multiple particle tracking study. *Polymer*, 58:170–179, 2015. ISSN 00323861. doi: 10.1016/j.polymer.2014.12.041.

- [121] A. Kowalczyk, C. Oelschlaeger, and N. Willenbacher. Tracking errors in 2d multiple particle tracking microrheology. *Measurement Science and Technology*, 26(1):015302, 2015. ISSN 0957-0233. doi: 10.1088/0957-0233/26/1/015302.
- [122] T. Kuboki, W. Chen, and S. Kidoaki. Time-dependent migratory behaviors in the long-term studies of fibroblast durotaxis on a hydrogel substrate fabricated with a soft band. *Langmuir*, 30(21):6187–6196, 2014. ISSN 0743-7463. doi: 10.1021/la501058j.
- [123] T. Kutlusoy, B. Oktay, N. K. Apohan, M. Süleymanoğlu, and S. E. Kuruca. Chitosan-co-hyaluronic acid porous cryogels and their application in tissue engineering. *International journal of biological macromolecules*, 103:366–378, 2017. ISSN 1879-0003. doi: 10.1016/j.ijbiomac.2017.05.067.
- [124] A. La Gatta, C. Schiraldi, A. Papa, A. D’Agostino, M. Cammarota, A. de Rosa, and M. de Rosa. Hyaluronan scaffolds via diglycidyl ether crosslinking: toward improvements in composition and performance. *Carbohydrate polymers*, 96(2):536–544, 2013. ISSN 1879-1344. doi: 10.1016/j.carbpol.2013.04.022.
- [125] G. Lai, Y. Li, and G. Li. Effect of concentration and temperature on the rheological behavior of collagen solution. *International journal of biological macromolecules*, 42(3):285–291, 2008. ISSN 1879-0003. doi: 10.1016/j.ijbiomac.2007.12.010.
- [126] S. K. Lai, Y.-Y. Wang, D. Wirtz, and J. Hanes. Micro-and macrorheology of mucus. *Advanced drug delivery reviews*, 61(2):86–100, 2009.
- [127] V. K. Lai, D. S. NedreLOW, S. P. Lake, B. Kim, E. M. Weiss, R. T. Tranquillo, and V. H. Barocas. Swelling of collagen-hyaluronic acid co-gels: An in vitro residual stress model. *Annals of biomedical engineering*, 44(10):2984–2993, 2016. ISSN 1573-9686. doi: 10.1007/s10439-016-1636-0.
- [128] E. N. Landis and D. T. Keane. X-ray microtomography. *Materials characterization*, 61(12):1305–1316, 2010.
- [129] R. Lanza, R. Langer, J. P. Vacanti, and A. Atala. *Principles of tissue engineering*. Academic press, 2020.
- [130] A. Lapolla, P. Traldi, and D. Fedele. Importance of measuring products of non-enzymatic glycation of proteins. *Clinical biochemistry*, 38(2):103–115, 2005. ISSN 0009-9120. doi: 10.1016/j.clinbiochem.2004.09.007.
- [131] O. Latinovic, L. A. Hough, and H. Daniel Ou-Yang. Structural and micromechanical characterization of type i collagen gels. *Journal of Biomechanics*, 43(3):500–505, 2010. ISSN 0021-9290. doi: 10.1016/j.jbiomech.2009.09.041.
- [132] A. Le Duc, B. Vergnes, and T. Budtova. Polypropylene/natural fibres composites: Analysis of fibre dimensions after compounding and observations of fibre rupture by rheo-optics. *Composites Part A: Applied Science and Manufacturing*, 42(11):

-
- 1727–1737, 2011. ISSN 1359835X. doi: 10.1016/j.compositesa.2011.07.027. URL <http://www.sciencedirect.com/science/article/pii/S1359835X11002338>.
- [133] C. Lee, A. Grodzinsky, and M. Spector. The effects of cross-linking of collagen-glycosaminoglycan scaffolds on compressive stiffness, chondrocyte-mediated contraction, proliferation and biosynthesis. *Biomaterials*, 22(23):3145–3154, 2001. ISSN 01429612. doi: 10.1016/S0142-9612(01)00067-9.
- [134] Y. W. Lee, W. J. Cho, and J. Y. Jang. Implantation material comprising biocompatible polymer, Sept. 2 2013. US Patent 8,822,551.
- [135] C. Lee-Thedieck, N. Rauch, R. Fiammengo, G. Klein, and J. P. Spatz. Impact of substrate elasticity on human hematopoietic stem and progenitor cell adhesion and motility. *Journal of Cell Science*, 125(Pt 16):3765–3775, 2012. ISSN 00219533. doi: 10.1242/jcs.095596.
- [136] Y. Lei, S. Gojgini, J. Lam, and T. Segura. The spreading, migration and proliferation of mouse mesenchymal stem cells cultured inside hyaluronic acid hydrogels. *Biomaterials*, 32(1):39–47, 2011. ISSN 01429612. doi: 10.1016/j.biomaterials.2010.08.103.
- [137] H. Li, J. M. Mattson, and Y. Zhang. Integrating structural heterogeneity, fiber orientation, and recruitment in multiscale ecm mechanics. *Journal of the mechanical behavior of biomedical materials*, 92:1–10, 2019. ISSN 1878-0180. doi: 10.1016/j.jmbbm.2018.12.023.
- [138] J. Lilla, D. Stickens, and Z. Werb. Metalloproteases and adipogenesis: A weighty subject. *The American Journal of Pathology*, 160(5):1551–1554, 2002. ISSN 00029440. doi: 10.1016/S0002-9440(10)61100-5.
- [139] B.-S. Liu, C.-H. Yao, Y.-S. Chen, and S.-H. Hsu. In vitro evaluation of degradation and cytotoxicity of a novel composite as a bone substitute. *Journal of Biomedical Materials Research Part A: An Official Journal of The Society for Biomaterials, The Japanese Society for Biomaterials, and The Australian Society for Biomaterials and the Korean Society for Biomaterials*, 67(4):1163–1169, 2003.
- [140] Y. Liu, C. Liang, X. Liu, B. Liao, X. Pan, Y. Ren, M. Fan, M. Li, Z. He, J. Wu, et al. Ages increased migration and inflammatory responses of adventitial fibroblasts via rage, mapk and nf- κ b pathways. *Atherosclerosis*, 208(1):34–42, 2010.
- [141] J. M. Lohre, L. Baclig, E. Wickham, S. Guida, J. Farley, K. Thyagarajan, R. Tu, and R. Quijano. Evaluation of epoxy ether fixed bovine arterial grafts for mutagenic potential. *ASAIO journal (American Society for Artificial Internal Organs: 1992)*, 39(2):106–113, 1993.
- [142] S.-L. Loo, W. B. Krantz, T.-T. Lim, A. G. Fane, and X. Hu. Design and synthesis of ice-templated psa cryogels for water purification: Towards tailored morphology

- and properties. *Soft Matter*, 9(1):224–234, 2013. ISSN 1744-683X. doi: 10.1039/C2SM26859K.
- [143] V. I. Lozinsky, F. M. Plieva, I. Y. Galaev, and B. Mattiasson. The potential of polymeric cryogels in bioseparation. *Bioseparation*, 10(4/5):163–188, 2001. ISSN 0923179X. doi: 10.1023/A:1016386902611.
- [144] V. I. Lozinsky, I. Y. Galaev, F. M. Plieva, I. N. Savina, H. Jungvid, and B. Mattiasson. Polymeric cryogels as promising materials of biotechnological interest. *Trends in Biotechnology*, 21(10):445–451, 2003. ISSN 0167-7799. doi: 10.1016/j.tibtech.2003.08.002.
- [145] W. Luo, H. Shitaye, M. Friedman, C. N. Bennett, J. Miller, O. A. Macdougald, and K. D. Hankenson. Disruption of cell-matrix interactions by heparin enhances mesenchymal progenitor adipocyte differentiation. *Experimental cell research*, 314(18):3382–3391, 2008. doi: 10.1016/j.yexcr.2008.07.003.
- [146] L. Ma, C. Gao, Z. Mao, J. Zhou, J. Shen, X. Hu, and C. Han. Collagen/chitosan porous scaffolds with improved biostability for skin tissue engineering. *Biomaterials*, 24(26):4833–4841, 2003. ISSN 01429612. doi: 10.1016/S0142-9612(03)00374-0.
- [147] A. Malandrino, M. Mak, R. D. Kamm, and E. Moeendarbary. Complex mechanics of the heterogeneous extracellular matrix in cancer. *Extreme Mechanics Letters*, 21:25–34, 2018. ISSN 2352-4316. doi: 10.1016/j.eml.2018.02.003.
- [148] B. M. Marín-Santibáñez, J. Pérez-González, and L. de Vargas. Shear rheometry and visualization of glass fiber suspensions. *Rheologica Acta*, 49(2):177–189, 2010. ISSN 0035-4511. doi: 10.1007/s00397-009-0418-0. URL <https://doi.org/10.1007/s00397-009-0418-0>.
- [149] R. A. Marklein and J. A. Burdick. Controlling stem cell fate with material design. *Advanced Materials*, 22(2):175–189, 2010. doi: 10.1002/adma.200901055.
- [150] C. F. Marques, G. S. Diogo, S. Pina, J. M. Oliveira, T. H. Silva, and R. L. Reis. Collagen-based bioinks for hard tissue engineering applications: a comprehensive review. *Journal of materials science. Materials in medicine*, 30(3):32, 2019. ISSN 1573-4838. doi: 10.1007/s10856-019-6234-x.
- [151] K. A. Marx, T. Zhou, A. Montrone, D. McIntosh, and S. J. Braunhut. Quartz crystal microbalance biosensor study of endothelial cells and their extracellular matrix following cell removal: Evidence for transient cellular stress and viscoelastic changes during detachment and the elastic behavior of the pure matrix. *Analytical Biochemistry*, 343(1):23 – 34, 2005. ISSN 0003-2697. doi: <https://doi.org/10.1016/j.ab.2005.05.013>.
- [152] Mason and Weitz. Optical measurements of frequency-dependent linear viscoelastic moduli of complex fluids. *Physical Review Letters*, 74(7):1250–1253, 1995. ISSN 0031-9007. doi: 10.1103/PhysRevLett.74.1250.

-
- [153] T. G. Mason. Estimating the viscoelastic moduli of complex fluids using the generalized stokes-einstein equation. *Rheologica Acta*, 39(4):371–378, 2000. ISSN 0035-4511. doi: 10.1007/s003970000094.
- [154] T. G. Mason, K. Ganesan, J. H. van Zanten, D. Wirtz, and S. C. Kuo. Particle tracking microrheology of complex fluids. *Physical Review Letters*, 79(17):3282–3285, 1997. ISSN 0031-9007. doi: 10.1103/PhysRevLett.79.3282.
- [155] R. J. McAnulty. Fibroblasts and myofibroblasts: Their source, function and role in disease. *The International Journal of Biochemistry & Cell Biology*, 39(4):666–671, 2007. ISSN 1357-2725. doi: <https://doi.org/10.1016/j.biocel.2006.11.005>.
- [156] R. J. McAnulty. Fibroblasts and myofibroblasts: Their source, function and role in disease. *The International Journal of Biochemistry & Cell Biology*, 39(4):666–671, 2007. ISSN 1357-2725. doi: 10.1016/j.biocel.2006.11.005.
- [157] C. T. McKee, J. A. Last, P. Russell, and C. J. Murphy. Indentation versus tensile measurements of young’s modulus for soft biological tissues. *Tissue engineering. Part B, Reviews*, 17(3):155–164, 2011. doi: 10.1089/ten.TEB.2010.0520.
- [158] F.-L. Mi, Y.-C. Tan, H.-C. Liang, R.-N. Huang, and H.-W. Sung. In vitro evaluation of a chitosan membrane cross-linked with genipin. *Journal of Biomaterials Science, Polymer Edition*, 12(8):835–850, 2001.
- [159] J. Michaelson, V. Hariharan, and H. Huang. Hyperglycemic and hyperlipidemic conditions alter cardiac cell biomechanical properties. *Biophysical journal*, 106(11):2322–2329, 2014.
- [160] E. Mittmann, S. Gallus, P. Bitterwolf, C. Oelschlaeger, N. Willenbacher, C. M. Niemeyer, and K. S. Rabe. A phenolic acid decarboxylase-based all-enzyme hydrogel for flow reactor technology. *Micromachines*, 10(12):795, 2019.
- [161] D. Mizuno, C. Tardin, C. F. Schmidt, and F. C. MacKintosh. Nonequilibrium mechanics of active cytoskeletal networks. *Science*, 315(5810):370–373, 2007.
- [162] J. D. Mott and Z. Werb. Regulation of matrix biology by matrix metalloproteinases. *Current opinion in cell biology*, 16(5):558–564, 2004. ISSN 0955-0674. doi: 10.1016/j.ceb.2004.07.010.
- [163] X. Murgia, P. Pawelzyk, U. F. Schaefer, C. Wagner, N. Willenbacher, and C.-M. Lehr. Size-limited penetration of nanoparticles into porcine respiratory mucus after aerosol deposition. *Biomacromolecules*, 17(4):1536–1542, 2016. ISSN 1525-7797. doi: 10.1021/acs.biomac.6b00164.
- [164] S. D. Nath, C. Abueva, B. Kim, and B. T. Lee. Chitosan–hyaluronic acid polyelectrolyte complex scaffold crosslinked with genipin for immobilization and controlled release of bmp-2. *Carbohydrate polymers*, 115:160–169, 2015.

- [165] S. Nayak, S. Dey, and S. C. Kundu. Skin equivalent tissue-engineered construct: co-cultured fibroblasts/ keratinocytes on 3d matrices of sericin hope cocoons. *PloS one*, 8(9):e74779, 2013. ISSN 1932-6203. doi: 10.1371/journal.pone.0074779.
- [166] L. J. Nesti, W.-J. Li, R. M. Shanti, Y. J. Jiang, W. Jackson, B. A. Freedman, T. R. Kuklo, J. R. Giuliani, and R. S. Tuan. Intervertebral disc tissue engineering using a novel hyaluronic acid-nanofibrous scaffold (hanfs) amalgam. *Tissue engineering. Part A*, 14(9):1527–1537, 2008. ISSN 1937-335X. doi: 10.1089/ten.tea.2008.0215.
- [167] F. H. Nestler, S. Hvidt, J. D. Ferry, and A. Veis. Flexibility of collagen determined from dilute solution viscoelastic measurements. *Biopolymers*, 22(7):1747–1758, 1983. ISSN 0006-3525. doi: 10.1002/bip.360220710.
- [168] N. Nijenhuis, D. Mizuno, J. A. E. Spaan, and C. F. Schmidt. High-resolution microrheology in the pericellular matrix of prostate cancer cells. *Journal of the Royal Society, Interface*, 9(73):1733–1744, 2012. ISSN 1742-5662. doi: 10.1098/rsif.2011.0825.
- [169] M. E. Nimni and R. D. Harkness. Molecular structures and functions of collagen. *Collagen Volume I Biochemistry*, 1988.
- [170] C. Nishi, N. Nakajima, and Y. Ikada. In vitro evaluation of cytotoxicity of diepoxy compounds used for biomaterial modification. *Journal of biomedical materials research*, 29(7):829–834, 1995.
- [171] B. Obradović, editor. *Cell and tissue engineering*. Springer, Berlin/Belgrade, 2012. ISBN 978-3-642-21912-2. doi: 10.1007/978-3-642-21913-9.
- [172] C. Oelschlaeger and N. Willenbacher. Rheological properties of aqueous solutions of cetylpyridinium chloride in the presence of sodium chlorate. *Rheologica Acta*, 50(7):655–660, 2011. ISSN 0035-4511. doi: 10.1007/s00397-011-0548-z.
- [173] C. Oelschlaeger, M. Cota Pinto Coelho, and N. Willenbacher. Chain flexibility and dynamics of polysaccharide hyaluronan in entangled solutions: a high frequency rheology and diffusing wave spectroscopy study. *Biomacromolecules*, 14(10):3689–3696, 2013. ISSN 1525-7797. doi: 10.1021/bm4010436.
- [174] C. Oelschlaeger, F. Bossler, and N. Willenbacher. Synthesis, structural and micromechanical properties of 3d hyaluronic acid-based cryogel scaffolds. *Biomacromolecules*, 17(2):580–589, 2016. ISSN 1525-7797. doi: 10.1021/acs.biomac.5b01529.
- [175] S. H. Oh, I. K. Park, J. M. Kim, and J. H. Lee. In vitro and in vivo characteristics of pcl scaffolds with pore size gradient fabricated by a centrifugation method. *Biomaterials*, 28(9):1664–1671, 2007. ISSN 01429612. doi: 10.1016/j.biomaterials.2006.11.024.

-
- [176] Oosten, Anne S. G. van, M. Vahabi, A. J. Licup, A. Sharma, P. A. Galie, F. C. MacKintosh, and P. A. Janmey. Uncoupling shear and uniaxial elastic moduli of semiflexible biopolymer networks: compression-softening and stretch-stiffening. *Scientific Reports*, 6:19270, 2016. ISSN 2045-2322. doi: 10.1038/srep19270.
- [177] F. K. Oppong and J. R. de Bruyn. Microrheology and jamming in a yield-stress fluid. *Rheologica Acta*, 50(4):317–326, 2011. ISSN 0035-4511. doi: 10.1007/s00397-010-0519-9.
- [178] S. C. Owen, S. A. Fisher, R. Y. Tam, C. M. Nimmo, and M. S. Shoichet. Hyaluronic acid click hydrogels emulate the extracellular matrix. *Langmuir*, 29(24):7393–7400, 2013. ISSN 0743-7463. doi: 10.1021/la305000w.
- [179] P. B. Pal, H. Sonowal, K. Shukla, S. K. Srivastava, and K. V. Ramana. Aldose reductase regulates hyperglycemia-induced huvec death via sirt1/ampk- α 1/mtor pathway. *Journal of molecular endocrinology*, 63(1):11–25, 2019. doi: 10.1530/JME-19-0080.
- [180] A. Papagiannopoulos, K. Sotiropoulos, and S. Pispas. Particle tracking microrheology of the power-law viscoelasticity of xanthan solutions. *Food Hydrocolloids*, 61:201–210, 2016. ISSN 0268005X. doi: 10.1016/j.foodhyd.2016.05.020.
- [181] A. Parekh and D. Velegol. Collagen gel anisotropy measured by 2-d laser trap microrheometry. *Annals of biomedical engineering*, 35(7):1231–1246, 2007. ISSN 1573-9686.
- [182] P. Pawelzyk, N. Mücke, H. Herrmann, and N. Willenbacher. Attractive interactions among intermediate filaments determine network mechanics in vitro. *PloS one*, 9(4):e93194, 2014. ISSN 1932-6203. doi: 10.1371/journal.pone.0093194.
- [183] M. P. Petrich, D. L. Koch, and C. Cohen. An experimental determination of the stress–microstructure relationship in semi-concentrated fiber suspensions. *Journal of Non-Newtonian Fluid Mechanics*, 95(2):101–133, 2000. ISSN 0377-0257. doi: 10.1016/S0377-0257(00)00172-5. URL <http://www.sciencedirect.com/science/article/pii/S0377025700001725>.
- [184] C. J. Petrie. The rheology of fibre suspensions. *Journal of Non-Newtonian Fluid Mechanics*, 87(2-3):369–402, 1999.
- [185] C. Piard, A. Jeyaram, Y. Liu, J. Caccamese, S. M. Jay, Y. Chen, and J. Fisher. 3d printed huvecs/mscs cocultures impact cellular interactions and angiogenesis depending on cell-cell distance. *Biomaterials*, 222:119423, 2019.
- [186] M. Pilavtepe, S. Recktenwald, R. Schuhmann, K. Emmerich, and N. Willenbacher. Macro-and microscale structure formation and aging in different arrested states of laponite dispersions. *Journal of Rheology*, 62(2):593–605, 2018.
- [187] A. Pizzoferrato, G. Ciapetti, S. Stea, E. Cenni, C. R. Arciola, D. Granchi, and Lucia. Cell culture methods for testing biocompatibility. *Clinical Materials*, 15(3):173–190, 1994. ISSN 0267-6605. doi: 10.1016/0267-6605(94)90081-7.

- [188] F. M. Plieva, P. Ekström, I. Y. Galaev, and B. Mattiasson. Monolithic cryogels with open porous structure and unique double-continuous macroporous networks. *Soft Matter*, 4(12):2418, 2008. ISSN 1744-683X. doi: 10.1039/b804105a.
- [189] A. Procopio, E. Malucelli, A. Pacureanu, C. Cappadone, G. Farruggia, A. Sargenti, S. Castiglioni, D. Altamura, A. Sorrentino, C. Giannini, E. Pereiro, P. Cloetens, J. A. M. Maier, and S. Iotti. Chemical fingerprint of zn-hydroxyapatite in the early stages of osteogenic differentiation. *ACS central science*, 5(8):1449–1460, 2019. ISSN 2374-7943. doi: 10.1021/acscentsci.9b00509.
- [190] A. Puisto, X. Illa, M. Mohtaschemi, and M. Alava. Modeling the rheology of nanocellulose suspensions. *Nordic Pulp & Paper Research Journal*, 27(2):277–281, 2012.
- [191] M. Rajabian, C. Dubois, and M. Grmela. Suspensions of semiflexible fibers in polymeric fluids: Rheology and thermodynamics. *Rheologica Acta*, 44(5): 521–535, 2005. ISSN 0035-4511. doi: 10.1007/s00397-005-0434-7. URL <https://link.springer.com/content/pdf/10.1007/s00397-005-0434-7.pdf>.
- [192] A. Ramazani S. A., A. Ait-Kadi, and M. Grmela. Rheology of fiber suspensions in viscoelastic media: Experiments and model predictions. *Journal of Rheology*, 45(4):945–962, 2001. ISSN 01486055. doi: 10.1122/1.1378026.
- [193] C. Rask-Madsen and G. L. King. Vascular complications of diabetes: Mechanisms of injury and protective factors. *Cell metabolism*, 17(1):20–33, 2013. doi: 10.1016/j.cmet.2012.11.012.
- [194] J. Ratanavaraporn, S. Damrongsakkul, N. Sanchavanakit, T. Banaprasert, and S. Kanokpanont. Comparison of gelatin and collagen scaffolds for fibroblast cell culture. *Journal of Metals, Materials and Minerals*, 16(1), 2017. ISSN 0857-6149.
- [195] S. Reichelt, J. Becher, J. Weisser, A. Prager, U. Decker, S. Moller, A. Berg, and M. Schnabelrauch. Biocompatible polysaccharide-based cryogels. *Materials science & engineering. C, Materials for biological applications*, 35:164–170, 2014. ISSN 0928-4931. doi: 10.1016/j.msec.2013.10.034.
- [196] G. C. Reilly and A. J. Engler. Intrinsic extracellular matrix properties regulate stem cell differentiation. *Journal of Biomechanics*, 43(1):55 – 62, 2010. ISSN 0021-9290. doi: <https://doi.org/10.1016/j.jbiomech.2009.09.009>. Special Issue on Cell Mechanobiology.
- [197] G. C. Reilly and A. J. Engler. Intrinsic extracellular matrix properties regulate stem cell differentiation: Special issue on cell mechanobiology. *Journal of Biomechanics*, 43(1):55–62, 2010. ISSN 0021-9290. doi: 10.1016/j.jbiomech.2009.09.009.
- [198] B. A. Roeder, K. Kokini, J. E. Sturgis, J. P. Robinson, and S. L. Voytik-Harbin. Tensile mechanical properties of three-dimensional type i collagen extracellular matrices with varied microstructure. *Journal of Biomechanical Engineering*, 124(2):214, 2002. ISSN 01480731. doi: 10.1115/1.1449904.

-
- [199] J. Roether, S. Bertels, C. Oelschlaeger, M. Bastmeyer, and N. Willenbacher. Microstructure, local viscoelasticity and cell culture suitability of 3d hybrid ha/collagen scaffolds. *PloS one*, 13(12):e0207397, 2018. ISSN 1932-6203. doi: 10.1371/journal.pone.0207397.
- [200] F. M. Ross. Opportunities and challenges in liquid cell electron microscopy. *Science*, 350(6267):aaa9886, 2015.
- [201] M. E. Rosti, L. Brandt, and D. Mitra. Rheology of suspensions of viscoelastic spheres: Deformability as an effective volume fraction. *Physical Review Fluids*, 3(1):012301, 2018.
- [202] S. Rother, V. D. Galiazzo, D. Kilian, K. M. Fiebig, J. Becher, S. Moeller, U. Hempel, M. Schnabelrauch, J. Waltenberger, D. Scharnweber, and V. Hintze. Hyaluronan/collagen hydrogels with sulfated hyaluronan for improved repair of vascularized tissue tune the binding of proteins and promote endothelial cell growth. *Macromolecular bioscience*, 2017. ISSN 1616-5195. doi: 10.1002/mabi.201700154.
- [203] M. Rubinstein and R. H. Colby. *Polymer physics*. Oxford university press New York, 2003.
- [204] T. Savin and P. S. Doyle. Static and dynamic errors in particle tracking microrheology. *Biophysical Journal*, 88(1):623–638, 2005. ISSN 00063495. doi: 10.1529/biophysj.104.042457.
- [205] P. J. Schilling, B. R. Karedla, A. K. Tatiparthi, M. A. Verges, and P. D. Herrington. X-ray computed microtomography of internal damage in fiber reinforced polymer matrix composites. *Composites Science and Technology*, 65(14):2071–2078, 2005.
- [206] I. Schoen, B. L. Pruitt, and V. Vogel. The yin-yang of rigidity sensing: How forces and mechanical properties regulate the cellular response to materials. *Annual Review of Materials Research*, 43(1):589–618, 2013. ISSN 1531-7331. doi: 10.1146/annurev-matsci-062910-100407.
- [207] K. M. Schultz and K. S. Anseth. Monitoring degradation of matrix metalloproteinases-cleavable peg hydrogels via multiple particle tracking microrheology. *Soft Matter*, 9(5):1570–1579, 2013. ISSN 1744-683X. doi: 10.1039/C2SM27303A.
- [208] K. M. Schultz, K. A. Kyburz, and K. S. Anseth. Measuring dynamic cell-material interactions and remodeling during 3d human mesenchymal stem cell migration in hydrogels. *Proceedings of the National Academy of Sciences of the United States of America*, 112(29):E3757–64, 2015. doi: 10.1073/pnas.1511304112.
- [209] D. Schulz Torres, T. M. Freyman, I. V. Yannas, and M. Spector. Tendon cell contraction of collagen–gag matrices in vitro: effect of cross-linking. *Biomaterials*, 21(15):1607–1619, 2000. ISSN 01429612. doi: 10.1016/S0142-9612(00)00051-X.

- [210] B. Seal. Polymeric biomaterials for tissue and organ regeneration. *Materials Science and Engineering: R: Reports*, 34(4-5):147–230, 2001. ISSN 0927796X. doi: 10.1016/S0927-796X(01)00035-3.
- [211] M. Seandel, K. Noack-Kunmann, D. Zhu, R. T. Aimes, and J. P. Quigley. Growth factor-induced angiogenesis in vivo requires specific cleavage of fibrillar type i collagen. *Blood*, 97(8):2323–2332, 2001.
- [212] M. A. Selyanin, P. Y. Boykov, and V. N. Khabarov. *Hyaluronic acid: Preparation, properties, application in biology and medicine / Mikhail A. Selyanin, Petr Ya. Boykov and Vladimir N. Khabarov ; translated from the Russian by scientific editor Dr. F. Polyak*. John Wiley & Sons, Hoboken, 2015. ISBN 9781118695937.
- [213] M. Sepehr, P. J. Carreau, M. Moan, and G. Ausias. Rheological properties of short fiber model suspensions. *Journal of Rheology*, 48(5):1023–1048, 2004.
- [214] A. Sharma, S. Bhat, V. Nayak, and A. Kumar. Efficacy of supermacroporous poly(ethylene glycol)-gelatin cryogel matrix for soft tissue engineering applications. *Materials science & engineering. C, Materials for biological applications*, 47:298–312, 2015. ISSN 0928-4931. doi: 10.1016/j.msec.2014.11.031.
- [215] M. Shayegan and N. R. Forde. Microrheological characterization of collagen systems: from molecular solutions to fibrillar gels. *PloS one*, 8(8):e70590, 2013. ISSN 1932-6203. doi: 10.1371/journal.pone.0070590.
- [216] R. V. Shevchenko, S. L. James, and S. E. James. A review of tissue-engineered skin bioconstructs available for skin reconstruction. *Journal of the Royal Society, Interface*, 7(43):229–258, 2010. ISSN 1742-5662. doi: 10.1098/rsif.2009.0403.
- [217] D. Singh, V. Nayak, and A. Kumar. Proliferation of myoblast skeletal cells on three-dimensional supermacroporous cryogels. *International journal of biological sciences*, 6(4):371, 2010.
- [218] V. P. Singh, A. Bali, N. Singh, and A. S. Jaggi. Advanced glycation end products and diabetic complications. *The Korean journal of physiology & pharmacology : official journal of the Korean Physiological Society and the Korean Society of Pharmacology*, 18(1):1–14, 2014. ISSN 1226-4512. doi: 10.4196/kjpp.2014.18.1.1.
- [219] M. J. Skaug and D. K. Schwartz. Tracking nanoparticle diffusion in porous filtration media. *Industrial & Engineering Chemistry Research*, 54(16):4414–4419, 2015.
- [220] L. R. Smith, S. Cho, and D. E. Discher. Stem cell differentiation is regulated by extracellular matrix mechanics. *Physiology*, 33(1):16–25, 2018. doi: 10.1152/physiol.00026.2017. PMID: 29212889.
- [221] J. Solon, I. Levental, K. Sengupta, P. C. Georges, and P. A. Janmey. Fibroblast adaptation and stiffness matching to soft elastic substrates. *Biophysical Journal*, 93(12):4453–4461, 2007. ISSN 00063495. doi: 10.1529/biophysj.106.101386.

-
- [222] A. Southan, M. Mateescu, V. Hagel, M. Bach, C. Schuh, C. Kleinhans, P. J. Kluger, S. Tussetschläger, I. Nuss, T. Haraszti, S. V. Wegner, J. P. Spatz, H. Boehm, S. Laschat, and G. E. M. Tovar. Toward controlling the formation, degradation behavior, and properties of hydrogels synthesized by aza-michael reactions. *Macromolecular Chemistry and Physics*, 214(16):1865–1873, 2013. ISSN 10221352. doi: 10.1002/macp.201300359.
- [223] J. R. Staunton, W. Y. So, C. D. Paul, and K. Tanner. High-frequency microrheology in 3d reveals mismatch between cytoskeletal and extracellular matrix mechanics. *Proceedings of the National Academy of Sciences*, 116(29):14448–14455, 2019. doi: 10.1073/pnas.1814271116.
- [224] A. Ström, A. Larsson, and O. Okay. Preparation and physical properties of hyaluronic acid-based cryogels. *Journal of Applied Polymer Science*, 132(29):n/a–n/a, 2015. ISSN 00218995. doi: 10.1002/app.42194.
- [225] D. G. Stupack and D. A. Cheresh. Ecm remodeling regulates angiogenesis: Endothelial integrins look for new ligands. *Science Signaling*, 2002(119):pe7–pe7, 2002. doi: 10.1126/stke.2002.119.pe7.
- [226] R. R. Sundararajakumar and D. L. Koch. Structure and properties of sheared fiber suspensions with mechanical contacts. *Journal of Non-Newtonian Fluid Mechanics*, 73(3):205–239, 1997. ISSN 0377-0257. doi: 10.1016/S0377-0257(97)00043-8. URL <http://www.sciencedirect.com/science/article/pii/S0377025797000438>.
- [227] L. H. Switzer and D. J. Klingenberg. Rheology of sheared flexible fiber suspensions via fiber-level simulations. *Journal of Rheology*, 47(3):759–778, 2003. ISSN 01486055. doi: 10.1122/1.1566034.
- [228] K. Tanner. High frequency active microrheology reveals mismatch in 3d tumor intracellular and extracellular matrix viscoelasticity. *Biophysical Journal*, 116(3):8a, 2019.
- [229] T. Teissier and É. Boulanger. The receptor for advanced glycation end-products (rage) is an important pattern recognition receptor (prp) for inflammaging. *Biogerontology*, pages 1–23, 2019.
- [230] C. T. Thorpe, C. P. Udeze, H. L. Birch, P. D. Clegg, and H. R. C. Screen. Specialization of tendon mechanical properties results from interfascicular differences. *Journal of the Royal Society, Interface*, 9(76):3108–3117, 2012. ISSN 1742-5662. doi: 10.1098/rsif.2012.0362.
- [231] K. Tomihata. Preparation of cross-linked hyaluronic acid films of low water content. *Biomaterials*, 18(3):189–195, 1997. ISSN 01429612. doi: 10.1016/S0142-9612(96)00116-0.
- [232] B. P. Toole, T. N. Wight, and M. I. Tammi. Hyaluronan-cell interactions in cancer and vascular disease. *Journal of Biological Chemistry*, 277(7):4593–4596, 2002.

- [233] D. Tousoulis, N. Papageorgiou, E. Androulakis, G. Siasos, G. Latsios, K. Tentolouris, and C. Stefanadis. Diabetes mellitus-associated vascular impairment: Novel circulating biomarkers and therapeutic approaches. *Journal of the American College of Cardiology*, 62(8):667–676, 2013. doi: 10.1016/j.jacc.2013.03.089.
- [234] A. Tripathi, T. Vishnoi, D. Singh, and A. Kumar. Modulated crosslinking of macroporous polymeric cryogel affects in vitro cell adhesion and growth. *Macromolecular bioscience*, 13(7):838–850, 2013. ISSN 1616-5195. doi: 10.1002/mabi.201200398.
- [235] C.-C. Tsai, R.-N. Huang, H.-W. Sung, and H. C. Liang. In vitro evaluation of the genotoxicity of a naturally occurring crosslinking agent (genipin) for biologic tissue fixation. *Journal of biomedical materials research*, 52(1):58–65, 2000.
- [236] J. R. Tse and A. J. Engler. Preparation of hydrogel substrates with tunable mechanical properties. *Current protocols in cell biology*, 47(1):10–16, 2010. ISSN 1934-2616. doi: 10.1002/0471143030.cb1016s47.
- [237] Y. Tseng and D. Wirtz. Mechanics and multiple-particle tracking microheterogeneity of α -actinin-cross-linked actin filament networks. *Biophysical journal*, 81(3):1643–1656, 2001.
- [238] Y. Tseng, T. P. Kole, and D. Wirtz. Micromechanical mapping of live cells by multiple-particle-tracking microrheology. *Biophysical Journal*, 83(6):3162–3176, 2002. ISSN 00063495. doi: 10.1016/S0006-3495(02)75319-8.
- [239] E. A. Turley, P. W. Noble, and L. Y. W. Bourguignon. Signaling properties of hyaluronan receptors. *Journal of Biological Chemistry*, 277(7):4589–4592, 2002.
- [240] M. T. Valentine, Z. E. Perlman, M. L. Gardel, J. H. Shin, P. Matsudaira, T. J. Mitchison, and D. A. Weitz. Colloid surface chemistry critically affects multiple particle tracking measurements of biomaterials. *Biophysical Journal*, 86(6):4004–4014, 2004. ISSN 00063495. doi: 10.1529/biophysj.103.037812.
- [241] L. van Hove. Correlations in space and time and born approximation scattering in systems of interacting particles. *Physical Review*, 95(1):249, 1954. doi: 10.1103/PhysRev.95.249.
- [242] A. S. van Oosten and P. A. Janmey. Extremely charged and incredibly soft: physical characterization of the pericellular matrix. *Biophysical Journal*, 104(5):961–963, 2013. ISSN 00063495.
- [243] S. van Vlierberghe, P. Dubruel, and E. Schacht. Biopolymer-based hydrogels as scaffolds for tissue engineering applications: A review: Biomacromolecules. *Biomacromolecules*, 12(5):1387–1408, 2011. ISSN 1525-7797. doi: 10.1021/bm200083n.
- [244] S. Varma, J. P. R. O. Orgel, and J. D. Schieber. Nanomechanics of type i collagen. *Biophysical Journal*, 111(1):50–56, 2016. ISSN 00063495. doi: 10.1016/j.bpj.2016.05.038.

-
- [245] D. Velegol and F. Lanni. Cell traction forces on soft biomaterials. i. microrheology of type i collagen gels. *Biophysical Journal*, 81(3):1786–1792, 2001. ISSN 00063495. doi: 10.1016/S0006-3495(01)75829-8.
- [246] T. Velnar, T. Bailey, and V. Smrkolj. The wound healing process: an overview of the cellular and molecular mechanisms. *The Journal of international medical research*, 37(5):1528–1542, 2009. ISSN 0300-0605.
- [247] C. Ventura, A. Blanco, C. Negro, P. Ferreira, F. Garcia, and M. Rasteiro. Modeling pulp fiber suspension rheology. *Tappi Journal*, 6(7):17–23, 2007.
- [248] P. K. Viji Babu, C. Rianna, U. Mirastschijski, and M. Radmacher. Nanomechanical mapping of interdependent cell and ecm mechanics by afm force spectroscopy. *Scientific reports*, 9(1):12317, 2019. doi: 10.1038/s41598-019-48566-7.
- [249] K. H. Vining and D. J. Mooney. Mechanical forces direct stem cell behaviour in development and regeneration. *Nature Reviews Molecular Cell Biology*, 18(12):728, 2017.
- [250] V. Vogel and M. Sheetz. Local force and geometry sensing regulate cell functions. *Nature reviews. Molecular cell biology*, 7(4):265–275, 2006. ISSN 1471-0072. doi: 10.1038/nrm1890.
- [251] M. Votteler, P. J. Kluger, H. Walles, and K. Schenke-Layland. Stem cell microenvironments—unveiling the secret of how stem cell fate is defined. *Macromolecular bioscience*, 10(11):1302–1315, 2010. doi: 10.1002/mabi.201000102.
- [252] T. A. Waigh. Microrheology of complex fluids. *Reports on Progress in Physics*, 68(3):685–742, 2005. ISSN 0034-4885. doi: 10.1088/0034-4885/68/3/R04.
- [253] G. Wang, W. Yu, and C. Zhou. Optimization of the rod chain model to simulate the motions of a long flexible fiber in simple shear flows. *European Journal of Mechanics - B/Fluids*, 25(3):337–347, 2006. ISSN 0997-7546. doi: 10.1016/j.euromechflu.2005.09.004. URL <http://www.sciencedirect.com/science/article/pii/S0997754605000749>.
- [254] H.-M. Wang, Y.-T. Chou, Z.-H. Wen, C.-Z. Wang, C.-H. Chen, and M.-L. Ho. Novel biodegradable porous scaffold applied to skin regeneration. *PloS one*, 8(6):e56330, 2013. ISSN 1932-6203. doi: 10.1371/journal.pone.0056330.
- [255] L. Wang, Z.-y. Li, Y.-p. Wang, Z.-h. Wu, and B. Yu. Dynamic expression profiles of marker genes in osteogenic differentiation of human bone marrow-derived mesenchymal stem cells. *Chinese medical sciences journal = Chung-kuo i hsueh k'o hsueh tsa chih*, 30(2):108–113, 2015. ISSN 1001-9294.
- [256] E. R. Weeks, J. C. Crocker, A. C. Levitt, A. Schofield, and D. A. Weitz. Three-dimensional direct imaging of structural relaxation near the colloidal glass transition. *Science*, 287(5453):627, 2000. doi: 10.1126/science.287.5453.627.

- [257] D. Weihs, T. G. Mason, and M. A. Teitell. Bio-microrheology: a frontier in microrheology. *Biophysical Journal*, 91(11):4296–4305, 2006. ISSN 00063495. doi: 10.1529/biophysj.106.081109.
- [258] K. J. Welsh, M. S. Kirkman, and D. B. Sacks. Role of glycated proteins in the diagnosis and management of diabetes: Research gaps and future directions. *Diabetes care*, 39(8):1299–1306, 2016. doi: 10.2337/dc15-2727.
- [259] M. P. E. Wenger, L. Bozec, M. A. Horton, and P. Mesquida. Mechanical properties of collagen fibrils. *Biophysical Journal*, 93(4):1255–1263, 2007. ISSN 00063495. doi: 10.1529/biophysj.106.103192.
- [260] WHO and Consultants. *Definition and diagnosis of diabetes mellitus and intermediate hyperglycaemia: Report of a WHO/IDF consultation*. World Health Organization, Geneva, Switzerland, 2006. ISBN 9241594934.
- [261] D. Wildenschild, C. Vaz, M. Rivers, D. Rikard, and B. Christensen. Using x-ray computed tomography in hydrology: systems, resolutions, and limitations. *Journal of Hydrology*, 267(3-4):285–297, 2002.
- [262] D. Wirtz. Particle-tracking microrheology of living cells: Principles and applications. *Annual Review of Biophysics*, 38(1):301–326, 2009. ISSN 1936-122X. doi: 10.1146/annurev.biophys.050708.133724.
- [263] J. Xie, Q. Zhang, T. Zhu, Y. Zhang, B. Liu, J. Xu, and H. Zhao. Substrate stiffness-regulated matrix metalloproteinase output in myocardial cells and cardiac fibroblasts: Implications for myocardial fibrosis. *Acta biomaterialia*, 10(6):2463–2472, 2014. doi: 10.1016/j.actbio.2014.01.031.
- [264] S. Yamamoto and T. Matsuoka. Dynamic simulation of rod-like and plate-like particle dispersed systems. *Computational materials science*, 14(1-4):169–176, 1999.
- [265] J. S. Young, A. R. Kannurpatti, and C. N. Bowman. Effect of comonomer concentration and functionality on photopolymerization rates, mechanical properties and heterogeneity of the polymer. *Macromolecular Chemistry and Physics*, 199(6):1043–1049, 1998. ISSN 10221352. doi: 10.1002/(SICI)1521-3935(19980601)199:6<1043::AID-MACP1043>3.3.CO;2-Q.
- [266] D. Zhang, X. Wu, J. Chen, and K. Lin. The development of collagen based composite scaffolds for bone regeneration. *Bioactive Materials*, 3(1):129–138, 2018. ISSN 2452-199X. doi: 10.1016/j.bioactmat.2017.08.004.
- [267] F. Zhang, C. He, L. Cao, W. Feng, H. Wang, X. Mo, and J. Wang. Fabrication of gelatin-hyaluronic acid hybrid scaffolds with tunable porous structures for soft tissue engineering. *International journal of biological macromolecules*, 48(3):474–481, 2011. ISSN 1879-0003. doi: 10.1016/j.ijbiomac.2011.01.012.

- [268] X.-Z. Zhang, Y.-Y. Yang, T.-S. Chung, and K.-X. Ma. Preparation and characterization of fast response macroporous poly(n -isopropylacrylamide) hydrogels. *Langmuir*, 17(20):6094–6099, 2001. ISSN 0743-7463. doi: 10.1021/la010105v.
- [269] J. Zhu and R. E. Marchant. Design properties of hydrogel tissue-engineering scaffolds. *Expert review of medical devices*, 8(5):607–626, 2011. doi: 10.1586/erd.11.27.